
**From the Institute of Anatomy**

**of the University of Lübeck**

**Director: Prof. Dr. med. Jürgen Westermann**

# Assessment of the T-lymphocyte Receptor Repertoire in the Experimental Model of Epidermolysis Bullosa Acquisita

Dissertation

for Fulfillment of

Requirements

for the Doctoral Degree

of the University of Lübeck

from the Department of Natural Sciences

Submitted by

Markus Arnold Niebuhr

from Wolfsburg

Lübeck 2019

| | |
|---|---|
| First referee: | PD. Dr.[in] rer. nat. Kathrin Kalies |
| Second referee: | Prof. Dr. rer. nat. Tamás Laskay |
| Chairman: | Prof. Dr. rer. nat. Norbert Tautz |
| Date of oral examination: | 14.02.2019 |

Approved for printing. Lübeck, 21.02.2019

*Denn man muss wissen, daß alle Erkenntnis zwei Enden habe,*
*bei denen man sie fassen kann, das eine a priori das andere a posteriori.*
Immanuel Kant

*So remember to look up at the stars and not down at your feet. Try to make sense of what you see and wonder about what makes the universe exist. Be curious.*
Stephen Hawking

# Table of Contents

## Abstract

**Background:** T-lymphocytes display a heterogeneous cell population that is characterized by a highly variable T-lymphocyte receptor. The repertoire of individual T-lymphocyte receptors has be analyzed in several studies focusing on autoimmunity. Thereby a disease-association of the T-lymphocyte receptor repertoire was detectable for some diseases, whereas in others no association was observable. In the experimental model of the dermal autoimmune disease Epidermolysis bullosa acquisita (EBA), the two disease-mandatory T-lymphocyte populations of skin immigrating T-lymphocytes ($T_{skin}$) and germinal center immigrating follicular helper T-lymphocytes ($T_{fh}$) are described in the literature. However, it is unknown, whether the T-lymphocyte receptor repertoire of $T_{skin}$ and $T_{fh}$ displays a specific shift under autoimmune condition. Therefore this dissertation addresses the question, whether the T-lymphocyte receptor$\beta$ repertoire of $T_{skin}$ and $T_{fh}$ is shifted in immunization induced EBA and if an overlap of both repertoires is detectable within an individual.

**Results:** Analysis of the $T_{skin}$ T-lymphocyte receptor$\beta$ repertoire resulted in no detectable characteristic for the skin immigrating T-lymphocytes by comparison among experimental groups. However, consideration of the $T_{fh}$ T-lymphocyte receptor$\beta$ repertoire among individuals resulted in an accumulation of identical $T_{fh}$ clonotypes, which specifically share the T-lymphocyte receptor$\beta$ V3-segment. Furthermore, $T_{fh}$ clonotypes were detected under autoimmune condition, that are shared among all analyzed individuals and thereby also exhibit an elevated V3-segment usage. In consideration of the $T_{fh}$ repertoire within an individual, it was found, that a highly uniform $T_{fh}$ repertoire exists among contralateral lymph nodes. Thereby, the uniformity is constituted at early time points and segregates during chronic establishment of EBA. Furthermore it could be shown, that $T_{fh}$ clonotypes of high frequency in germinal centers are also present in the skin of an individual, although this immigration is not different among experimental groups.

**Conclusion:** In immunization induced EBA a divergent picture for the disease-association of the T-lymphocyte receptor$\beta$ repertoire was found. Whereas the $T_{skin}$ repertoire does not show a specific shift under autoimmune condition, the $T_{fh}$ repertoire comprises a specific shift in immunization induced EBA. Thereby, the results obtained in this dissertation suggest the highly identical $T_{fh}$ T-lymphocyte receptor$\beta$ clonotypes in germinal centers, which specifically share the V3-segment, as possible causative link for induction of EBA. This data encourages further studies to analyze the effect for the pathogenic development of experimental EBA, by specific depletion of T-lymphocytes that express the T-lymphocyte receptor$\beta$ V3-segment.

## Zusammenfassung

**Hintergrund:** T-Lymphozyten stellen eine heterogene Gruppe an Zellen dar, die durch eine hohe Variabilität des T-Lymphozyten Rezeptors charakterisiert ist. In einer Vielzahl an Studien mit dem Fokus auf Autoimmunität wurde die Veränderung des Repertoires an T-Lymphozyten-Rezeptoren untersucht. Dabei zeigten einige Studien krankheitsspezifische Unterschiede im Repertoire der T-Lymphozyten-Rezeptoren, wohingegen in anderen Studien keine Unterschiede nachweisbar waren. In der Literatur sind für das immunisierungs-basierte Modell der dermalen Autoimmunerkrankung Epidermolysis bullosa acquisita (EBA) die zwei obligatorischen T-Lymphozyten Populationen der Haut-immigrierenden T-Lymphozyten ($T_{Haut}$) und der Keimzentrums-immigrierenden follikulären T-Helferzellen ($T_{fh}$) beschrieben. Für die beiden Populationen der $T_{Haut}$ und $T_{fh}$ ist allerdings eine spezifische Veränderung des T-Lymphozyten-Rezeptor Repertoires in der immunisierungs basierten EBA nicht bekannt. Daher befasst sich diese Dissertation mit der Frage, ob das T-Lymphozyten-Rezeptor$\beta$ Repertoire der $T_{Haut}$ und $T_{fh}$ in der immunisierungs basierten EBA verändert ist und ob es zu einer Überlappung der Populationen innerhalb von Individuen kommt.

**Ergebnisse:** Die Analyse des T-Lymphozyten-Rezeptor$\beta$ Repertoires der $T_{Haut}$ hat keine charakteristische Veränderung der Haut-immigrierenden T-Lymphozyten zwischen den experimentellen Gruppen ergeben. Bei der Untersuchung der $T_{fh}$ hingegen zeigte sich, dass unter Autoimmunbedingungen T-Lymphozyten-Rezeptor$\beta$ Klonotypen spezifisch zwischen einzenen Individuen akkumulieren und dabei vermehrt das T-Lymphozyten-Rezeptor$\beta$ V3-Segment aufweisen. Zusätzlich konnte beweisen werden, dass idente $T_{fh}$ Klonotypen zwischen allen untersuchten Individuen existieren, die dabei ebenfalls vermehrt das V3-Segment besitzen. Bei der Untersuchung von $T_{fh}$ innerhalb von Individuen konnte festgestellt werden, dass das $T_{fh}$ Repertoire zwischen Keimzentren in kontralateralen Lymphknoten unter Autoimmunbedingungen hoch ident ist. Diese hohe Identität wird dabei zu frühen Krankheitszeitpunkten etabliert und seggregiert während der chronischen Entwicklung der immunisierungs-basierten EBA. Zusätzlich konnte ein Zusammenhang zwischen dem Repertoire der $T_{fh}$ und der $T_{Haut}$ gefunden werden. Hierbei stellte sich heraus, dass hoch frequente $T_{fh}$ Klonotypen in der Haut vorhanden sind, es dabei allerdings keine Unterschiede zwischen den experimentellen Gruppen gibt.

**Fazit:** In der immunisierungs-basierten EBA hat sich ein uneinheitliches Bild zu krankheitsspezifischen Unterschieden im T-Lymphozyten-Rezeptor$\beta$ Repertoire ergeben. Auf der einen Seite

zeigt das Repertoire der $T_{Haut}$ keine Veränderungen unter Autoimmunbedingungen. Hingegen auf der anderen Seite konnte für das Repertoire der $T_{fh}$ eine deutliche Veränderung unter Autoimmunbedingungen gezeigt werden. Die in dieser Dissertation erhobenen Daten deuten daher an, dass hoch idente $T_{fh}$ T-Lymphozyten-Rezeptor$\beta$ Klonotypen, die das T-Lymphozyten-Rezeptor$\beta$ V3-Segment aufweisen, eine mögliche kausale Ursache für die Krankheitsentstehung im immunisierungs-basierten Modell der EBA sind. Auf Grundlage dieser Daten kann in weiterführenden Studien der Einfluss einer spezifischen Depletion von V3-Segment-exprimierenden T-Lymphozyten auf die pathogene Entwicklung der experimentellen EBA untersucht werden.

# 1 Introduction

## 1.1 The immune system

The immune system preserves the host's integrity by a collective interplay of individual components and protects the body against biologically different pathogens and abnormal cell growth. During evolution, a diverse framework including organs, anatomical epithelial- and endothelial barriers, a highly specialized cellular compartment, alongside a variety of soluble or humoral components was developed. Jointly, components of the immune system fight against invading pathogens with the aim of clearance. Thereby mechanisms of the immune system must be specifically directed against foreign targets and highly adjustable. Therefore, the key mechanism of immune responses is a precise regulation between broad recognition of pathogens and a narrow targeting of exogenous structures. Otherwise pathogens might remain unrecognized or loss of self-tolerance might lead to unwanted harm or autoimmunity (Murphy and Weaver, 2016).

### 1.1.1 Innate immune system

Anatomical barriers, like the skin, display the primary line of protection against infective invasion. As a result, the physical shielding prevents an exposure of the host to environmental factors and pathogens. Upon bypassing, invading pathogens are initially sensed and detected by the innate immune system, mediating an autonomous and pathogen-unspecific response. Here the humoral compartments of the complement system, a multilateral protein framework, directly fight against invading pathogens and induce inflammation by a multitude of degradation and signaling processes. Inflammation-sensitive cells, like macrophages and neutrophils, are attracted to the site of invasion. They sense via innate pattern recognition receptors, specific for pathogens or cellular damage. Upon pattern recognition, innate immune cells are activated and begin to directly eliminate the invading pathogens by phagocytosis. In addition, inflammation is initialized and amplified by releasing pro-inflammatory cytokines and cell attracting chemokines. These processes are initiated nearly instantaneously after barrier-breaching and last for days. However, the innate immune system relies on the recognition of consistent pattern and does not contain an intrinsic mechanism to individually adapt to the invading pathogen (Abbas et al., 2017).

### 1.1.2 Adaptive immune system

Time delayed, the pathogen-specific response of the adaptive immune system is initiated by tissue resident dendritic cells (DC), interlinking both, the innate and adaptive system. This particular cell

type functions as an antigen presenting cell (APC) and ingests extracellular content via phagocytosis. Intracellularly, DCs process and fragment incorporated proteins, load peptides (called antigens) onto major histocompatibility (MHC) complex molecules and transport the antigen-loaded MHC complex to the cytoplasmic membrane. In parallel, DCs migrate to the compartment-draining lymph node via the lymphatic system. After entering, DCs localize in the paracortical area of the lymph node, where the antigen-loaded MHC molecules are presented to T-lymphocytes. After recognizing an antigen via the T-lymphocyte receptor, T-lymphocytes are activated and differentiate. Depending on the differentiation, T-lymphocytes are able to fulfill extensive effector-functions like activation of macrophages and cognate B-lymphocyte help. In parallel to T-lymphocytes, B-lymphocytes are activated by endogenous recognition of soluble antigens via the B-lymphocyte receptor. Upon activation, B-lymphocytes constitute the formation of germinal centers (GC), where they undergo maturation and differentiate into antibody-producing long-lived plasma cells. As final result of the germinal center reaction, plasma cells emerge and secret high affine antibodies. During initiation of the adaptive immune response, T- and B-lymphocytes mediate, in contrast to the innate immune system, a pathogen-tailored reaction over days and weeks. This enables a specific control and clearance of a multitude pathogen-range. Following both processes, the immune response is attenuated. Thereby T- and B-lymphocytes establish an immunological memory, enabling a faster and more effective secondary response. Despite the distinction, both the innate and adaptive immune system are mutually dependent and effect each other reciprocally to ensure the comprehensive functionality (Murphy and Weaver, 2016).

## 1.2 The T-lymphocyte

T-lymphocytes display a very heterogeneous cellular population, capable to fulfill multitude functionalities like various effector and regulatory functions (Gong et al., 2014). Thereby the heterogeneity is not only based on different functionalities, it is mainly based on the highly variable T-lymphocyte receptor. This receptor is individually generated during cellular maturation and constructed as a heterodimer, consisting of an $\alpha$- and a $\beta$-chain (Fig. 1.1).

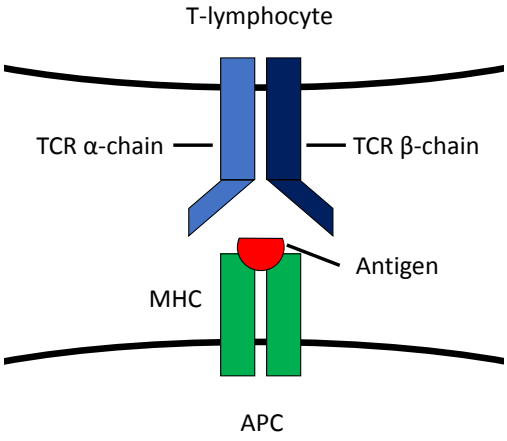


**Figure 1.1: Schematic structure of the T-lymphocyte receptor - MHC interaction.** The T-lymphocyte receptor is found on the surface of T-lymphocytes and consists of an $\alpha$- and a $\beta$-chain. It is capable to recognizes antigens presented via the MHC complex on the surface of APCs.

### 1.2.1 Development of T-lymphocytes

As part of the lymphoid linage, T-lymphocytes arise in the bone marrow from hematopoietic stem cells. As cellular progenitors, not expressing the T-lymphocyte receptor, they migrate into the thymus, the site of primary T-lymphocyte maturation. During the process of thymopoiesis, T-lymphocytes first initialize the expression of the T-lymphocyte receptor$\beta$ chain, which consists of different genetic alleles. For mice, 36 variable- (V), 2 diversity- (D), 14 joining- (J) and 2 constant-segments (C) are encoded genetically in the $\beta$-chain locus. Whereof, pseudogene-substracted, 22 V-, 2 D-, 11 J- and 2 C-segments are functional (Bosc et al., 2005b). During expression of the $\beta$-chain, the process of somatic recombination is initiated, causing a random rearrangement of somatic DNA fragments (Fig. 1.2 A). In an initial process, a D-segment and a J-segment are recombined via RAG enzymes, resulting in a DJ-segment (Sadofsky, 2001). In two consecutive steps, a V-segment and afterwards a C-segment are RAG-mediated attached to the DJ-segment. This results in a huge variety of different possibilities, in which the VDJC-segments of the T-lymphocyte receptor$\beta$ chain are recombinable (Sadofsky, 2001; Schatz and Spanopoulou, 2005). During this rearrangement however, also random nucleotides are additionally integrated between the VD- and DJ-segment, further increasing variability of the rearranged $\beta$-chain (Fig. 1.2 B) (Komori et al., 1993; Gilfillan et al., 1993). Thus, downstream the MHC interacting complementarity-determining region (CDR) 1 and 2 (Marrack et al., 2008), the hyper-variable CDR3 region is located, spanning from the downstream V-segment to the upstream J-segment (Yassai et al., 2009). The random

rearrangement holds the possibility of a defective rearranged $\beta$-chain. Therefore, cells with an out-of-frame or defective reading frame of the rearranged T-lymphocyte receptor$\beta$-chain undergo apoptosis (Dempsey, 2011).

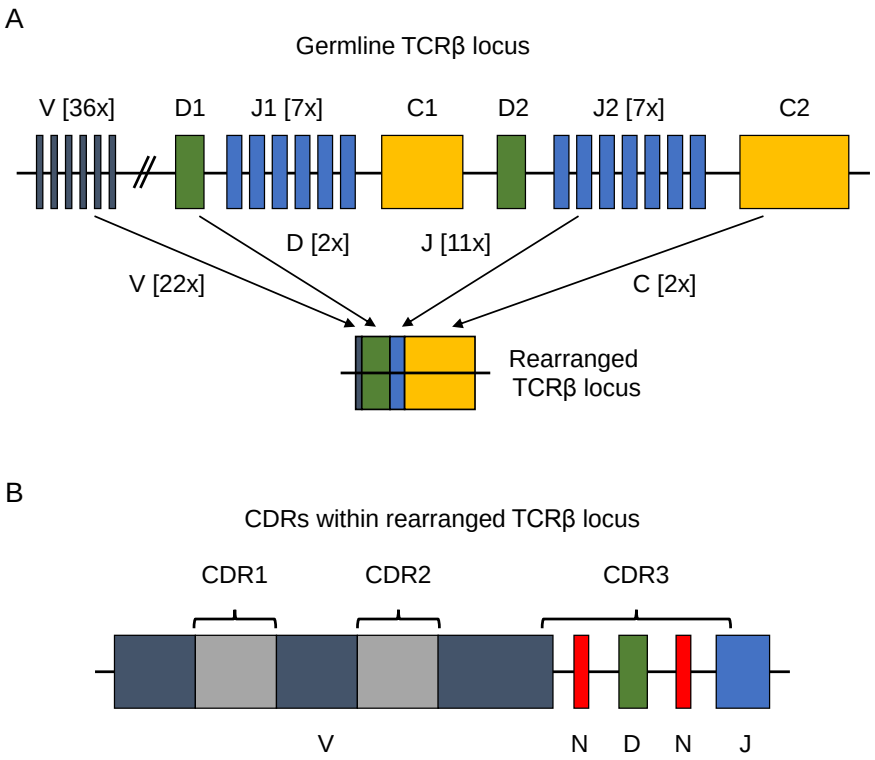


**Figure 1.2: Somatic recombination of the murine T-lymphocyte receptor$\beta$ locus.** A) During T-lymphocyte maturation the germline T-lymphocyte receptor$\beta$ locus is rearranged by combination of a single variable- (V), diversity- (D), joining- (J) and constant-segment (C) (Giudicelli et al., 2005; Lefranc et al., 2004). While this random process, 22 V-, 2 D-, 11 J- and 2 C-segment are composed individually on cellular level. B) Additionally, random nucleotides (N) are integrated between the VD- and DJ-segment, further diversifying the CDR3 region (Komori et al., 1993; Gilfillan et al., 1993). Figure adapted from Laydon et al. (2015).

After expression of the T-lymphocyte receptor$\beta$ chain, the maturation of T-lymphocytes is continued by rearrangement of the T-lymphocyte receptor$\alpha$ chain. Likewise, the $\beta$-chain, the $\alpha$-chain is generated by somatic recombination, although lacking a D-segment in the rearranged $\alpha$-chain (Krangel et al., 2004; Krangel, 2009). For mice, 98 V-, 60 J- and 1 C-segment are genetically encoded in the $\alpha$-chain locus, of which 84 V-, 38 J- and 1 C-segments are functional (Bosc et al., 2005a). Also the $\alpha$-chain consists of the CDR 1 and 2, as well as the hyper-variable CDR3 region.

Co-expression of the $\alpha/\beta$-chain completes the T-lymphocyte receptor, harboring a total of six CDRs. Whereby both CDR1 and 2 mediate binding to MHC complexes. The combined tertiary structure of the $\alpha$- and $\beta$-chains CDR3 is capable to interact with antigens in the MHC cleft, making it the hallmark-definition of a T-lymphocyte $\alpha/\beta$ clonotype. Thereby, theoretical estimations assume that $10^{20}$ T-lymphocyte clonotypes may possibly rearranged, although it is expected that only $5x10^{6}$ different clonotypes are simultaneously present in mice (Zarnitsyna et al., 2013; Lythe et al., 2016). This difference is based on positive and negative selection, eliminating the majority of T-lymphocyte clonotypes due to binding abilities (Starr et al., 2003; Klein et al., 2014). Selection is initiated by co-expression of both T-lymphocyte co-receptors CD4 and CD8, resulting in a double positive state (Klein et al., 2014). At this time point, T-lymphocytes are positively selected for their capability to bind endogenous MHC class I or II molecules. Here, weak or a too strong binding of the CDR1 and 2 regions to MHC molecules results in cellular apoptosis. Additionally, T-lymphocytes undergo a linage commitment during positive selection. This results in the single positive state of $CD4^+$ T-lymphocytes, specific for MHC class II, or $CD8^+$ T-lymphocytes, specific for MHC class I. Subsequently, linage specific T-lymphocytes undergo negative selection, to maintain self-tolerance. For that, endogenous proteins are expressed, processed and loaded onto MHC class I and II molecules. T-lymphocytes then bind the auto-antigen loaded MHC molecules and only T-lymphocytes, expressing self-tolerant T-lymphocyte receptors, survive the selection and are capable to emigrate out of the thymus. These naïve T-lymphocytes then migrate via the blood into secondary lymphatic organs to encounter antigen-presentation via APCs, in order to differentiate into effector T-lymphocytes.

### 1.2.2 Activation and differentiation of $CD4^+$ T-lymphocyte subsets

After leaving the thymus, naïve $CD4^+$ T-lymphocytes circulate via the bloodstream and constantly enter secondary lymphatic organs, like lymph nodes, searching for foreign antigens (Kaune et al., 2015). After entering the T-lymphocyte zone (TCZ) in the paracortical area of the lymph node, $CD4^+$ T-lymphocytes permanently interact with DCs via a physical connection between the T-lymphocyte receptor and the MHC class II. Thereby, they scan presented antigens via the T-lymphocyte receptor CDR3 antigen binding site (Rudensky et al., 1991). In the vast majority of interactions no activation of $CD4^+$ T-lymphocytes is initiate. However upon recognizing their foreign antigen, an enhanced and serial interaction with the DC results in a stimulatory signal (Friedl and Gunzer, 2001; Huang et al., 2010). Based on this intense and reoccurring interplay, $CD4^+$ T-lymphocytes are activated. Thereby, co-stimulatory signaling between T-lymphocytes

and DCs is required for activation, otherwise an inactive anergic state of $CD4^+$ T-lymphocytes is induced (Gimmi et al., 1993). Thus, signaling between the most important interactions CD28-CD80/CD86 or ICOS-ICOSL represents the keystone in functional T-lymphocyte activation (June et al., 1994; Hutloff et al., 1999; Sharpe and Abbas, 2006). During activation, clonal expansion via proliferation of antigen-specific $CD4^+$ T-lymphocytes is initiated by the T-lymphocyte growth factor IL2 (Morgan et al., 1976). Thereby, intensity of both signals, the T-lymphocyte receptor stimulation and co-stimulation, determine the rate of clonal expansion (Jenkins et al., 1991).

Following activation, the differentiation of $CD4^+$ T-lymphocytes into T-lymphocyte helper ($T_H$) subsets is initialized, such as $T_H1$, $T_H2$, $T_H9$, $T_H17$, $T_H21$, $T_{reg}$ and $T_{fh}$ (Fig. 1.3). Thereby, each individual subset mediates an unique and crucial functionality for the adaptive immune response.

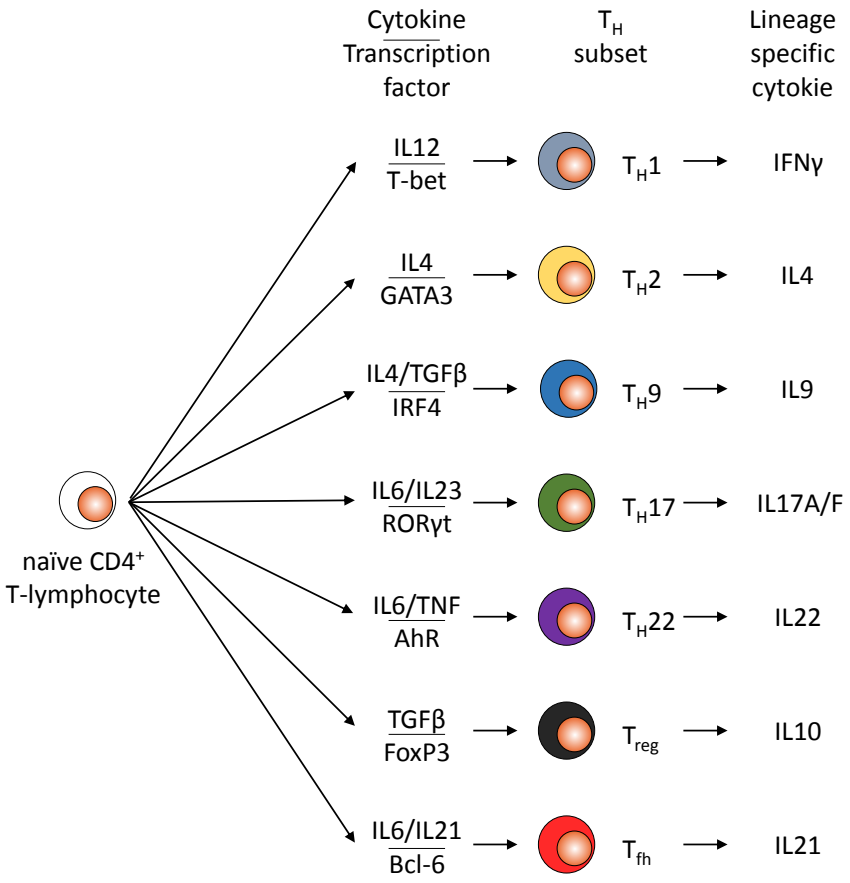


**Figure 1.3: Differentiation of $CD4^+$ T-lymphocytes into $T_H$ subsets.** Cytokine depended differentiation of naïve $CD4^+$ T-lymphocytes into $T_H$ subsets. Thereby, each subset is characterized by a lineage-specific transcription factor and cytokine secretion (Tripathi and Lahesmaa, 2014).

As one factor for $T_H$ differentiation, the cytokine milieu during activation was described (O'Garra and Murphy, 1996). Thereby, the differentiation of each $T_H$ subset is induced by a specific cytokine

or cytokine composition. As second factor for $T_H$ differentiation, the T-lymphocyte receptor signaling strength during the T-lymphocyte receptor - MHC class II interaction was identified (Tubo et al., 2013). Thus, the differentiation of $T_H$ subsets is based on two factors, which affect the fate of differentiation: cytokine milieu and T-lymphocyte receptor signaling strength.

In this dissertation, the focus will be specifically on $T_H$ subsets, of which a T-lymphocyte receptor signaling strength was determined and which were already shown to be involved in the experimental model of the autoimmune disease Epidermolysis Bullosa Acquisita. Therefore, germinal center immigrating $T_{fh}$ and the skin immigrating $T_H1$, $T_H2$ and $T_{reg}$, which are collectively considered as $T_{skin}$, are analyzed. In the following, the essential functions of $T_{fh}$ and $T_{skin}$ are explained in detail.

### 1.2.3 Functional characteristics of $T_{fh}$

Upon initial activation in the TCZ of lymph nodes via DCs, the differentiation of $T_{fh}$ is initiated by IL6 and IL21 (Nurieva et al., 2008). Both cytokines jointly initialize expression of the $T_{fh}$ specific transcription factor Bcl-6, which was shown to be obligatory for differentiation and actively suppresses differentiation into other subsets (Yu et al., 2009; Nurieva et al., 2009; Johnston et al., 2009). In parallel to Bcl-6, the chemokine receptor CxCR5 is expressed and mediates chemotaxis towards the cortical B-lymphocyte zone (BCZ) (Crotty, 2014). This migration is induced by B-lymphocytes, which release the cytokine CxCL13, the ligand of CxCR5 (Moser, 2015). At the TCZ-BCZ border, a secondary activation of $T_{fh}$ is mediated by B-lymphocytes presenting their specific antigen via MHC class II and providing the co-stimulatory ICOSL molecule (Xu et al., 2013). During this secondary activation via T-lymphocyte receptor - MHC class II interaction, antigen-specific $T_{fh}$ increase the level of CxCR5 and additionally induce a high expression of PD-1 and ICOS, which leads to a robust establishment of the $T_{fh}$ phenotype (Crotty, 2014). Expressing all three marker at high levels, $T_{fh}$ are able to migrate into the BCZ. Besides cytokines, the T-lymphocyte receptor signaling strength, was evaluated for the $T_{fh}$ differentiation. Thereby, it was shown, that a high to very high signaling strength is essential for their development (Tubo and Jenkins, 2014). Furthermore, this high to very high signaling strength was linked to the ability of $T_{fh}$ to migrate into the BCZ and represents an important check point for robust establishment of the phenotype (Tubo et al., 2013).

After BCZ-entry $T_{fh}$ and B-lymphocytes jointly constitute germinal centers. Here, $T_{fh}$ function as the essential check point for B-lymphocytes during affinity maturation, class switching and

differentiation into long-lived plasma cells. Initially, the release of the $T_{fh}$ signature cytokine IL21 promotes proliferation and differentiation towards plasma cells (Qi, 2016). During this maturation, B-lymphocytes are located in the dark zone (DZ) of the germinal center and undergo affinity maturation, including a somatic alteration of the B-lymphocyte receptor DNA. After completing, a transition into the light zone (LZ) is conducted and somatically altered B-lymphocytes compete for positive selection via $T_{fh}$ (Qi, 2016). This selection is a three-stage process: (I) a $T_{fh}$ has to recognize the MHC class II presented antigen on the surface of a B-lymphocyte, (II) a B-lymphocyte mediated co-stimulation via ICOS-ICOSL has to exceed a certain threshold, which leads to (III) an externalization of CD154 on the surface of $T_{fh}$ (Liu et al., 2015). This enables the necessary CD40/CD154 interaction for positive B-lymphocyte selection (Liu et al., 2015). Thereby, the presentation of an unrecognized antigen or a too low ICOSL-ICOS interaction prevents the CD40/CD154 signaling, which was shown to be the crucial step for B-lymphocyte selection (Kawabe et al., 1994). Based on this process $T_{fh}$ select between functional and non-function alteration of the B-lymphocyte receptor (Crotty, 2014). Alongside selection, $T_{fh}$ also direct the maturation of B-lymphocytes via the cytokine milieu, which leads to shifting antibody sub-classes (Stavnezer et al., 2008). During germinal center reaction, the process of DZ-entry, somatic DNA alteration, LZ transition and $T_{fh}$ mediated selection is a reoccurring process. It is repeated until long-lived plasma cells are selected via $T_{fh}$ and leave the germinal center to secrete high affine antibodies. Thus, $T_{fh}$ directly mediate the B-lymphocyte maturation in germinal centers of lymph nodes by functioning as an indispensable check point.

### 1.2.4 Functional characteristics of $T_{skin}$

$T_{skin}$ are different from $T_{fh}$ since they leave lymph nodes after activation and migrate into peripheral tissues.

#### 1.2.4.1 $T_H1$

$T_H1$ are activated by an antigen encounter in the TCZ of a lymph node. After the initial activation via T-lymphocyte receptor - MHC class II interaction, an IL2 and IL12 milieu directs the differentiation towards $T_H1$ cells. Thereby, IL12 mediates an early expression of IFN$\gamma$ and stimulates expression of the $T_H1$ key transcription factor T-bet (Szabo et al., 2000; Tripathi and Lahesmaa, 2014). In parallel to the $T_H1$ fate decision, also an active inhibition of differentiation towards other $T_H$ subtypes is initiated via IL12 (Kaplan et al., 1996). As secondary determinator for differentiation the T-lymphocyte receptor signaling strength was determined. Thereby the differentiation towards $T_H1$ requires a low to medium signaling strength (Tubo et al., 2013; Tubo and Jenkins,

2014). During further differentiation, $T_H1$ cells up-regulate necessary expression of cytokines and receptors to conduct effector-functions in peripheral tissues. These include expression of the pro-inflammatory signature cytokine IFN$\gamma$. Furthermore, the chemokine receptors CxCR3 and CCR5 are expressed, which specifically direct lymphocyte trafficking into inflamed tissues (Groom and Luster, 2011).

After leaving the lymph node and extravasation into peripheral tissues such as the skin, $T_H1$ cells fulfill their effector-function by constituting a pro-inflammatory IFN$\gamma$ milieu. Thereby, they are crucial for the clearance of intracellular pathogens by stimulating classical activation of macrophages, to enhance their phagocytosis and intracellular degradation of microorganisms (Nathan et al., 1983). Consequently, $T_H1$ are the main initiators of cell-mediate phagocytosis in peripheral tissues and thereby conduct to clearance.

#### 1.2.4.2 $T_H2$

After activation in the TCZ of a lymph node, the IL4-mediated differentiation towards $T_H2$ is initiated. Thereby, signaling of the IL4 receptor was found to initiate and regulate expression of the $T_H2$ key transcription factor GATA3 (Ouyang et al., 1998; Farrar et al., 2001). By expressing GATA3, the fate decision towards $T_H2$ is initiated and the transcription factor intrinsically inhibits differentiation towards other $T_H$ subtypes (Ouyang et al., 1998; Zhu et al., 2006). In parallel to the cytokine-initiated differentiation, T-lymphocyte receptor signaling strength necessary for $T_H2$ was assessed. Thereby it was found, that $T_H2$ differentiation is initiated by a weak signaling strength, below the level necessary for $T_H1$ differentiation (Tubo et al., 2013; Tubo and Jenkins, 2014; van Panhuys, 2016). Throughout further differentiation processes, the endogenous transcription of the anti-inflammatory signature cytokine IL4 is initiated (Murphy and Reiner, 2002).

$T_H2$ fulfill their effector-function in tissues and participate in an immunological response to extracellular parasites like helminths. Furthermore, by constituting an anti-inflammatory IL4 milieu they are able to alternatively activate macrophages and thereby induce tissue repair (Zhu, 2015).

#### 1.2.4.3 $T_{reg}$

Natural $T_{reg}$ originated in the thymus and, upon an antigen encounter, inducible $T_{reg}$ are activated via the cytokine TGF$\beta$. The signaling of the TGF$\beta$ receptor was linked to expression of the $T_{reg}$ key transcription factor FoxP3 (Chen et al., 2003; Selvaraj and Geiger, 2007). Thereby expression of FoxP3 was also shown to be necessary and sufficient for $T_{reg}$ induction (Ziegler, 2006). Although, the importance of FoxP3 for the $T_{reg}$ phenotype was demonstrated, FoxP3 was shown to be not constitutively expressed (Ziegler, 2006). However, expression of the signature cytokine IL10 does

not correlate with the expression status of FoxP3 (Ng et al., 2013). Unlike $T_H1$ and $T_H2$, a specific T-lymphocyte receptor signaling strength, necessary for the differentiation towards $T_{reg}$ is unknown.

The effector-function of $T_{reg}$ in peripheral tissues is control of the immune response to foreign and self antigens. Thereby, secretion of the anti-inflammatory IL10 is described to modulate an immune response by attenuating a pro-inflammatory milieu (Jankovic et al., 2010). Additionally, $T_{reg}$ are able to reduce the expression of co-stimulatory molecules on APCs and thereby are able to reduce activation and differentiation of T-lymphocytes during immune reactions (Grant et al., 2015).

## 1.3 The Epidermolysis bullosa acquisita

In healthy organisms, the host's integrity is preserved by a state in which the immune system is tolerant to auto-antigens. If this tolerance is defective or resolved, the immune system begins to target host's tissues, resulting in the state of autoimmunity. Although, the fundamental mechanism causing autoimmunity is unknown yet, auto-reactive T-lymphocytes are seen as the major mediator (Dornmair et al., 2003; Pilli et al., 2017). As described in Chapt. 1.2.1 the key mechanism to preserve tolerance is the negative selection during thymopoiesis. Thereby, this process is based on decision between a restrict deletion of possible auto-reactive T-lymphocytes and an impairment of immune reaction against pathogens by too strict deletion. Thus, a low number of auto-reactive T-lymphocytes is seen as physiological and does not automatically result in an autoimmune disease (Murphy and Weaver, 2016). Rather, it is though that an interplay of genetic predisposition, environmental factors and infections cause the break of tolerance to auto-antigens (Vojdani et al., 2014; Ceccarelli et al., 2016; Jörg et al., 2016).

In general, autoimmune diseases can be classified into two groups: (I) T-lymphocyte-mediated and (II) T- and B-lymphocyte-mediated autoimmune diseases. Thereby, the auto-antibody mediated autoimmune diseases Epidermolysis bullosa acquisita (EBA) represents an example for a T- and B-lymphocyte-mediated disease (Mihai and Sitaru, 2007; Kasperkiewicz et al., 2016).

The human EBA is a chronic autoimmune skin blistering disease caused by auto-antibodies targeting the non-collagenous domain 1 (NC1) of type VII collagen (COL7), present at the dermal-epidermal junction (DEJ) of the skin (Woodley et al., 1984; Lapiere et al., 1993). COL7 forms anchoring fibrils and is one essential protein for the integrity of skin, by connecting the dermal and epidermal layer (Pollard et al., 2017). In clinical presentation of EBA, this integrity is disrupted

causing the development of sub-epidermal blisters, leading to erythema and erosions. For studying the underlying pathomechanisms, an experimental EBA model has been developed. Thereby this model represents an ideal way to study $T_{fh}$ and $T_{skin}$ during pathogenesis.

### 1.3.1 Mouse model of immunization induced EBA

In the experimental EBA model, the disease in mice is induced by an injection of the recombinant fragment mCOL7c, derived from the NC1 domain of murine COL7 (Sitaru et al., 2006). By using the strong adjuvant TiterMax, the break of tolerance to mCOL7c is achieved (Bennett et al., 1992). The emergence of clinical symptoms in the immunization induced EBA can be divided into the **induction-phase**, where $T_{fh}$ are activated and migrate into germinal center, and the **effector-phase**, where $T_{skin}$ immigrate into the skin and clinical symptoms emerge.

During the **induction-phase of EBA** (Fig. 1.4 A) the disease is induced by a loss of tolerance to mCOL7c. The initial activation of auto-reactive T-lymphocytes is mediated by DCs (Iwata et al., 2013). Thereby, the MHC class II haplotype H2s, expressed in SJL/J mice, was linked to the pathogenic induction (Ludwig et al., 2011). After initial activation a functional bifurcation of T-lymphocytes is initialized. On the one hand, a differentiation into $T_H1$, polarizing the draining lymph node towards a pro-inflammatory IFN$\gamma$ milieu, was shown to be crucial for EBA induction (Hammers et al., 2011). On the other hand, the differentiation into $T_{fh}$, mandatory for auto-antibody production, is initiated. In parallel to T-lymphocytes, auto-reactive B-lymphocytes are activated and the $T_{fh}$ dependent formation of germinal centers is initialized (Iwata et al., 2013). Thereby, a $CD4^+$ T-lymphocyte depletion was shown to completely abrogate auto-antibody production, whereas $CD8^+$ T-lymphocyte depletion was irrelevant for disease induction (Iwata et al., 2013). During the maturation of B-lymphocytes into plasma cells, an IFN$\gamma$ based shifting of antibody sub-classes was shown towards complement-fixing IgG2b and IgG2c, which are directly linked to the pathogenesis (Hammers et al., 2011). Additionally, activation of auto-reactive B-lymphocytes and production of auto-antibodies is concentrated in draining lymph nodes (Kasperkiewicz et al., 2011; Tiburzy et al., 2013).

In the **EBA effector-phase** (Fig. 1.4 B), $T_{skin}$ were identified to contribute during effector-phase. In a study specifically focusing on the EBA effector-phase, a general infiltration of $CD4^+$ T-lymphocytes and a strong up-regulation of IFN$\gamma$ was found in the skin (Bieber et al., 2017b). Thereby, the IFN$\gamma$ expression was attributed to $T_H1$ and shown to exceed $T_H2$ cytokine expres-

sion (Bieber et al., 2017b). Furthermore, by unspecific blocking of T-lymphocyte emigration out of lymph nodes, a relieved disease progression could be achieved (Maass, 2015). Thus, it can be assumed that the presence of $T_{skin}$, whereof especially $T_H1$, contribute to EBA progression. However, the specific role of $T_{reg}$ during the effector-phase was also assessed. Thereby, the depletion of $T_{reg}$ resulted in a worsened phenotype with an increased IFN$\gamma$ expression in wounds (Bieber et al., 2017b). Therefore, it is reasonable that $T_{skin}$ play a substantial role during effector-phase of EBA. Furthermore, it seems necessary for wound formation, that a pro-inflammatory $T_H1$ milieu exceeds the anti-inflammatory $T_H2/T_{reg}$ milieu.

However, the actual formation of sub-epidermal blisters in the skin is induced by auto-antibodies targeting mCOL7 and myeloid cells. Upon deposition of the complement-fixing IgG2b and IgG2c auto-antibodies at the DEJ, the complement system is activated (Sitaru et al., 2006; Mihai et al., 2007). As consequence neutrophils are actively recruited into the skin and they release reactive oxygen species (ROS) in response to the immune complexes (Chiriac et al., 2007; Kasperkiewicz et al., 2012). Ultimately, the released ROS leads to disruption of dermal-epidermal adherence and formation of sub-epidermal blisters, causing erythema and erosions (Shimanovich et al., 2004).

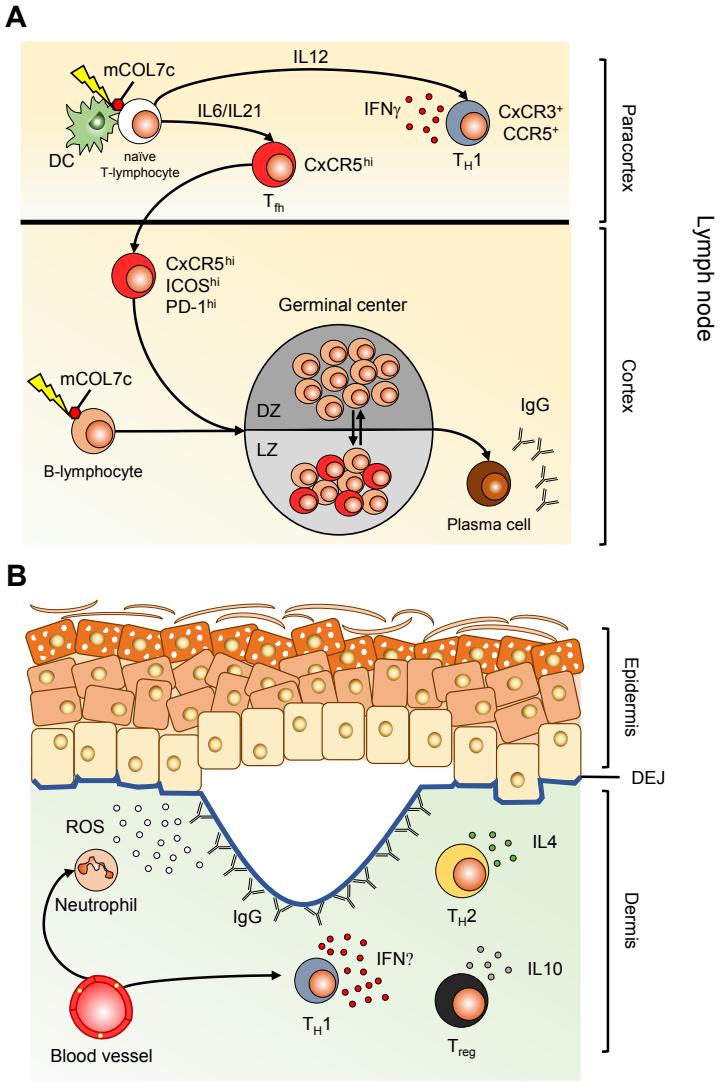


**Figure 1.4: Role of T-lymphocytes in immunization induced EBA.** A) Illustration of the EBA induction-phase in draining lymph nodes. In response to mCOL7c, auto-antibody production in GCs is directed by $T_{fh}$. Parallel, $T_H1$ constitute a pro-inflammatory IFN$\gamma$ milieu. B) Illustration of the EBA effector-phase in the skin. Neutrophils mediate disruption of dermal-epidermal adherence. Of the $T_{skin}$, $T_H1$ constitute a pro-inflammatory IFN$\gamma$ milieu, which exceeds the anti-inflammatory $T_H2/T_{reg}$ milieu.

In summary for immunization induced EBA, $T_{fh}$ within germinal centers were identified to be mandatory for auto-antibody production in draining lymph nodes and $T_{skin}$ are contributors during the effector-phase in the skin. Thereby, for both $T_{fh}$ and $T_{skin}$ only their effector-functions are described in the literature. However, the underlying repertoire of T-lymphocyte receptors is neglected and it is not known, whether this effector-functions are bystander processes or if a specific repertoire of T-lymphocyte receptors is involved in the emergence of EBA. Since a MHC class II restriction

has been demonstrated for immunization induced EBA (Ludwig et al., 2011), it conceivable, that due to this restriction a homogeneous set of T-lymphocyte clonotypes arise among individual mice during thymic selection. Thereby, it is also imaginable, that the set of auto-antigen specific $T_{fh}$ and $T_{skin}$ is homogeneous among individual mice and subsequently identical auto-antigen specific $T_{fh}$ and $T_{skin}$ clonotypes are activated in an autoimmune response against mCOL7c. This assumption is supported by a general MHC-association to autoimmunity (Ridgway and Fathman, 1998; Matzaraki et al., 2017) and a study focusing on the T-lymphocyte receptor$\beta$ repertoire of monozygous twins. In this study it could be shown, that the T-lymphocyte receptor$\beta$ repertoire of twins, sharing identical MHC alleles, is significantly more identical compared to unrelated individuals (Zvyagin et al., 2014). Thus, the MHC class II restriction makes an emergence of identical disease and presumably auto-antigen specific T-lymphocytes under autoimmune condition highly likely and enables the hypothesis, that an identical $T_{fh}$ and $T_{skin}$ T-lymphocyte receptor repertoire is involved in the pathogenic development of immunization induced EBA.

## 1.4 T-lymphocyte receptor repertoire in autoimmune diseases

The T-lymphocyte receptor repertoire has been investigated in several studies, focusing on changes under autoimmune condition. Thereby, it is reported to be a double-edged sword: whereas some studies report a connection between the T-lymphocyte receptor repertoire and autoimmune diseases, other where unable to detect a relation. In the skin related autoimmune disease systemic lupus erythematosus the T-lymphocyte receptor repertoire of skin infiltrating T-lymphocytes is assumed to recognize a restricted set of auto-antigens and is thought to be specifically involved in the dermal disease manifestation (Kita et al., 1998). In contrast, analysis of the T-lymphocyte receptor repertoire in the dermal autoimmune diseases psoriasis and atopic dermatitis showed no specific accumulation and a highly divers repertoire of skin immigrating T-lymphocytes (Harden et al., 2015). Furthermore, also specific characteristics of the T-lymphocytes receptor CDR3 region were assessed in several studies, focusing on skin unrelated autoimmune diseases. Thereby, skewing towards a longer CDR3 region was found under autoimmune condition (Okajima et al., 2009), whereas an other study reported no skewing and an unaffected length of the CDR3 region (Niemi et al., 2015). In addition to the CDR3 length, also the usage of T-lymphocyte receptor V- and J-segments were analyzed. Thereby, the V-segment usage was found to be altered (Kita et al., 1998; Yoshizawa et al., 1999; VanderBorght et al., 2000; Epperson et al., 2001) and also a shift in the J-segment usage was detected (Haegert et al., 1999; Epperson et al., 2001). Also in a combined V-J-segment assessment, a disease-characteristic usage was also found in a study (Clemente et al.,

2013). In contrast to V- and J-segment disease-association, in a skin related autoimmune disease, no preferred usage was observable (Brunner et al., 2017). Thus, a divergent association of the T-lymphocyte receptor repertoire to skin related or autoimmune diseases in general is found in the literature, indicating that an association is a disease specific phenomenon.

Since the T-lymphocyte receptor repertoire in autoimmune diseases is a double-edged sword, the question arose, whether a disease association of the T-lymphocyte receptor repertoire is detectable for the immunization induced mouse model of EBA. In this model, $T_{fh}$ are the checkpoint during maturation of auto-reactive B-lymphocytes and $T_{skin}$ are contributors during the effector-phase in skin. Thus, it is highly interesting to specifically focus on the T-lymphocyte receptor repertoire of those subsets and address the questions, (I) whether either subset shifts under autoimmune condition and (II) if both subsets overlap in an individual? To answer these questions, the T-lymphocyte receptor repertoire of both subsets was determined.

### 1.4.1 Determination of the T-lymphocyte receptor repertoire

To analyze the T-lymphocyte receptor repertoire, a highly sensitive and specific methodology is required. Thereby the level of resolution is the crucial determinator between quantitative and qualitative analysis. Techniques like cloning of individual T-lymphocyte receptors and subsequent individual sequencing, enable a qualitative analysis of the nucleotide and amino acid composition of the CDR3 region, but it is not feasible for a high number of T-lymphocytes (Birkholz et al., 2009). In contrast, techniques like flow cytometry or spectratyping are capable to analyze a multitude number of T-lymphocytes in parallel, but are only able to quantify the T-lymphocyte receptor V- and J-segment content or CDR3 length, lacking detailed information of the CDR3 composition (Pannetier et al., 1993; van den Beemd et al., 2000; Ciupe et al., 2013). Recently, a comprehensive analysis of the T-lymphocyte receptor repertoire was enabled by Next Generation Sequencing (NGS), combining the qualitative analysis of the CDR3 region with a high quantitative throughput (Benichou et al., 2012; Six et al., 2013; Calis and Rosenberg, 2014).

For this dissertation, an analysis of the T-lymphocyte receptor$\beta$ chain was conducted using the Illumina sequencing platform. In principle, the analysis is based on generating millions of DNA fragments spanning the T-lymphocyte receptor$\beta$ CDR3 region and carrying specific adapters at the 3' and 5' end. These DNA fragments are covalently bound to a glass-surface and sequenced simultaneously. During sequencing, an individual complementary nucleotide, carrying a defined fluorophore, is enzymatically attached to the DNA fragment. In an alternating processes the incorporated nucleotide is identified via emission of the fluorophore. This process, called sequencing-by-synthesis,

facilitates high sensitivity and a high signal-to-noise-ratio (Fuller et al., 2009). As output, the Illumina platform typically provides millions to billions of sequences, called reads, associated with individual scores, which indicate sequencing quality (Ewing and Green, 1998). Thereby, each read corresponds to an individual DNA fragment and represents a single information of a T-lymphocyte receptor$\beta$ CDR3 region. Based on this enormous dataset, a simultaneous consideration of quantitative and qualitative aspects of T-lymphocyte receptor$\beta$ clonotypes can be achieve. Therefore, NGS represents the ideal technique to analyze the T-lymphocyte receptor$\beta$ repertoire of $T_{fh}$ and $T_{skin}$ in immunization induced EBA.

## 1.5 Aim of the study

T-lymphocytes are a heterogeneous population, which is capable to fulfill different effector-functions. Thereby, the heterogeneity is based on the highly variable T-lymphocyte receptor, representing an individual characteristic of each T-lymphocyte. In autoimmune diseases, T-lymphocytes are seen as mediator for the break of tolerance and trigger for disease induction. In comprehensive studies, focusing on the repertoire of T-lymphocyte receptors under autoimmune condition, a varying picture between association to the disease and disease-independence is published in the literature. In immunization induced EBA, an indispensable involvement of $T_{fh}$ during induction-phase and $T_{skin}$ during the effector-phase was shown. Although their effector-functions have been addressed in the past, nothing is known about the T-lymphocyte receptor repertoire in experimental EBA. Therefore, the present study focuses on analysis of the T-lymphocyte receptor$\beta$ repertoire and addresses the following questions:

I. Does the T-lymphocyte receptor$\beta$ repertoire of $T_{skin}$ and $T_{fh}$ shifts during EBA?

   - Do identical T-lymphocyte receptor$\beta$ clonotypes accumulate among individual mice in skin lesions?
   - Do identical T-lymphocyte receptor$\beta$ clonotypes accumulate among individual mice in germinal centers?

II. Do $T_{fh}$ and $T_{skin}$ overlap within an individual?

   - Is the T-lymphocyte receptor$\beta$ repertoire of $T_{fh}$ identical among germinal centers of the left and right draining lymph node?
   - Is the T-lymphocyte receptor$\beta$ repertoire of $T_{fh}$ and $T_{skin}$ identical?

# 2 Materials and Methods

## 2.1 Materials

### 2.1.1 Laboratory animals

10 to 12 week old female SJL/J mice were purchased from Charles River Laboratory (Sulzfeld, Germany) and held under specific-pathogen-free (SPF) conditions in the animal facility of the University of Lübeck (Gemeinsame Tierhaltung der Universität zu Lübeck). Animal housing was conducted under the terms of the German animal welfare act. Conditions included a constant day/night rhythm and an *ad libitum* provision of water and chow.

### 2.1.2 Reagents and kits

Experiments were conducted using reagents and kits mentioned in Tab. 2.1.

**Table 2.1: Utilized reagents and kits.**

| Name | Manufacturer |
|---|---|
| Acetic acid 100% | Carl Roth GmbH & Co. KG, Germany |
| Acetone 99.8% | Carl Roth GmbH & Co. KG, Germany |
| Agarose peqGOLD | VWR International GmbH, Germany |
| Aquatex | Merck KGaA, Germany |
| Bepanthen Augen- und Nasensalbe | Bayer AG, Germany |
| Bovine Serum Albumin (IgG-free) | Sigma-Aldrich Inc., USA |
| Bromophenol Blue | Sigma-Aldrich Inc., USA |
| Chloroform 99% | Carl Roth GmbH & Co. KG, Germany |
| Coomassie Brilliant Blue | Sigma-Aldrich Inc., USA |
| 4',6-Diamidino-2-Phenylindole (DAPI) | Thermo Fisher Scientific, USA |
| N,N-Dimethylformamide | Sigma-Aldrich Inc., USA |
| 1,4-Dithiothreitol (DTT) | Sigma-Aldrich Inc., USA |
| 5x DNA Loading Buffer Blue | Bioline Reagents, UK |
| DNase I | Thermo Fisher Scientific, USA |
| dNTP Mix 10mM each | Thermo Fisher Scientific, USA |
| Entellan | Merck KGaA, Germany |

| | |
|---|---|
| Eosin-G 1% | Merck KGaA, Germany |
| Ethanol 99.8% | Carl Roth GmbH & Co. KG, Germany |
| ExtrAvidin Alkaline Phosphatase | Sigma-Aldrich Inc., USA |
| ExtrAvidin Peroxidase | Sigma-Aldrich Inc., USA |
| Fast Blue RR Salt | Sigma-Aldrich Inc., USA |
| Fast Red RR Salt | Sigma-Aldrich Inc., USA |
| Formaldehyde 37% | Merck KGaA, Germany |
| Formamide 99% | Sigma-Aldrich Inc., USA |
| Glycerol 99.5% | Sigma-Aldrich Inc., USA |
| Hematoxylin Solution (Mayer's) | Merck KGaA, Germany |
| Hydrochloric acid 37% | Sigma-Aldrich Inc., USA |
| HyperLadder 100bp | Bioline Reagents, UK |
| immunPREP RNA Mini Kit | Analytik Jena, Germany |
| Isopropanol 99.95% | Carl Roth GmbH & Co. KG, Germany |
| Ketanest S (25mg/ml) | Pfizer Inc., USA |
| Liquid DAB+ Substrate | Agilent Technologies, Inc., USA |
| 2-Mercaptoethanol (98%) | Sigma-Aldrich Inc., USA |
| Methanol 99.9% | Carl Roth GmbH & Co. KG, Germany |
| Midi Gel Adapter | Thermo Fisher Scientific, USA |
| MiSeq Reagent Kit v2 300 cycle | Illumina INC, USA |
| Mowiol 4-88 | Sigma-Aldrich Inc., USA |
| MTBIvc reagent system (i1-18) | iRepertoire Inc., USA |
| Multiplex PCR Kit | QIAGEN N.V., Netherlands |
| Naphthol AS-MX phosphate | Sigma-Aldrich Inc., USA |
| NuPAGE Antioxidant | Thermo Fisher Scientific, USA |
| NuPAGE 4-12% Bis-Tris Protein Gel | Thermo Fisher Scientific, USA |
| NuPAGE MES SDS Running Buffer | Thermo Fisher Scientific, USA |
| OneStep RT-PCR Kit | QIAGEN N.V., Netherlands |
| PageRuler Prestained Protein Ladder | Thermo Fisher Scientific, USA |
| Paraformaldehyde | Carl Roth GmbH & Co. KG, Germany |
| PerfeCTa NGS Quantification Kit | Quantabio, USA |
| PhiX Control v3 | Illumina INC, USA |

| | |
|---|---|
| Propidium Iodide staining Solution | Becton, Dickinson and Company, USA |
| QIAquick Gel Extraction Kit | QIAGEN N.V., Netherlands |
| QuantiFluor RNA System | Promega Corporation, USA |
| Rompun (20mg/ml Xylazine) | Bayer Vital GmbH, Germany |
| Roti-GelStain | Carl Roth GmbH & Co. KG, Germany |
| Sodium azide ($NaN_3$) | Sigma-Aldrich Inc., USA |
| Sodium chloride (NaCl) | Merck KGaA, Germany |
| Sodium chloride solution 0.9% | Braun AG, Germany |
| Sodium dodecyl sulfate (SDS) | Thermo Fisher Scientific, USA |
| Sodium hydroxide (NaOH) | Carl Roth GmbH & Co. KG, Germany |
| SYBR Green PCR Master Mix | Thermo Fisher Scientific, USA |
| TaqMan Universal PCR Master Mix | Thermo Fisher Scientific, USA |
| Tissue freezing medium | Leica Instruments GmbH, Germany |
| TiterMax classic | Sigma-Aldrich Inc., USA |
| Tris base | Sigma-Aldrich Inc., USA |
| Trypan blue 0.4% | Thermo Fisher Scientific, USA |
| Tween 20 | Serva Electrophoresis GmbH, Germany |
| UltraPure Glycine | Thermo Fisher Scientific, USA |
| Xylene 99% | Merck KGaA, Germany |

### 2.1.3 Solutions and buffer

The solutions and buffer mentioned in Tab. 2.2 were experimentally used.

**Table 2.2: Utilized solutions and buffer.**

| **Name** | **Composition** |
|---|---|
| Anesthetic solution | 100mg/kg Ketanest S, 10mg/kg Rompun, Sodium chloride solution 0.9% |
| APAAP-substrate | 0.5mM Naphthol AS-MX phosphate, 250mM N,N-Dimethylformamide, 1mM Levamisole, Tris-buffer 0.1M |
| Coomassie Blue destaining solution | 10% v/v acetic acid, 40% v/v methanol, laboratory grade $H_2O$ |

| | |
|---|---|
| Coomassie Blue staining solution | 0.2% w/v Coomassie Brilliant Blue, 10% v/v acetic acid, 40% v/v methanol, laboratory grade $H_2O$ |
| DAPI staining solution | 3.5mM DAPI, PBS |
| FACS Buffer | 0.5mM EDTA, 0.5% w/v BSA (IgG-free), PBS |
| Fast Blue staining solution | 3mM Fast Blue RR Salt, APAAP-substrate |
| Fast Red staining solution | 1.5mM Fast Red RR Salt, APAAP-substrate |
| IHC antibody dilution buffer | 1% w/v BSA (IgG-free), 0.5% w/v $NaN_3$, PBS |
| Immunofluorescence blocking solution | 0.5% w/v BSA (IgG-free), PBS |
| Laemmli Buffer | 25mM Tris, 192mM glycine, 0.1% w/v SDS, 0.01% w/v Bromophenol blue, laboratory grade $H_2O$ |
| Library dilution buffer | 10 mM Tris, 0.1% Tween 20, laboratory grade $H_2O$, pH adjusted to 8.5 |
| NaOH (1M) | 1M NaOH, laboratory grade $H_2O$ |
| PAGE running buffer | 5% v/v NuPAGE MES SDS Running Buffer, 0.25% NuPAGE Antioxidant (only in cathodic-buffer-chamber), laboratory grade $H_2O$ |
| PAGE sample dilution buffer | 15mM DTT, 20% v/v Glycerol, 2.5% v/v 2-Mercaptoethanol, 1x Laemmli Buffer |
| PBS | 2.5mM KCl, 1.5mM $KH_2PO_4$, 140mM NaCl, 6.5mM $Na_2HPO_4$, laboratory grade $H_2O$, pH adjusted to 7.25 |
| TAE Buffer | 40mM Tris base, 20mM acetic acid, 1mM EDTA, laboratory grade $H_2O$, pH adjusted to 7.6 |
| TBS-Tween | 50mM Tris base, 0,05% Tween 20, 0,8% NaCl, laboratory grade $H_2O$, pH adjusted to 7.6 |
| Tris-buffer (0.1M) | 0.1M Tris base, laboratory grade $H_2O$, pH adjusted to 8.2 |

### 2.1.4 Consumables

Consumables mentioned in Tab. 2.3 were utilized for experimental trials.

**Table 2.3: Utilized consumables.**

| Name | Manufacturer |
|---|---|
| 26/30-Gauge needle | Braun AG, Germany |
| 50$\mu$m/70$\mu$m Cell strainer | Greiner Bio One, Austria |
| 96 Well Multiply PCR Plates | Sarstedt AG & Co., Germany |
| CryoPure Tube 1.6ml | Sarstedt AG & Co., Germany |
| FACS Tubes 5ml | Becton, Dickinson and Company, USA |
| Flow Cytometer Calibration and Size Reference Beads | Thermo Fisher Scientific, USA |
| Glass slides and coverslips | Gerhard Menzel GmbH,Germany |
| MembraneSlide 1.0 Pen NF | Carl Zeiss Microscopy GmbH, Germany |
| MicroFine Insuline syringes, 1ml | Becton, Dickinson and Company, USA |
| NuPage Novex 4-12% Bis-Tris-Gel 1.0mm x 12 well | Life Technologies, USA |
| Omnifix 1ml Syringes | Braun AG, Germany |
| PARAFILM M | Sigma-Aldrich Inc., USA |
| PCR Optical Adhesive Cover | Life Technologies, USA |
| Reaction tubes 0.2ml, 0.5ml, 1.5ml, 2ml, 5ml | Sarstedt AG & Co., Germany |
| Reaction tubes 15ml, 50ml | Nerbe plus, Germany |
| Pipette tips 10$\mu$l, 20$\mu$l, 100$\mu$l, 200$\mu$l, 1000$\mu$l | Nerbe plus, Germany |
| Pipette tips 10$\mu$l, 200$\mu$l, 1000$\mu$l | Sarstedt AG & Co., Germany |
| Safe Lock Tubes 1.5ml | Eppendorf AG, Germany |
| Scalpel blades | Dimeda Instrumente GmbH, Germany |
| Superfrost Plus Microscope Slides | Thermo Fisher Scientific, USA |
| Thermanox coverslips | Thermo Fisher Scientific, USA |

### 2.1.5 Primer

For quantitative RT-PCR (qRT-PCR) gen-specific primer, producing an amplicon of 100bp to 220bp and spanning at least an exon-exon junction, were used for amplification. Exact sequences, utilized concentration and NCBI Accession Number are specified in Tab. 2.4.

**Table 2.4: Gene-specific primer used for quantitative RT-PCR.**

| Primer | | Sequence | Concentration (nM) | NCBI Accession Number |
|---|---|---|---|---|
| $\beta$Actin | for | 5'GATGCTCCCCGGGCTGTATT | 25 | NM_007393 |
| | rev | 5'GGGGTACTTCAGGGTCAGGA | 25 | |
| FoxP3 | for | 5'ACTCGCATGTTCGCCTAC | 90 | NM_054039.2 |
| | rev | 5'TCCCTTCTCGCTCTCCACTC | 90 | |
| | probe | 5'CCGCCACCTGGAAGAATGCCATCCG | 20 | |
| GAPDH | for | 5'GACGGCCGCATCTTCTTGT | 90 | NM_008084.3 |
| | rev | 5'CACACCGACCTTCACCATTTT | 90 | |
| | probe | 5'CAGTGCCAGCCTCGTCCCGTAGA | 20 | |
| GATA3 | for | 5'GGTACTGGGCACTACCTTTG | 25 | NM_008091.3 |
| | rev | 5'TGGTGGTGGTCTGACAGTTC | 25 | |
| IFN$\gamma$ | for | 5'GCAAGGCGAAAAAGGATGC | 90 | NM_008337.3 |
| | rev | 5'GACCACTCGGATGAGCTCATTG | 90 | |
| | probe | 5'TGCCAAGTTTGAGGTCAACAACCCACAG | 20 | |
| IL4 | for | 5'GAGACTCTTTCGGGCTTTTCG | 90 | NM_021283.2 |
| | rev | 5'AGGCTTTCCAGGAAGTCTTTCAG | 90 | |
| | probe | 5'CCTGGATTCATCGATAAGCTGCACCATG | 20 | |
| IL10 | for | 5'TCCCTGGGTGAGAAGCTGAAG | 90 | NM_010548.2 |
| | rev | 5'CACCTGCTCCACTGCCTTG | 90 | |
| | probe | 5'CTGAGGCGCTGTCATCGATTTCTCCC | 20 | |
| MLN51 | for | 5'CCAAGCCAGCCTTCATTCTTG | 90 | NM_138660.2 |
| | rev | 5'TAACGCTTAGCTCGACCACTCTG | 90 | |
| | probe | 5'CACGGGAACTTCGAGGTGTGCCTAAC | 20 | |
| T-bet | for | 5'ACTGGATGCGACAGGAAG | 25 | NM_019507.2 |

| | | |
|---|---|---|
| rev | 5'GCGGCTGGTACTTATGGAG | 25 |

### 2.1.6 Antibodies

For immunohistochemistry (IHC), immunofluorescence (IF) and fluorescence-activated cell sorting (FACS) antibodies mentioned in Tab. 2.5 were utilized. All antibodies were titrated prior experimental usage for an optimal signal to noise ratio.

**Table 2.5: Utilized antibodies.**

| **Antibody** | **Clone** | **Manufacturer** |
|---|---|---|
| Biotin hamster anti-mouse TCR$\beta$ chain | H57-597 | Becton, Dickinson and Company, USA |
| Biotin rabbit anti-rat IgG | polyclonal | Southern Biotech, Inc., USA |
| Donkey anti-mouse IgG FITC | polyclonal | Jackson ImmunoResearch, USA |
| Goat anti-hamster IgG | polyclonal | abcam, UK |
| Rat anti-mouse CD4 | L3T4 | Becton, Dickinson and Company, USA |
| Rat anti-mouse CD4 APC | GK1.5 | BioLegend, USA |
| Rat anti-mouse CD4 PE | RM4-5 | Becton, Dickinson and Company, USA |
| Rat anti-mouse CD8$\alpha$ | 53-6.7 | Becton, Dickinson and Company, USA |
| Rat anti-mouse CD8$\alpha$ BV510 | 53-6.7 | BioLegend, USA |
| Rat anti-mouse CD8$\alpha$ PE | 53-6.7 | BioLegend, USA |
| Rat anti-mouse CD45R (B220) | RA3-6B2 | Becton, Dickinson and Company, USA |
| Rat anti-mouse CD45R (B220) PerCP-Cy 5.5 | RA3-6B2 | Thermo Fisher Scientific, USA |
| Rat anti-mouse CD185 (CxCR5) PE/Cy7 | L138D7 | BioLegend, USA |
| Rat anti-mouse CD279 (PD-1) BV421 | 29.F1A12 | BioLegend, USA |

| | | |
|---|---|---|
| Rat anti-mouse Gr-1 (Ly6G) | RB6-8C5 | Becton, Dickinson and Company, USA |
| Rat anti-mouse IgD FITC | 11-26c.2a | Becton, Dickinson and Company, USA |
| Rat anti-mouse Ki-67 | 16A8 | BioLegend, USA |
| TruStain fcX (anti-mouse CD16/32 antibody) | | BioLegend, USA |

### 2.1.7 Devices and instruments

Experiments were accomplished using devices and instruments delineated in Tab. 2.6.

**Table 2.6: Technical devices and instruments.**

| **Name** | **Manufacturer** |
|---|---|
| ABI PRISM 7900 HT | Applied Biosystems, Germany |
| AccuBlock Digital Dry Baths | Labnet International INC, USA |
| AxioCamHR digital camera | Carl Zeiss Microscopy GmbH, Germany |
| AxioCamIC | Carl Zeiss Microscopy GmbH, Germany |
| Axiophot optical microscope | Carl Zeiss Microscopy GmbH, Germany |
| Axioskop 2 plus optical microscope | Carl Zeiss Microscopy GmbH, Germany |
| Axiovert 200 | Carl Zeiss Microscopy GmbH, Germany |
| Calibration slide universal | Carl Zeiss Microscopy GmbH, Germany |
| Centrifuge 5417R (Rotor: F-45-30-11) | Eppendorf AG, Germany |
| Criterion Cell | Bio-Rad Laboratories Inc., USA |
| EBOX VX 5 | VILBER LOURMAT GmbH, Germany |
| Electrical nail file | Tchibo Certified Merchandise, Germany |
| Eppendorf Research plus pipettes | Eppendorf AG, Germany |
| FACS Aria III | Becton, Dickinson and Company, USA |
| FTSS 355-50 | CryLaS GmbH, Germany |
| Galaxy Mini Microcentrifuge | VWR International GmbH, Germany |
| Gel Electrophoresis Apparatus Criterion Cell | Bio-Rad Laboratories Inc., USA |

| | |
|---|---|
| Heraeus Megafuge 1.0 R (Rotor: 75002704) | Thermo Fisher Scientific, USA |
| Humidity chamber | Sigma-Aldrich Inc., USA |
| Hyrax Cryostat C50 | Carl Zeiss Microscopy GmbH, Germany |
| IKA MS2 Minishaker Vortexer | IKA works INC, USA |
| Microlaser-System SYS63TE/PA7 | Carl Zeiss Microscopy GmbH, Germany |
| MiniSpin Plus Centrifuge (Rotor: F-45-12-11) | Eppendorf AG, Germany |
| MiSeq System | Illumina INC, USA |
| Mitsubishi P95DW | Mitsubishi Electric, Japan |
| Neubauer improved counting chamber | Glaswarenfabrik Karl Hecht GmbH, Germany |
| N-XBO 75 | Carl Zeiss Microscopy GmbH, Germany |
| Odyssey Infrared Imaging System | Li-Cor Biosciences, USA |
| Olympus DP72 | Olympus Ag, Germany |
| PALM MicroBeam | Carl Zeiss Microscopy GmbH, Germany |
| PerfectBlue Gel System Mini L | VWR International GmbH, Germany |
| PowerPac Basic Power Supply | Bio-Rad Laboratories Inc. , USA |
| Power Supply LNG 350-6 Economy Line | Heinzinger electronic GmbH, Germany |
| Primus 25 Thermal Cycler | Eurofins Genomics GmbH, Germany |
| Primus 96 Plus Thermal Cycler | Eurofins Genomics GmbH, Germany |
| StepOne Plus Real-Time PCR | Thermo Fisher Scientific, USA |
| Thermomixer comfort | Eppendorf AG, Germany |
| Titramax 100 | VWR International GmbH, Germany |
| Quantus Fluorometer | Promega Corporation, USA |
| Vacuum Centrifuge Concentrator 5301 (Rotor: F-45-48-11) | Eppendorf AG, Germany |
| Vortex-Genie 2 | Scientific Industries INC, USA |

### 2.1.8 Software

Data generation, processing and analysis was done using the application-specific software specified in Tab. 2.7.

**Table 2.7: Software for data generation, processing and analysis.**

| Name | Developer |
|---|---|
| ABI 7900 HT detection System 2.4 | Applied Biosystems, Germany |
| Adobe Illustratur CS3 11.0.0 | Adobe Systems Incorporated, USA |
| Adobe Photoshop CS3 10.0.1 | Adobe Systems Incorporated, USA |
| AxioVision 4.9.1.2 | Carl Zeiss Microscopy GmbH, Germany |
| AxioVision 6.1 | Carl Zeiss Microscopy GmbH, Germany |
| Clono Suite | Institute of Anatomy, University of Lübeck, Germany (Fähnrich et al., 2017) |
| FACSDIVA V8.0.1 | Becton, Dickinson and Company, USA |
| FASTX Barcode splitter | Hannon Lab, Howard Hughes Medical Instute, USA |
| FlowJo v10.0.8r1 | FlowJo LLC, USA |
| GraphPad Prism 6 | GraphPad Software, Inc., USA |
| ImageJ 1.51j | Max Planck Institute of Molecular Cell Biology and Genetics Germany (Schindelin et al., 2012) |
| KIEL | Markus Schilhabel, Institute of Clinical Molecular Biology, Kiel University, Germany |
| Microsoft Excel 2013 | Microsoft Germany GmbH, Germany |
| MiTCR | Pirogov Russian National Research Medical University, Russia (Bolotin et al., 2013) |
| PALMRobo v4.8.0.1 | Carl Zeiss Microscopy GmbH, Germany |
| Pear 0.9.8 | The Exelixis Lab, Heidelberg Institute for Theoretical Studies, Germany (Zhang et al., 2014) |

| | |
|---|---|
| R 3.4.4 | R Foundation for Statistical Computing, Austria (R Core Team, 2015) |
| Step One Software v2.3 | Thermo Fisher Scientific, USA |
| tcR | Pirogov Russian National Research Medical University, Russia (Nazarov et al., 2015) |
| TeX 3.14159265 | Knuth D.E. |
| TeXstudio 2.12.6 | van der Zander B., Sundermeyer J., Braun D., Hoffmann T. |

## 2.2 Methods

### 2.2.1 Animal experiments

All animal experiments were approved by the Ministry of Energy, Agriculture, the Environment, Nature and Digitalization of Schleswig-Holstein (Ministerium für Energiewende, Landwirtschaft, Umwelt, Natur und Digitalisierung Schleswig-Holstein) and executed by certified personal. Tab. 2.8 reflects the entirety of animal experiment, which were approved, worked on or for this dissertation. Experiments were conducted after a convalescence of 1-2 weeks. Animals were randomly assigned to treatment groups and cage-effects were excluded by co-housing of treatment groups.

**Table 2.8: Animal experiment applications.**

| **Reference number** | **Delineation** |
|---|---|
| V242-45884/2016 (90-7/16) | Charakterisierung des vWFA2-induzierten EBA-Modells der Maus und Untersuchung des Einflusses mechanischer Reizung auf die Wundentstehung |
| V242-7224.122-1 (35-3/12) | Modulation des Verlaufs einer Autoimmunerkrankung der Haut durch Adjuvantien-Untersuchungen am aktvien Mausmodell der EBA |
| V312-72241.122-1 (106-10) | Die Expression der FC$\gamma$-Rezeptoren im Verlauf einer Autoimmunerkrankung der Haut - Untersuchung am aktiven Mausmodell der EBA |
| V312-72241.122-1 (104-10) | Einfluss einer mechanischen und chemischen Reizung der Haut auf die Entstehung von autoimmuninduzierten Blasen - Untersuchungen am aktiven Mausmodell der EBA |

| | |
|---|---|
| V312-72241.122-1 (92-7/09) | Etablierung von Entzündungsmarkern zur Charakterisierung des Kankheitszustandes einer an Epidermolysis Bullosa Aquisita erkrankten Haut |
| 23/A11/05 | Untersuchung zur Kinetik der Ausbildung von Autoimmunerkrankungen am Beispiel der Epidermolysis Bullosa Acquisita |

Animal experiments V312-72241.122-1 (106-10), V312-72241.122-1 (104-10), V312-72241.122-1 (92-7/09) and 23/A11/05 were conducted prior to this dissertation and analyzed with regard to divergent research question by Hammers et al. (2011) and Ellebrecht et al. (2016). Tissue sample obtained from the animal experiments were provided by the cryo-biobank of the Institute of Anatomy (University of Lübeck) for this dissertation.

#### 2.2.1.1 Validation of recombinant proteins

The recombinant proteins mCOL7c-GST (calculated mass 49.5kDa) and GST (calculated mass 26kDa) were generated as described by Sitaru et al. (2005) and kindly provided by the Lübeck Institute of Experimental Dermatology (University of Lübeck). Prior utilization, the concentration and purity of the recombinant proteins was validated via discontinuous and denaturating polyacrylamide gel electrophoresis (PAGE) (Fig. 2.1) according to Laemmli (1970). Protein samples were completely denatured using PAGE sample dilution buffer and incubation at 95°$C$ for 5min. A volume of 5$\mu$l diluted sample was loaded into individual pockets of the discontinuous NuPAGE 4-12% Bis-Tris Protein Gel. Separation was conducted at 200V for 35min. After separation, the gel was retrieved form the mounting device and pockets were removed. Proteins were fixed in 15% acetic acid for 2h and stained using Coomassie Blue staining solution for 15min (Tal et al., 1985). Excessive dye was removed by four-time consecutive washing using Coomassie Blue destaining solution for 30min. Following destaining, the gel was washed in laboratory grade $H_2O$ o/n. The quantitative analysis, compared to a Bovine serum albumin-standard (BSA), and visualization was carried out using the Odyssey Infrared Imaging System. Until utilization, individual preparations of the recombinant proteins were stored at -80°$C$.

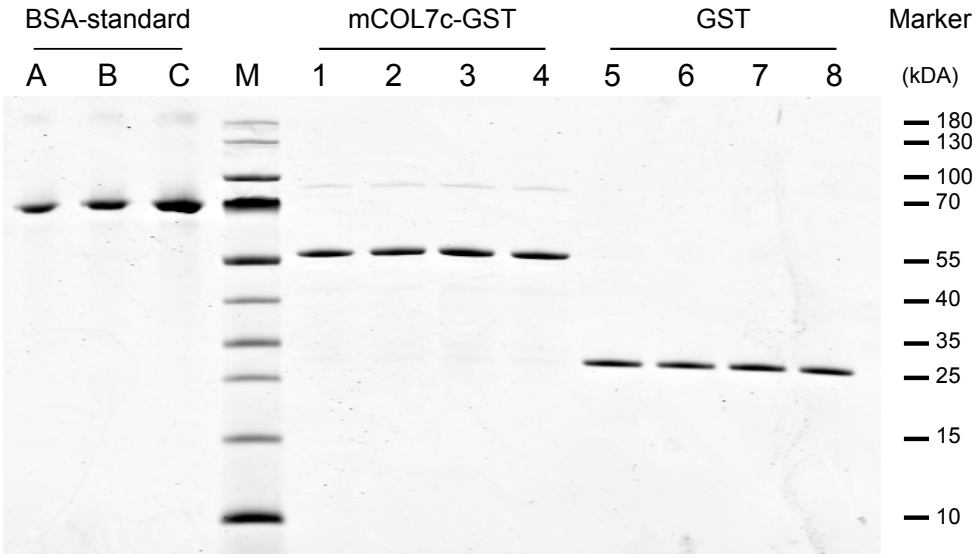


**Figure 2.1: Discontinuous and denaturating PAGE of the recombinant proteins mCOL7c-GST and GST.** Lanes A-C represent a BSA-standard (calculated mass 66.5kDa) in defined quantities (A $\widehat{=}$ 0.5$\mu$g, B $\widehat{=}$ 1$\mu$g, C $\widehat{=}$ 2$\mu$g). Lanes 1-4 represent individual preparations of mCOL7c-GST. Lanes 5-8 represent individual preparations of GST. Lane M represents the prestained protein PAGE-ladder (sizes of individual bands is schematically delineated alongside the gel).

#### 2.2.1.2 Induction of immunization induced EBA

For immunization an emulsion of PBS, GST or mCOL7c-GST in the adjuvant TiterMax was prepared under sterile conditions according to Tab. 2.9 (Hunter et al., 1981; Bennett et al., 1992). Each immunization batch was prepared immediately prior application by vortexing for 30-40min at 4°$C$ until complete emulsification.

**Table 2.9: Components of the immunization batch.**

| Protein stock ($2\mu g/\mu l$) | PBS | TiterMax | Final protein concentration ($\mu g/\mu l$) | Molarity (mM) |
|---|---|---|---|---|
| - | 50% | 50% | - | - |
| GST 13% | 37% | 50% | 0.26 | 0.01 |
| mCOL7c-GST 25% | 25% | 50% | 0.50 | 0.01 |

Laboratory animals were anesthetized, by i.p. injection of anesthetic solution, for 20-30min. 60$\mu$l of the prepared immunization batch was s.c. injected in either hind footpad (Sitaru et al., 2006). Eyes of anesthetized animals were covered with Bepanthen and awakening was monitored until full recovery.

#### 2.2.1.3 Scratching of the skin

For scratching, mice were anesthetized by i.p. injection of anesthetic solution for 20-30min. The inner side of both ears was exposed and the skin was scratched via a mechanical nail file until a size-standardized and non-bleeding wound remained. Using this approach, the epidermis was removed and the dermis remained intact (Maass, 2015).

#### 2.2.1.4 Assessment of affected ear area

The assessment of the affected ear area was performed as described by Bieber et al. (2017a). For individual evaluation laboratory animals were anesthetized by i.p. injection of anesthetic solution for 20-30min. The area exhibiting erythema, dermal wounds and crusts was evaluated in relation to the total ear area. All assessments were conducted by the same person, counteracting emerging evaluator variations.

#### 2.2.1.5 Organ extraction

Laboratory animals were sacrificed in deep $O_2/CO_2$ anesthesia by cervical dislocation or blood removal by cardiopuncture. Desired organs (ears and contralateral popliteal lymph nodes) were prepared *in situ* and either snap frozen using liquid nitrogen or short-term stored in PBS at $4°C$. For long-term storage, organs were transferred into cryotubes and stored at -$80°C$ until preparation. Organ extraction was carried out under clean and sterilized conditions.

### 2.2.2 Laser microdissection

Laser microdissection (MD) was used for the precise isolation of *in vivo* compartments within intact anatomical structures of the popliteal lymph nodes (Fig. 2.2) (Fend et al., 1999; Kalies et al., 2008). The dissection was conducted using a toluidine blue stained 12$\mu$m cryo-dissected lymph node sample. Individual compartments were identified by reference to B220/Ki-67 (identification and localization of germinal centers) and in discrimination to B220/TCR$\beta$ (identification and localization of the TCZ) stained 12$\mu$m serial sections. For germinal centers a volume of 4.5x$10^7$ $\pm$ 1x$10^7 \mu m^3$ was collected by pooling multiple individual germinal centers. The volume was deter-

mined as product of the area and thickness of the cryosection. Samples were lysed in 350$\mu$l Lysis solution RL for 30min at RT and stored at -20°$C$ until further processing.

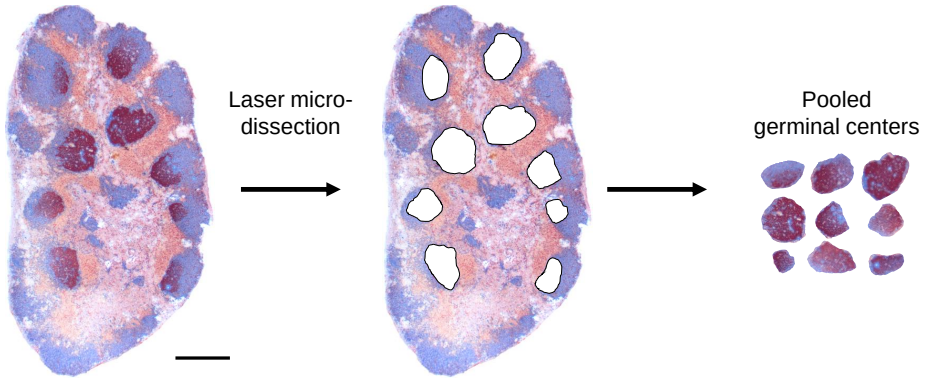


**Figure 2.2: Laser microdissection of germinal centers from draining lymph nodes.** Via a UV-laser coupled microscope, individual germinal centers were isolated form tissue sections. Dissection was implemented using a Toluidine blue stained section. As illustration an immunohistochemically stained lymph node is depicted, featuring staining for B-lymphocytes (blue = B220), T-lymphocytes (brown = TCR$\beta$) and proliferating cells (red = Ki-67). Scale bar $\widehat{=}$ 1.000$\mu$m.

### 2.2.3 Nucleic acid isolation

Nucleic acids were isolated using the immunPREP RNA Mini Kit according to the manufacturer's instructions. For further processing, laser microdissected samples were filled to 700$\mu$l Lysis solution RL. Skin biopsies (for qRT-PCR analysis 10 sections and for T-lymphocyte receptor$\beta$ repertoire 40 sections) were cryo-dissected into 12$\mu$m segments and lysed in 700$\mu$l Lysis solution RL. Samples were vortexed for 1min and afterwards cell walls and DNA were sheared via a 26-Gauge needle. 700$\mu$l 70% ethanol was added for nucleic acid precipitation and the solution was applied onto a Spinfilter R. Nucleic acids were allowed to bind to the column at 10.000g for 2min. Flow trough was discarded and the column was washed using 500$\mu$l high salt (HS) wash buffer at 10.000g for 1min. After discarding the flow trough, a secondary wash was conducted using 700$\mu$l low salt (LS) wash buffer at 10.000g for 1min. Afterwards the column was dried at 10.000g for 2min. Bound nucleic acids were released from the column by applying 40$\mu$l RNase-free $H_2O$ for 1min and subsequently eluted for 1min at 2.500g. Nucleic acid yield was increased by re-applying the eluate for 1min and repeated centrifugation at 2.500g for 1min. The sample volume was reduced by a 18 min evaporation step in a vacuum centrifuge at 60°$C$ and 240g to a final volume of 8$\mu$l.

### 2.2.4 gDNA digestion

1$\mu$l DNase I buffer and 1$\mu$l DNase I were added to the isolated 8$\mu$l nucleic acid solution of 2.2.3 and incubated at 25°$C$ for 20min. gDNA digestion was terminated by adding 1.5$\mu$l 15mM EDTA and subsequent incubation at 70°$C$ for 10min.

### 2.2.5 cDNA synthesis

For cDNA synthesis 8$\mu$l master mix, containing 4$\mu$l RevertAid 5x buffer, 2$\mu$l RNase-free $H_2O$, 1$\mu$l 10mM of each dNTP and 1$\mu$l 50$\mu$M random hexamers, was added to the 11.5$\mu$l gDNA-digested solution of 2.2.4 and incubated for 10min at 25°$C$. Reverse transcription was initiated by adding 0.5$\mu$l 200U/$\mu$l RevertAid Reverse Transcriptase and incubation at 42°$C$ for 60min. Enzymatic activity was terminated by an incubation at 70°$C$ for 10min. The transcribed cDNA was subsequently stored at -20°$C$ until utilization.

### 2.2.6 Quantitative RT-PCR

Transcribed cDNA of 2.2.5 was diluted 1:2 for qRT-PCR analysis using laboratory grade $H_2O$ and 1$\mu$l was added into a well of a 96 well plate. 19$\mu$l master mix, containing 10$\mu$l SYBR Green PCR Master Mix or TaqMan Universal PCR Master Mix, 7$\mu$l laboratory grade $H_2O$ and 2$\mu$l primer/probe (used concentration specified at 2.1.5), was added into each well. All qRT-PCR experiments were conducted in technical duplicates and ran on the StepOnePlus System. Amplification was achieved using specifications given in Tab. 2.10, whereby a melting curve has only been acquired if a SYBR Green based qRT-PCR was conducted.

**Table 2.10: Quantitative RT-PCR cycling conditions.**

| | Temperature | Time | Cycles |
|---|---|---|---|
| Initial denaturation | 95°C | 10min | 1 |
| Denaturation | 95°C | 45sec | 50 |
| Annealing and elongation | 60°C | 60sec | |
| Melting curve | 95°C | 15sec | 1 |
| | 60°C - 95°C | 15sec per 0.5°C | |

Amplification results were analyzed using the Step One Software v2.3. The relative gene expression level was ascertained as Cycle of threshold ($C_T$), representing the elongation cycle in which the

amplification-specific fluorescent signal exceeds background fluorescence. Relative quantification of the gene expression was considered in relation to the $C_T$ of the housekeeping genes MLN51, GAPDH and $\beta$Actin (Kalies et al., 2006). The expression stability of the housekeeping genes among all experimental conditions was determined by analysis prior experiments (Hellemans et al., 2007; Ling and Salvaterra, 2011). For the experiments, an expression stability, expressed as coefficient of variation, of 0.1 was defined as upper limit (Tab. 2.11).

**Table 2.11: Expression stability of utilized housekeeping genes.**

| Housekeeping gene | Mean $C_T$±SD | Coefficient of variation |
|---|---|---|
| MLN51 | 27.8±1.0 | 0.04 |
| GAPDH | 21.8±1.0 | 0.05 |
| $\beta$Actin | 17.0±1.2 | 0.07 |

For normalization of gene expression levels, a normalization factor ($N_F$) of all utilized housekeeping genes was calculated as the geometric mean $C_T$ (Vandesompele et al., 2002):

$$N_F = \sqrt[3]{\overline{C_T}\ MLN51 * \overline{C_T}\ GAPDH * \overline{C_T}\ \beta Actin}$$

Using the resulting $N_F$, the relative gene expression was calculated as (Livak and Schmittgen, 2001):

$$2^{\Delta C_T} = 2^{((N_F)-(\overline{C_T}\ gene\ of\ interest))}$$

The relative gene expression was further normalized as the quotient of control group expression levels, resulting in expression fold changes, following the formula (Livak and Schmittgen, 2001):

$$2^{-\Delta\Delta C_T} = 2^{-\Delta C_T\,(\text{examined})} \,/\, \overline{2^{-\Delta C_T\,(\text{control})}}$$

### 2.2.7 Sequencing of the T-lymphocyte receptor$\beta$ repertoire

#### 2.2.7.1 RNA quantification

The quantity of extracted RNA was determined using the QuantiFluor RNA System. 1$\mu$l gDNA-digested solution of 2.2.4 was diluted 1:100 using 1x TE buffer. QuantiFluor RNA Dye working-solution was prepared prior quantification by diluting QuantiFluor RNA Dye 1:1.000 using 1x TE buffer. 100$\mu$l diluted gDNA-digested solution and 100$\mu$l QuantiFluor RNA Dye working solution were combined and incubated for 5min at RT in the dark, allowing the dye to bind to the RNA. The RNA content was quantified using the Quantus Fluorometer with the allocated RNA-low protocol.

#### 2.2.7.2 Amplicon rescued multiplex PCR

Gene-specific preparation of T-lymphocyte receptor$\beta$ sequencing libraries was achieved by utilizing an amplicon rescued multiplex PCR (arm-PCR) containing two consecutive PCR steps (Han et al., 2006; Wang et al., 2010). For that, the commercially available MTBIvc reagent system was used, whereby 24 forward and reverse primer target the T-lymphocyte receptor$\beta$ V- or C-segment, respectively (Fig. 2.3 A).

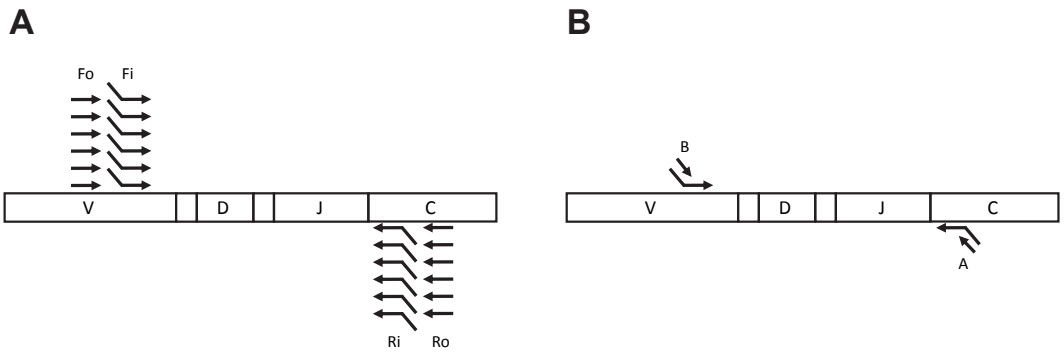


**Figure 2.3: Schematic procedure of the arm-PCR.** A) During the first PCR step gene specific primer target the V- and C-segment. The forward-out (Fo) and forward-in (Fi) primer are reverse-complementary to the V-segment, the reverse-out (Ro) and reverse-in (Ri) are reverse-complementary to the C-segment. Non-annealing parts of Fi and Ri introduce sequences necessary for Illimuna sequencing (Ri introduces PE PCR Primer 1.0 and Fi introduces PE PCR Primer 2.0). Also a sample specific index-sequence is introduced via the Ri primer. B) During the second PCR step communal Illuima primer A (PE PCR Primer 1.0) and B (PE PCR Primer 2.0) were used for exponential amplification.

In the first PCR step (Fig. 2.3 A), a reverse transcription and a multiplex-nested PCR was conducted successively. 10$\mu$l gDNA-digested solution of 2.2.4 was added to 15$\mu$l master mix, containing 5$\mu$l 5x OneStep RT-PCR Buffer, 1$\mu$l 10 mM each dNTP Mix, 3$\mu$l MTBIvc primer -carrying a sample specific index sequence-, 1$\mu$l OneStep RT-PCR Enzyme Mix and 5$\mu$l RNase-free $H_2O$. The total amount of utilized RNA was capped at 500ng. If necessary, the differential volume was compensated using RNase-free $H_2O$. For all investigated samples a No Template Control (NTC) was carried out under identical condition. Reverse transcription and multiplex-nested PCR was achieved using specifications given in Tab. 2.12.

**Table 2.12: arm-PCR: reverse transcription and multiplex-nested PCR.**

| | Temperature | Time | Cycles |
|---|---|---|---|
| Reverse transcription | 50°C | 40min | 1 |
| Denaturation | 95°C | 15min | |
| Denaturation | 94°C | 30sec | 15 |
| Annealing | 60°C | 2min | |
| Elongation | 72°C | 30sec | |
| Denaturation | 94°C | 30sec | 10 |
| Elongation | 72°C | 2min | |
| Final elongation | 72°C | 10min | 1 |

In the second PCR step (Fig. 2.3 B), an exponential amplification was achieved using amplicon specific communal Illumina primer (PE PCR Primer 1.0 and PCR Primer 2.0). 1$\mu$l PCR product of the first step was added to a master mix, containing 12.5$\mu$l Multiplex PCR Master Mix, 2.5$\mu$l communal Illumina primer and 9$\mu$l laboratory grade $H_2O$. For amplification the specified conditions given in Tab. 2.13 were used. Until further utilization samples were stored at -20°$C$.

**Table 2.13: arm-PCR: amplification PCR.**

| | Temperature | Time | Cycles |
|---|---|---|---|
| Initial denaturation | 95°C | 15min | 1 |
| Denaturation | 94°C | 30sec | 40 |
| Annealing | 60°C | 30sec | |
| Elongation | 72°C | 30sec | |
| Final elongation | 72°C | 5min | 1 |

#### 2.2.7.3 Agarose gel electrophoresis

Amplification during arm-PCR was verified by agarose gel electrophoresis. For accurate product-separation 2% w/v agarose was dissolved in 1x TAE buffer at 95°C. The solution was cooled to 65°C and 1:10.000 vol% Roti-GelStain was added before pouring into an applicable gel-tray. 25$\mu$l of the second arm-PCR step was mixed with 5$\mu$l 5x DNA Loading Buffer Blue and loaded onto the gel. For product-size estimation 5$\mu$l HyperLadder 100bp was loaded into first pocket of every gel and separation was achieved by applying 110V power for 40min. Subsequent separation, the

gel was monitored using UV light and captured with a fixed exposure time of 64ms using the EBOX VX5. According to the manufacturer's instructions, single product bands at approximately 280-300bp were considered as complete amplified products, with respect to corresponding NTCs not carrying any product at 280-300bp and only showing an unspecific band at approximately 140-150bp (Fig. 2.4). Positively amplified samples were cut out in a cutting-range equivalent to 250-330bp and stored at -20°$C$ until further processing.

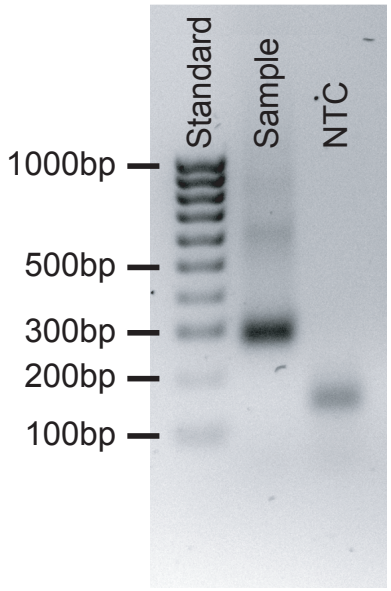


**Figure 2.4: Representative arm-PCR-product gel.** 2% agarose gel showing the arm-PCR product at 280-300bp in the lane loaded with the sample and no sample-specific amplification in the NTC lane.

#### 2.2.7.4 DNA-gel-extraction

DNA-gel-extraction was performed using the QIAquick Gel Extraction Kit, according to manufacturer's instructions. Gel slices were weighted and 3x the volume of buffer QG was added to 1x the volume of gel (gel volume was considered as: 1mg = 1$\mu$l). Following an incubation at 50°C for 10min (if necessary, incubation time was prolonged until complete dissolving), 1x the volume of isopropanol was added to the sample. 700$\mu$l sample-solution was added to a QIAquick spin column and DNA was allowed to bind to the column at 12.000g for 1min (for volumes greater than 700$\mu$l, DNA binding was repeated consecutively). Flow trough was discarded and the column was washed using 500$\mu$l buffer QG at 12.000g for 1 min. After discarding the flow trough, a secondary wash was performed by incubation for 3min using 750$\mu$l buffer PE and subsequent centrifugation at 12.000g for 1min. Afterwards the column was dried at 12.000g fo 1min. Bound DNA was eluted by incuba-

tion for 1min using 10$\mu$l buffer EB and centrifugation at 12.000g for 1min. Eluted T-lymphocyte receptor$\beta$ sequencing libraries were stored at -20°$C$ until further processing.

#### 2.2.7.5 Sequencing library quantification

The concentration of T-lymphocyte receptor$\beta$ sequencing libraries was determined by qRT-PCR using the PerfeCTa NGS Quantification Kit according to the manufacturer's instructions. T-lymphocyte receptor$\beta$ sequencing libraries were diluted 1:10.000 using 1x Library Dilution buffer. 4$\mu$l of the diluted T-lymphocyte receptor$\beta$ sequencing library was added into a well of a 96 well plate. 4$\mu$l of the standards 1-5 (containing 0.0005pM to 5pM amplifiable standards with a length of 426bp) and 4$\mu$l laboratory grade $H_2O$ as NTC were added into the lowest row of wells. 16$\mu$l master mix, containing 10$\mu$l 2x PerfeCta SYBR Green SuperMix, 0.6$\mu$l Illumina Primer Mix and 5.4$\mu$l laboratory grade $H_2O$, was added into each well. All qRT-PCR experiments for NGS library quantification were conducted in technical duplicates and ran on the ABI PRISM 7900 HT. Amplification was achieved using specifications given in Tab. 2.14.

**Table 2.14: PCR conditions for sequencing library quantification.**

| | Temperature | Time | Cycles |
|---|---|---|---|
| Initial denaturation | 95°C | 5min | 1 |
| Denaturation | 95°C | 20sec | 35 |
| Annealing | 60°C | 30sec | |
| Elongation | 72°C | 45sec | |
| Melting curve | 95°C | 15sec | 1 |
| | 60°C - 95°C | 15sec per 0.5°C | |

Amplification results were analyzed using the ABI 7900 HT detection System 2.4. Baseline setting was standardized from 3 to 8 and the threshold was set to 0.2 in all performed experiments. Based on standard amplification-curves, the $C_T$ values of each analyzed sample was converted to the raw concentration.

According to the manufacturer's protocol, absolute library concentration is calculated as:

$$size\ corrected\ concentration\ (pM) = raw\ concentration\ (pM) * \frac{standard\ fragment\ length\ (bp)}{amplicon\ fragment\ length\ (bp)}$$

Standard fragment length of the PerfeCTa NGS Quantification Kit is given as 426bp. For T-lymphocyte receptor$\beta$ sequencing libraries, prepared using the MTBIvc reagent system, the amplicon fragment length was considered as 280 bp (Fig. 2.4). Therefore, the size-corrected concentration was calculated as:

$$size\ corrected\ concentration\ (pM) = raw\ concentration\ (pM) * 1.52$$

Including the dilution factor, the absolute concentration of the T-lymphocyte receptor$\beta$ sequencing library was calculated as:

$$library\ concentration\ (nM) = size\ corrected\ concentration\ (pM) * 10.000$$

#### 2.2.7.6 Next-Generation Sequencing

The T-lymphocyte receptor$\beta$ sequencing libraries were analyzed using the Illumina MiSeq platform equipped with the MiSeq Reagent Kit v2 300 cycles. 6 individual T-lymphocyte receptor$\beta$ sequencing libraries were analyzed in parallel, all carrying an unique and sample-specific index-sequence. Prior sequencing all samples were normalized to a concentration of 2nM using library dilution buffer. For sequencing a pool of the 6 individual samples was prepared by combining 5$\mu$l of each 2nM sample. 5$\mu$l of the sample-pool was denatured using 5$\mu$l freshly prepared 0.2M NaOH for 5min at 20°C and subsequently filled up using 990$\mu$l HT1 buffer resulting in a 10pM sample-pool. 450$\mu$l of the 10pM sample-pool was further diluted using 150$\mu$l HT1 buffer resulting in a 7.5pM sample-pool.

As an internal Illimuna sequencing control, PhiX Control v3 was used. 2$\mu$l 10nM PhiX library was combined with 3$\mu$l library dilution buffer and denatured using 5$\mu$l 0.2M NaOH for 5min at 20°C. The solution was filled up using 990$\mu$l HT1 buffer resulting in a 20pM PhiX library. 375$\mu$l 20pM PhiX library was diluted using 225$\mu$l HT1 buffer resulting in a 12.5pM PhiX library.

For sequencing 510$\mu$l of the 7.5pM sample-pool and 90$\mu$l 12.5pM PhiX library were combined and loaded into the MiSeq reagent cartridge. The flow cell was rinsed using laboratory grade $H_2O$ and cleaned from particles. Sequencing was conducted as 150bp paired-end sequencing utilizing Illumina PE Read 1/2 Sequencing Primer. The device was set to generate FASTQ files. Individual sequencing runs were assessed based on PhiX sequencing quality, density of clusters (k/mm$^2$) and the cluster passed filter (%). Runs displaying a cluster density of 750k/mm$^2$ $\pm$ 150 and a cluster past filter rate >90% were categorized as successful sequencing runs.

#### 2.2.7.7 Data preprocessing

Each sequencing run yielded two separate FASTQ files, representing the individual information of the forward and reverse read. Data demultiplexing, processing and T-lymphocyte receptor$\beta$ detection was conducted using the computational front end ClonoCalc 2.1 (Fähnrich et al., 2017). The process of data preprocessing using ClonoCalc 2.1 is schematically depicted in Fig. 2.5. Initially, demultiplexing of sequenced samples was achieved using the FASTX Barcode Splitter and based on the underlying sample specific index sequence. While quality assessment during barcode splitting, reads harboring >0 nucleotide mismatches within the index sequence were discarded. Resulting FASTQ file represented the forward read, to which the corresponding reverse reads was identified using the program KIEL, via coordinate matching. Index specific forward and reverse reads were subsequently merged to a combined read using the program PEAR (Zhang et al., 2014). During assembly, the Phred quality score of individual reads was assessed and reads exhibiting a score <30 were discarded (Ewing and Green, 1998). Using assembled reads, MiTCR was used for IMGT-GENE/DB based T-lymphocyte receptor$\beta$ extraction (Bolotin et al., 2013; Lefranc et al., 2015). T-lymphocyte receptor$\beta$ containing reads were identified by sequence-mapping against the murine T-lymphocyte receptor$\beta$ gene locus. As final output, tables were generated containing detailed T-lymphocyte receptor$\beta$ information, such as the CDR3 amino acid sequence, read count, read frequency, VDJ composition and number of nucleotide insertions. T-lymphocyte receptor$\beta$ clonotypes are denoted as unique CDR3 amino acid sequences.

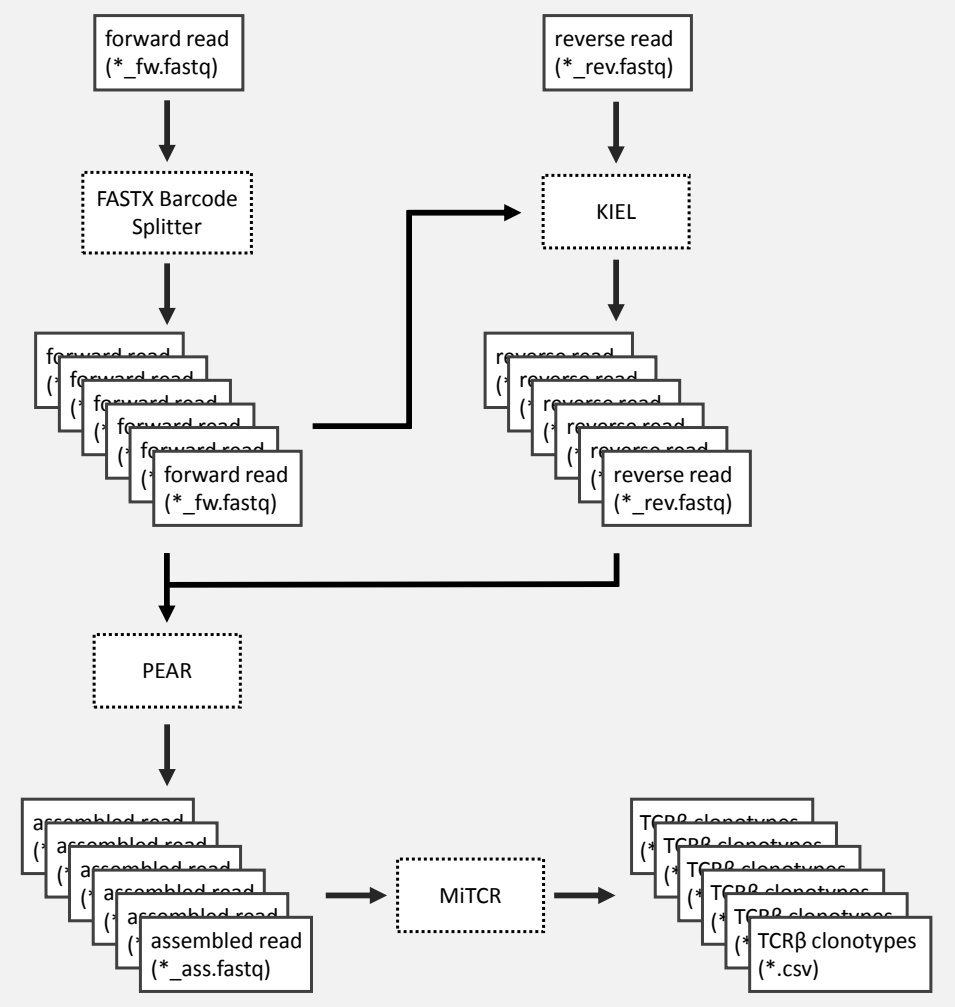


**Figure 2.5: Next-Generation Sequencing data preprocessing.** Schematic depiction of NGS data preprocessing. Forward reads were demultiplexed based on the sample specific index sequence and identification of corresponding reverse reads was performed by coordinate matching. Individual forward and reverse reads were assembled and T-lymphocyte receptor$\beta$ clonotypes were identified as unique CDR3 amino acid sequences.

#### 2.2.7.8 Data evaluation

Data evaluation was performed using the R platform and is based on the tcR package or Clono Suite functions (R Core Team, 2015; Nazarov et al., 2015; Fähnrich et al., 2017). Only annotated T-lymphocyte receptor$\beta$ clonotypes, defined as in-frame T-lymphocyte receptor$\beta$ clonotypes with a copy number $\geq 2$ were further considered (Madi et al., 2014). Evaluation of the frequency distribution revealed a very low frequency for the vast majority of annotated T-lymphocyte receptor$\beta$

clonotypes. Thus, to avoid any artificial diversity, which could originate from unpredictable PCR errors (Best et al., 2015) or unrelated bystander T-lymphocytes, only annotated T-lymphocyte receptor$\beta$ clonotypes with a relative abundance above the median were kept and are evaluated in this dissertation. These are referred to as T-lymphocyte receptor$\beta$ clonotypes. An overview of annotated T-lymphocyte receptor$\beta$ clonotypes and T-lymphocyte receptor$\beta$ clonotypes can be seen in Tab. S1 and Tab. S2.

#### 2.2.7.8.1 Comparative repertoire analysis

Clonotype dispersion within an individual sample was calculated using the **Gini coefficient** (Gini, 1912) as follows:

$$G = 1 - 2\int_0^1 L(X)dX$$

$$L(X) \text{ Lorenz curve}$$

This coefficient is determined as the ratio of area on the Lorenz curve diagram (Gastwirth, 1971). The coefficient is unitless and ranges from $G = 0$ (the abundance of all T-lymphocyte receptor$\beta$ clonotypes is equal) to $G = 1$ (one T-lymphocyte receptor$\beta$ clonotype represents the entire repertoire) (Heather et al., 2017).

Comparative analysis of the T-lymphocyte receptor$\beta$ clonotypes among two samples, including a sample size correction, was calculated using the **Jaccard-Index** (Jaccard, 1908) as follows:

$$J(A,B) = \frac{|A \cap B|}{|A \cup B|}$$

$$\text{A} = \text{clonotypes of T-lymphocyte receptor}\beta \text{ sample A}$$
$$\text{B} = \text{clonotypes of T-lymphocyte receptor}\beta \text{ sample B}$$

The index calculates the ratio of clonotypes that are identical between two samples and divides it by the number of clonotypes that exclusively exist in either sample. It is unitless and ranges from $J = 0$ (no shared clonotypes) to $J = 1$ (an identical T-lymphocyte receptor$\beta$ repertoire in both samples).

The sample size corrected and frequency-including comparison of T-lymphocyte receptor$\beta$ clonotypes among two samples was calculated using the **Morisita-Horn-Index** (Morisita, 1962; Horn, 1966) as follows:

$$C_{MH} = \frac{2\sum_{i=1}^{S} x_i y_i}{\left(\frac{\sum_{i=1}^{S} x_i^2}{X^2} + \frac{\sum_{i=1}^{S} y_i^2}{Y^2}\right) XY}$$

$x_i$ = quantity of T-lymphocyte receptor$\beta$ clonotypes $i$ within sample X

$y_i$ = quantity of T-lymphocyte receptor$\beta$ clonotypes $i$ within sample Y

S = quantity of unique T-lymphocyte receptor$\beta$ clonotypes

This index identifies the number of identical T-lymphocyte receptor$\beta$ clonotypes between two individual repertoires and takes their relative frequency into count. The index is unitless and ranges from $C_{MH} = 0$ (no congruence) to $C_{MH} = 1$ (an identical T-lymphocyte receptor$\beta$ repertoire).

To identify similarities or differences among the combined T-lymphocyte receptor$\beta$ V-J-segments a **principal component analysis (PCA)** was conducted. This method reduces complexity and dimensionality of a complex relation into a two-dimensional arrangement (Miqueu et al., 2010; Dash et al., 2017). Exemplary for the combined V-J-segment analysis, the relationship of 242 possible V-J-segment combinations is reduced to a two-dimensional illustration. Thereby, a similar V-J-segment usage results in a clustering, whereas a different, in a separation.

### 2.2.8 Fluorescence-activated cell sorting

#### 2.2.8.1 Staining and analysis

Fluorescence-activated cell sorting (FACS) was used for analysis and isolation of surface-stained cells form draining lymph nodes. Single cell suspension was obtained by homogenization of lymph nodes trough a 70$\mu$m mesh using a plunger. The suspension was taken up in 25ml PBS and centrifuged at 300g for 10min at 4°C. The supernatant was discarded and cells were taken up in 1ml FACS buffer. 4x$10^6$ cells were aliqouted and used for cell surface staining. In order to block unspecific binding of staining-antibodies, 1$\mu$l of anti-CD16/CD32 antibody (1mg/ml) was added to the cells and incubated at 4°C for 15min. Blocked cells were centrifuged at 300g for 10min at 4°C, the supernatant was discarded. Fluorochrome-conjugated antibodies were prepared in 100$\mu$l FACS buffer and added to the cells. Surface-staining was achieved in the dark for 30min at 4°C. All antibodies were titrated prior experimental usage for an optimal signal to noise ratio. Staining was stopped by centrifugation at 300g for 10min at 4°C. Cells were then resuspended in 300$\mu$l FACS buffer, filtered trough a 50$\mu$m mesh and prior acquisition via the FACS LSR III, 1$\mu$l Propidium iodide solution (0.1mg/ml) was added.

For cell sorting, desired cell populations were selected via the FACSDIVA software and collected in 300$\mu$l FACS buffer. Afterwards, sorted cells were centrifuged at 10.000g for 10min at 4°C. The resulting pellet was resuspended in Lysis solution RL and samples were stored until further preparation at -20°C.

#### 2.2.8.2 Data evaluation

During FACS measurement, events were recoded using the FACSDIVA software as compensated FCS files (version 3.0). Compensation was used to reduce overlapping signals between emission spectra of the used fluorochromes and adjusted via single stained controls (Bagwell and Adams, 1993). All gates for cell-sorting and data evaluation were set according to fluorescence minus one (FMO) controls (Mahnke and Roederer, 2007).

### 2.2.9 Immunohistological staining methods

Immunohistological staining was used for identification, detection and localization of different cell types and anatomical structures. An application specific methodology was used, either based on different chemical properties or epitope recognition of antibodies. Visualization was conducted by direct staining of cellular structures, enzymatic substrate-turnover or linkage of fluorochromes to antibodies. All staining were conducted in the dark using a humidity chamber. Incubations were performed under constant movement using an orbital shaker and antibodies were titrated prior experimental usage for an optimal signal to noise ratio. If not mentioned separately, all steps were conducted at RT.

#### 2.2.9.1 Cryosections

Cryosections of tissues samples were prepared using the Hyrax Cryostat C50. Snap frozen tissues were embedded in tissue freezing medium and cut until a plain cut-level was present. Individual 12$\mu$m sections were mounted onto slides and dried for at least 1h. For nucleic acid isolation individual sections were collected in 1.5ml Safe Lock Tubes, lysed in 700$\mu$l Lysis solution RL and stored until further preparation at -20°C.

#### 2.2.9.2 Hematoxylin and Eosin staining

Consideration of histological structures in different tissues was achieved by Hematoxylin and Eosin (H&E) staining. Initially samples were fixed using a composite solution of methanol and acetone (1:1) for 10min at -20°C and rinsed twice using PBS for 5min. Staining of acidic cellular structures

was achieved using Hematoxylin (diluted 1:5 in PBS) for 10min. Remaining chemicals were washed off by twice incubating in PBS for 5min and bluing was carried out by incubation in PBS for 10min. Subsequently samples were desalted by rinsing in laboratory grade $H_2O$ and alkaline cell structures were counterstained via Eosin for 1-3min. Remaining dye was removed by incubation in laboratory grade $H_2O$ for 5 min. Slides were dehydrated using an ascending alcohol series (70% - 99.8% ethanol) and three times incubation in xylene for 2-3min. Subsequently samples were mounted using Entallan and coverslips.

#### 2.2.9.3 Gr-1 staining

Dermal identification of neutrophils was conducted by staining for the myeloid-derived cell-marker Gr-1 (Ly6G). Samples were fixed using a composite solution of methanol and acetone (1:1) for 10min at -20°C and rinsed twice in TBS-Tween for 5min. Sections were incubated using the anti-mouse Gr-1 antibody for 1h and rinsed twice in TBS-Tween for 5min. As secondary antibody the biotinylated anti-rat IgG antibody was applied, incubated for 30min and unbound antibody was removed by rinsing twice using TBS-Tween for 5min. Conjugation of ExtrAvidin Alkaline Phosphatase was carried out for 30min and remaining substances were washed away by twofold rinsing in TBS-Tween for 5min. Visualization of neutrophils was achieved by application of Fast Red staining solution for 25min. Following rinsing twice, using TBS-Tween for 5min, acidic cellular structures were stained using Hematoxylin for 20sec to 2min and blued by incubation in PBS for 10min. Subsequent rinsing twice using PBS, samples were mounted using Aquatex and coverslips.

#### 2.2.9.4 CD4/CD8$\alpha$ staining

Detection of T-lymphocytes in the skin was achieved by staining for the T-lymphocyte co-receptors CD4 and CD8$\alpha$. Sections were fixed using a composite solution of methanol and acetone (1:1) for 10min at -20°C and rinsed in TBS-Tween for 10min. Primary antibodies, either anti-mouse CD4 or anti-mouse CD8$\alpha$ were applied for 1h and unbound antibody was removed by rinsing in TBS-Tween fo 10min. Incubation with Biotinylated anti-rat IgG antibody was done for 30min and samples were washed using TBS-Tween for 10min. Conjugation of ExtrAvidin Alkaline Phosphatase was carried out for 30min and remaining substances were washed away by rinsing in TBS-Tween for 10min. Either co-receptor was visualized by incubation with Fast Red staining solution for 25min, followed by rising in TBS-Tween for 10min. Acidic cellular structures were stained using Hematoxylin for 20sec to 2min and blued by incubation in PBS for 10min. Subsequent rinsing twice using PBS, samples were mounted using Aquatex and coverslips.

#### 2.2.9.5 Ki-67/B220 staining

Identification of germinal centers in lymph nodes was achieved by staining for proliferating B-lymphocytes. Therefore, the constitutively expressed pan-B-lymphocyte marker B220 (Coffman and Weissman, 1981) and Ki-67 (Gerdes et al., 1991), a proliferation marker which is expressed during all phases of mitosis, were utilized. First, cryosections were fixed using chloroform for 10min and acetone for 10min. After rinsing in TBS-Tween for 10 min, the samples were fixed using 4% PFA for 45min at 4°C. Subsequent rinsing in TBS-Tween for 10min, the primary anti-mouse Ki-67 antibody was applied o/n. Unbound antibodies were washed away by incubation in TBS-Tween for 10min and the secondary biotinylated anti-rat IgG antibody was added for 30min. Subsequent rinsing using TBS-Tween, ExtrAvidin Alkaline Phosphatase was applied for 30min and remaining substances were washed away using TBS-Tween for 10min. Visualization of proliferating cells was achieved by application of Fast Red staining solution for 25min. Following rinsing in TBS-Tween for 10 min, the primary anti-mouse B220 antibody was applied for 1h. Remaining antibodies were removed by rinsing in TBS-Tween for 10min. As secondary antibody, the biotinylated anti-rat IgG antibody was added, incubated for 30 min and unbound antibodies were washed away using TBS-Tween for 10min. ExtrAvidin Alkaline Phosphatase was applied for 30min, samples were washed using TBS-Tween and B-lymphocytes were visualized using Fast Blue staining solution. After rinsing in TBS-Tween for 10 min, samples were mounted using Aquatex and coverslips.

#### 2.2.9.6 TCR$\beta$/B220 staining

Classification and delineation of the BCZ and TCZ during MD was realized by staining for the pan-B-lymphocyte marker B220 and the T-lymphocyte receptor$\beta$. Cryosections were fixed using a composite solution of methanol and acetone (1:1) for 10min at -20°C and rinsed in TBS-Tween for 10min. The primary biotinylated anti-mouse TCR$\beta$ antibody was applied for 1h and unbound antibodies were removed by rinsing in TBS-Tween for 10min. Subsequently, samples were incubated with ExtrAvidin Peroxidase for 30min and remaining substances were washed away using TBS-Tween for 10min. Visualization of T-lymphocytes was performed by incubation with Liquid DAB+ Substrate for 5min and a following washing step using TBS-Tween for 10min. Samples were further incubated using the primary anti-mouse B220 antibody for 1h and unbound antibodies were washed away by rinsing with TBS-Tween for 10min. The secondary biotinylated anti-rat IgG antibody was applied for 30min and remaining antibodies were removed by rinsing in TBS-Tween for 10min. ExtrAvidin Alkaline Phosphatase was applied for 30min and samples were rinsed using TBS-Tween for 10min. B-lymphocytes were visualized using Fast Blue staining solution. Subsequently, samples

were rinsed in TBS-Tween for 10min and mounted using Aquatex and coverslips.

#### 2.2.9.7 Ki-67/TCR$\beta$/B220 combined staining

For a joint staining of proliferating cell, T-lymphocytes and B-lymphocytes the protocols of the Ki-67/B220 and TCR$\beta$/B220 staining were combined. Initially, proliferating cells were visualized as described in 2.2.9.5. Afterwards, the combined staining for TCR$\beta$/B220 was conducted as described in 2.2.9.6.

#### 2.2.9.8 Toluidine blue staining

For laser microdissection, cryosections were mounted on film slides and stained using Toluidin blue. Samples were fixed by incubation in 75% ethanol for 10min, rinsed using laboratory grade $H_2O$ for 2min and stained by applying 0.1% Toluidine blue for 2min. Subsequent the samples were rinsed two times using laboratory grade $H_2O$ for 2min and dehydrated by incubation in 96% ethanol for 15sec. Stained slides were stored at -80°$C$ until further processing.

#### 2.2.9.9 Immunofluorescence staining

Identifying of dermal deposition of IgG at the DEJ was carried out via a direct immunofluorescence staining. Skin sections were fixed using a composite solution of methanol and acetone (1:1) for 10min at -20°C and were rinsed in TBS-Tween for 10min. Afterwards the anti-mouse IgG FITC antibody was applied and samples were incubated for 1h. After rinsing with TBS-Tween for 10min, nuclei were stained using 1:10.000 DAPI staining solution for 5min. Following rinsing in TBS-Tween for 10min, samples were mounted using Mowiol and coverslips.

The visualization of $CD4^+$ and $CD8^+$ T-lymphocytes within germinal centers of lymph nodes was realized via a direct immunofluorescence staining. Tissue samples were fixed using a composite solution of methanol and acetone (1:1) for 10min at -20°C and were rinsed in TBS-Tween for 10min. Samples were subsequently, blocked using immunofluorescence blocking solution for 20min and rinsed in TBS-Tween for 10min. Anti-mouse CD4 PE or anti-mouse CD8$\alpha$ PE antibodies were applied together with the anti-mouse IgD FITC antibody. Samples were incubated for 1h and afterwards rinsed using TBS-Tween for 10min. Nuclei were stained using 1:10.000 DAPI staining solution for 5min. Samples were rinsed in TBS-Tween for 10min and mounted using Mowiol and coverslips.

### 2.2.10 Microscopy and digital image analysis

The Axiophot light microscope was used to acquire representative areas of immunohistochemically stained skin or lymph node sections. Prior acquisition, the illumination was set up according to Köhler (1893). White balance was set to the background and related images were taken using an equal exposure time.

Immunofluorescence was visualized using the Axioskop 2 plus microscope. All images were captured after black-tuning, using an identical exposure time and equal ISO-setting. Both values were adjusted prior analysis to the corresponding positive and negative controls.

#### 2.2.10.1 Determination of dermal T-lymphocyte and $T_{fh}$ frequencies

The cellular frequency of T-lymphocytes in the skin and $T_{fh}$ in germinal centers was assessed using a standardized ImageJ analysis pipeline. Immunohistochemical stainings were segregated into individual colors using the function "Colour Deconvolution", a threshold was set globally and individual cells were partitioned using the function "Watershed". For skin samples, the entire area of the cryosection was utilized and the number of stained dermal T-lymphocytes was determined using the function "Analyze Particles". Obtained results were validated using a digital overlay. For germinal centers, the area of an individual germinal center was defined using a Ki-67/B220 staining and transfered to the corresponding TCR$\beta$/B220 staining via the function "Restore selection". The number of stained $T_{fh}$ was determined using the function "Analyze Particles" and results were validated using a digital overlay (Fig. 2.6). For T-lymphocytes in the skin, four cryosection and for $T_{fh}$, ten individual germinal centers were analyzed and the respective mean frequency was used for further evaluation.

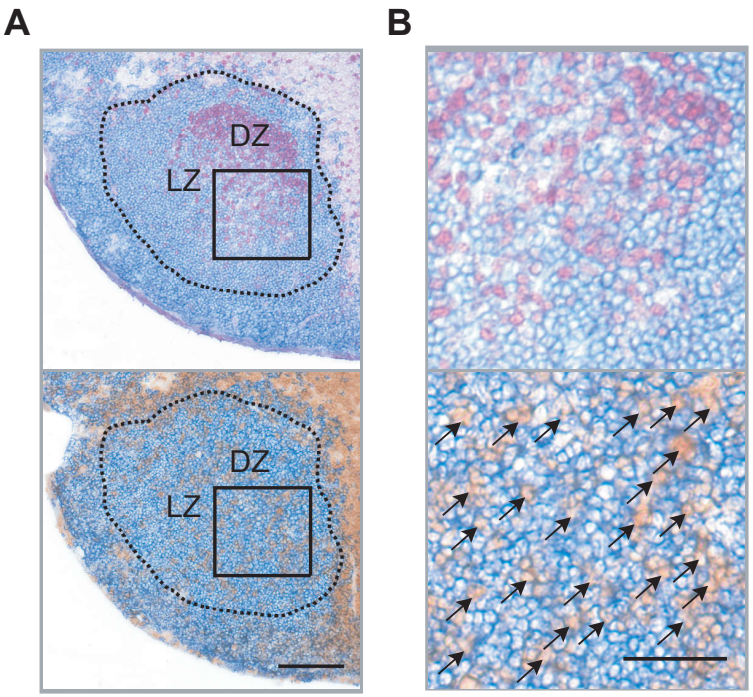


**Figure 2.6: Representative depiction of $T_{fh}$ frequency-determination in germinal centers.** Immunohistochemical staining of a serial lymph node section, depicting an identical germinal center. A) The area of a germinal center was identified via a Ki-67/B220 staining and transfered to the corresponding TCR$\beta$/B220 staining. Dashed line represents the germinal center area, solid line the area of magnification. Scale bar $\widehat{=}$ 100$\mu$m. B) Magnification of an area within the germinal center. Arrows indicate individual $T_{fh}$. For a clearer and better presentation, only a proportion of the identified $T_{fh}$ are highlighted via an arrow. Scale bar $\widehat{=}$ 50$\mu$m. B-lymphocytes (blue = B220), T-lymphocytes (brown = TCR$\beta$) and proliferating cells (red = Ki-67)) are stained. DZ = dark zone, LZ = light zone.

For assessment of the area, a calibration slide was used to define the absolute scale via the function "Set scale". Determination of the area was done using the function "Measure". The volume was further determined as product of the area and thickness of the cryosection. The frequency of T-lymphocyte was extrapolated as quotient of T-lymphocyte number and the volume.

#### 2.2.10.2 Determination of germinal center area in the B-lymphocyte zone

The relative proportion of the germinal center area within the BCZ was determined using a standardized ImageJ analysis pipeline. Whole lymph node sections were stained for Ki-67/B220. For assessment of the area, a calibration slide was used to define scale via the function "Set scale". The BCZ area was determined using the function "Measure". Likewise, the cumulative area of all germinal centers per cryosection was determined. The relative proportion of the germinal center

area within the BCZ was calculated as quotient. For each sample three individual cryosection were evaluated and the mean proportion was used for evaluation.

### 2.2.11 Statistical analysis

Data were analyzed using GraphPad Prism 6 or the open-access statistical software R v 3.4.4 and is presented as arithmetic mean ± standard deviation (SD). During analysis a visual examination was performed according to Tukey (1977). Single outlier were identified via Grubbs test (Grubbs, 1950) and when reaching significance, individual data points were excluded from the analysis. Each data set was tested for normal distribution using the D'Agostino-Pearson omnibus test (D'Agostino and Pearson, 1973). For comparison of two independent groups, the Mann-Whitney U-test (for a non-parametric data set) was used. Three or more groups were compared using One-way ANOVA with Dunnett's post-hoc test (Dunnett, 1955) or Kruskal-Wallis test (non-parametric data sets) with Dunnett's post-hoc test. Two-Way ANOVA with Dunnett's post-hoc test was used for data of three or more groups, which was based on two independent classification factors. The comparison of one-dimensional distributions was achieved using the Kolmogorov-Smirnov test (Miqueu et al., 2007). Statistical significance is denoted as: * $p < 0.05$, ** $p < 0.01$, *** $p < 0.001$.

# 3 Results

T-lymphocytes are seen as the major mediator for induction of autoimmunity. Thereby, the T-lymphocyte receptor repertoire has been investigated under autoimmune condition and showed different involvements. In the autoimmune model of immunization induced EBA, the contribution of dermal immigrating $T_{skin}$ was shown for the effector-phase. In addition, also the germinal center immigrating $T_{fh}$ were shown to be necessary for generation of disease associated auto-antibodies. However, data about the T-lymphocyte receptor repertoire of $T_{skin}$ and $T_{fh}$ are missing. Therefore, this thesis addresses, whether (I) the T-lymphocyte receptor$\beta$ repertoire of $T_{skin}$ and $T_{fh}$ shifts under autoimmune condition and (II) if $T_{fh}$ and $T_{skin}$ clonotypes overlap within an individual.

## 3.1 Dermal disruption model: scratching mediated $T_{skin}$ immigration with maintained mCOL7c specific $T_H1$ milieu

Immunization induced EBA is a chronic autoimmune disease, characterized by auto-antibodies targeting the dermal structure protein mCOL7. During pathogenesis, dermal wounds emerge, which are caused by a disruption of the dermal-epidermal adherence and subsequently formation of sub-epidermal blisters. For induction of experimental EBA, the groups PBS/TM, GST/TM and mCOL7c-GST/TM are defined. Thereby, the utilized control groups PBS/TM and GST/TM enable the distinction from auto-antigen independent processes and facilitate the detection of EBA-specific changes in T-lymphocyte receptor$\beta$ repertoire. All experimental groups represent an activation of T-lymphocytes in draining lymph nodes, but differ in the use of peptide free and peptide based immunizations and the discrimination between xeno- and auto-antibodies (Tab. 3.1). By comparison of PBS/TM against mCOL7c-GST/TM, the TiterMax mediated antigen-unspecific activation enables an exclusion of bystander T-lymphocytes (Bennett et al., 1992). Utilization of the GST/TM control group permits, on the one hand, a comparison against auto-antigen independent T-lymphocyte activation via a xeno-antigen. On the other hand, since the auto-antigen is linked to GST (Sitaru et al., 2005), this control is necessary for the detection of auto-antigen specific effects after mCOL7c-GST/TM immunization (Leyendeckers et al., 2003). Thus, an effect in response to the auto-antigen mCOL7c is only detectable by direct comparison against both control groups and has to exceed both, bystander and xeno-antigen specific effects. Also, the induction of antibodies differs between GST/TM and mCOL7c-GST/TM administration. Thereby, GST results only in xeno-antibodies (Rao et al., 2003), whereas mCOL7c-GST additional induces auto-antibodies (Sitaru et al., 2006).

**Table 3.1: Immunological conditions induced among different immunization groups.**

| Immunization group | T-lymphocyte activation in lymph nodes | Peptide immunization | Antibodies |
|---|---|---|---|
| PBS/TM | + | - | - |
| GST/TM | + | + (xeno-antigen) | + (xeno) |
| mCOL7c-GST/TM | + | + (auto-antigen) | + (auto) |

To investigate the emergence of clinical symptoms and dermal antibody deposition, SJL/J mice are immunized according to Fig. 3.1. Thereby, the experiment is running for a total of 28 days, which exceeds the time point of disease onset by 7 days (Hammers et al., 2011).

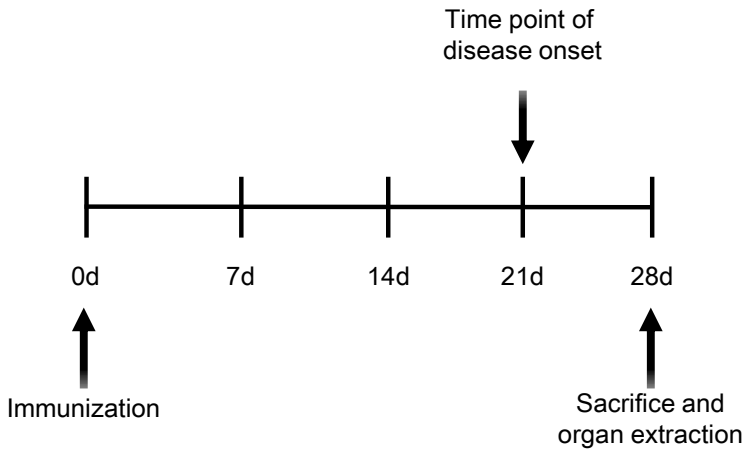


**Figure 3.1: Experimental setup for investigation of dermal wound induction.** SJL/J mice were either naïve or immunized using PBS/TM, GST/TM or mCOL7c-GST/TM (compounded according to Tab. 2.9) into both hind foot pads (Sitaru et al., 2006). The experiment was terminated on experimental day 28.

The emergence of EBA wounds is restricted to the mCOL7c-GST/TM immunization (Fig. 3.2 A). Thereby, typical fur-loss and wounds around the snout, eye and ear are observable. In a direct immunofluorescence (DIF) staining of skin biopsies, a deposition of IgG auto-antibodies is also only detectable at the DEJ after mCOL7c-GST/TM immunization (Fig. 3.2 B). In comparison to the other experimental groups, no difference compared to the naïve steady state is observable.

Thus, as expected, only the auto-antibody inducing mCOL7c-GST/TM immunization results in the EBA phenotype and shows a deposition of IgG at the DEJ.

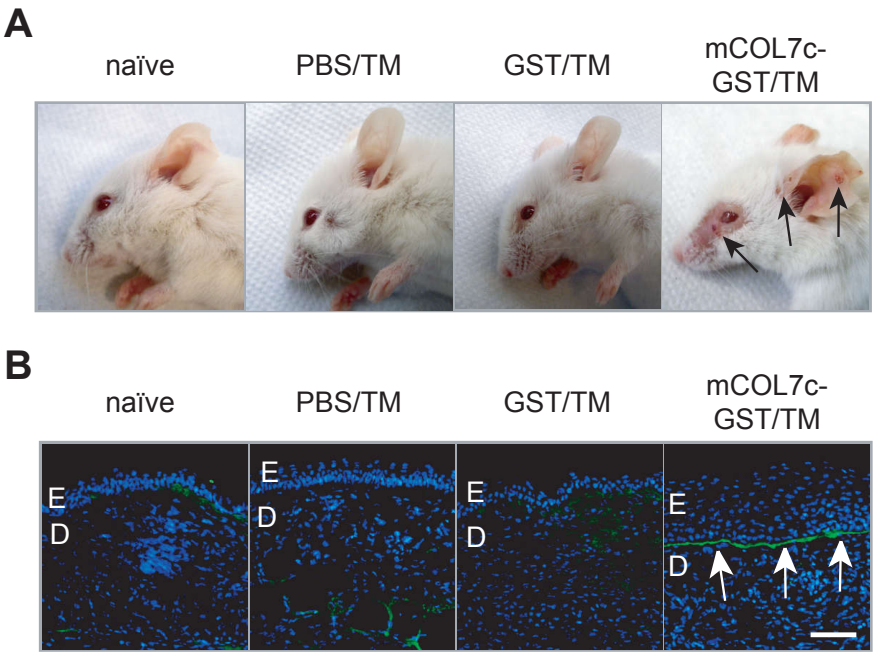


**Figure 3.2: Representative depiction of EBA wounds and IgG deposition at the DEJ among immunization groups.** SJL/J mice were either naïve or immunized using PBS/TM, GST/TM or mCOL7c-GST/TM into both hind foot pads. The experiment was terminated 28 days after immunization. A) Representative depictions of immunized mice. Arrows point at EBA wounds and specifically show erythema, dermal wounds and fur-loss. B) Deposition of IgG at the DEJ, visualized via DIF (green = IgG, blue = DAPI). Arrows point at IgG deposition. E = epidermis, D = dermis, Scale bar $\widehat{=}$ 100$\mu$m.

In summary, the appearance of EBA wounds and deposition of IgG among the immunization groups is restricted to the auto-antigen based mCOL7c-GST/TM immunization. In contrast, the remaining experimental groups do not show an EBA phenotype or general disease implications. This implies, that only after mCOL7c-GST/TM immunization an inflammatory immigration of $T_{skin}$ into dermal wounds is observable. However, to answer, whether the $T_{skin}$ T-lymphocyte receptor$\beta$ repertoire shifts under autoimmune condition, the repertoire found in EBA wounds has to be considered with regard to the $T_{skin}$ repertoire in controls. Thus, it is necessary to establish a model to compare the $T_{skin}$ repertoire of EBA mice to.

### 3.1.1 Activated $T_H1$ T-lymphocytes immigrate in endogenous wounds

Since is known that $T_{skin}$ immigrate into EBA wounds, it is initially assessed, which $T_H$-profile $T_{skin}$ in endogenous wounds exhibit. For that, mice are immunized using either PBS/TM or mCOL7c-GST/TM according to Fig. 3.1. Skin samples are collected on experimental day 28 and cellular frequencies, as well as the gene expression of $T_{skin}$-associated genes is analyzed.

In immunohistochemically stained skin sections a general thickening and immigration of neutrophils is detectable in HE and Gr-1 stainings only after mCOL7c-GST/TM immunization, respectively (Fig. 3.3 A). Additionally, an immigration of $CD4^+$, but no $CD8^+$ T-lymphocytes are observable. Quantification of the $CD4^+$ T-lymphocyte immigration via a computer based quantification (as described in Chap. 2.2.10.1) results in $50x10^2$ $\pm 5x10^2$ $CD4^+$ cells per $mm^3$ after mCOL7c-GST/TM immunization, whereas significantly less are detectable in the PBS/TM control with $3x10^2$ $\pm 1x10^2$ $CD4^+$ cells per $mm^3$ (Fig. 3.3 B). For $CD8^+$ T-lymphocytes no difference is detectable between mCOL7c-GST/TM and PBS/TM. Thus, the EBA typical dermal thickening, neutrophil and T-lymphocyte immigration is restricted to the auto-antigen based mCOL7c-GST/TM immunization. Evaluating $T_{skin}$-specific cytokines and transcription factors, IFN$\gamma$ along with T-bet and IL10 are significantly up-regulated in endogenous wounds (Fig. 3.3 C). Therefore, it has to be concluded that activated $T_H1$ immigrate into EBA wounds and constitute a pro-inflammatory milieu via IFN$\gamma$ expression.

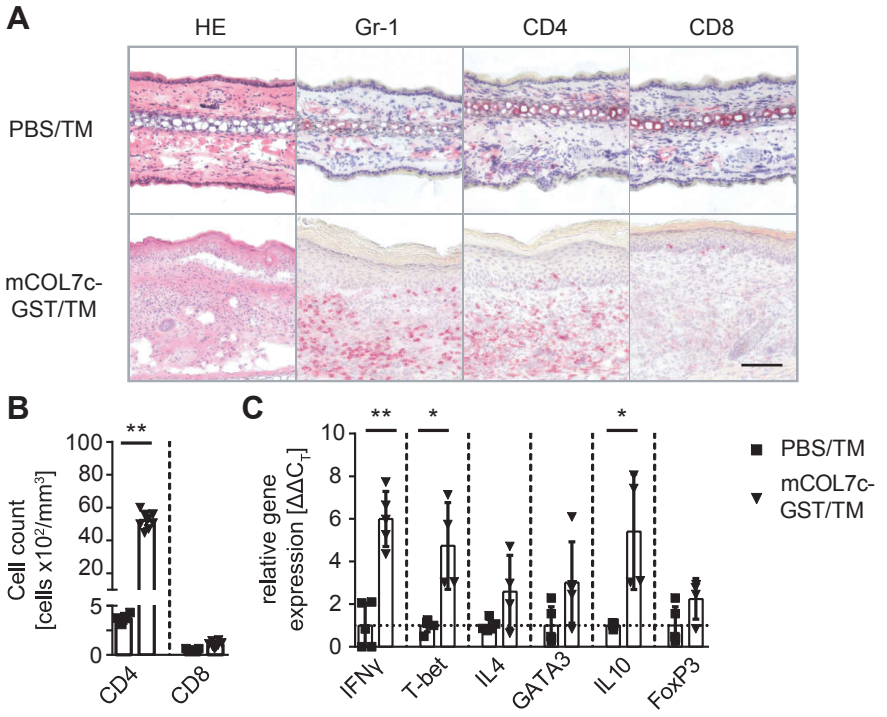


**Figure 3.3: Endogenous wounds in immunization induced EBA feature the recruitment of activated $T_H1$.** SJL/J mice were immunized using PBS/TM or mCOL7c-GST/TM into both hind foot pads. 28 days after immunization, skin samples were obtained, A) stained with HE or for the cell specific marker Gr-1, CD4 and CD8. Upper panel represents PBS/TM and lower panel mCOL7c-GST/TM. B) Cell numbers of $CD4^+$ and $CD8^+$ T-lymphocytes were evaluated via a computer based quantification (as described in Chap. 2.2.10.1). C) mRNA levels of $T_{skin}$ specific cytokines and transcription factors were determined using qRT-PCR, adjusted to the normalization factor ($N_F$) and normalized to the mean expression value of the PBS/TM group (as described in Chap. 2.2.6). Dashed line represents mean expression value of the PBS/TM group. n=4-5, scale bar $\widehat{=}$ 100$\mu$m, data is expressed as means ± SD, * $p<0.05$, ** $p<0.01$, Mann-Whitney U-test.

### 3.1.2 T-lymphocyte immigration can be induced by epidermal disruption

To compare the T-lymphocyte receptor$\beta$ repertoire of $T_{skin}$ among the immunization groups, a dermal immigration of T-lymphocytes in the non autoimmune groups has to be induced. To distinguish between the repertoire of $T_{skin}$, which specifically immigrate in response to the auto-antigen from bystander activated and random immigrating $T_{skin}$, the two control groups PBS/TM and GST/TM are used. Thereby, PBS/TM represents bystander activation of T-lymphocytes in draining lymph nodes and since the auto-antigen mCOL7c is linked to GST, the GST/TM immunization controls for auto-antigen unspecific activation of T-lymphocytes. To induce an immunization independent

immigration of $T_{skin}$ in those control groups, skin wounds are induced by scratching.

SJL/J mice are immunized according to Fig. 3.1 and at time point of disease onset, 21 days after immunization, in all experimental groups both inner sides of the ears are scratched. This is shown to remove the epidermis, while leaving the dermis intact and results in an uniform induction of wounds (Maass, 2015). Skin samples are obtained at experimental day 28 and are immunohistochemically stained with HE and for the cell specific marker Gr-1, CD4 and CD8. In an overview of representative pictures a general thickening and immigration of neutrophils is observable, displaying an uniform dermal inflammation (Fig. 3.4 A). In addition, a localization of $CD4^+$, but no $CD8^+$ T-lymphocyte-localization is detectable in scratched skin. Quantifying the number of $CD4^+$ and $CD8^+$ T-lymphocytes via a computer based quantification, reveals no differences between the immunization groups (Fig. 3.4 B). This data show, that scratching generally results in dermal inflammation and most importantly leads to an immunization independent immigration of T-lymphocytes in induced wounds. In a separate experiment, evaluating the long-term effect of scratching, it could be additionally shown, that only after mCOL7c-GST/TM immunization chronic wounds remain, whereas complete healing occurs in the other experimental groups (Fig. S1). However, since the immunization independent T-lymphocyte immigration is achieved, the question emerge, whether the pro-inflammatory $T_H1$ and an IL10 milieu, found in endogenous wounds, is maintained after scratching.

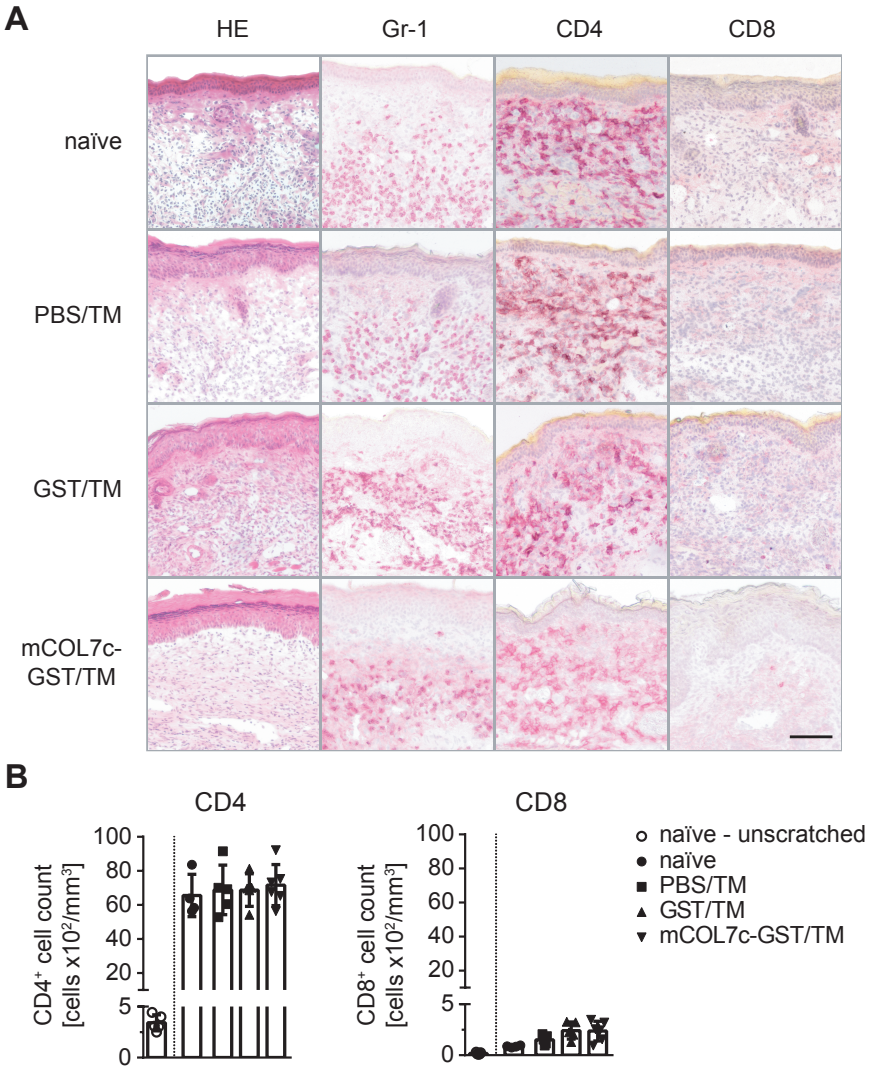


**Figure 3.4: CD4$^+$ T-lymphocytes immigrate immunization independent into scratched skin.** SJL/J mice were either naïve or immunized using PBS/TM, GST/TM or mCOL7c-GST/TM. The skin of both ears was scratched 21 days after immunization and on experimental day 28 skin samples were obtained. A) Skin sections were stained with HE and for the cell specific marker Gr-1, CD4 and CD8. B) Cell number of CD4$^+$ and CD8$^+$ T-lymphocytes was assessed via a computer based quantification. Additionally, the homeostatic CD4$^+$ and CD8$^+$ T-lymphocyte frequency in unscratched naïve skin is depicted as baseline indicator. n=4-6, scale bar $\widehat{=}$ 100$\mu$m, data is expressed as means ± SD, Kruskal-Wallis test with Dunnett's post-hoc test.

### 3.1.3 $T_H1$ and IL10 milieu are maintained after scratching in mCOL7c-GST/TM immunized mice

To test whether the pro-inflammatory $T_H1$ and an IL10 milieu of endogenous wounds is maintained after scratching, specific cytokines and transcription factors of the $T_{skin}$ subsets are an-

alyzed via a gene expression assay. The prototypical $T_H1$ cytokine IFN$\gamma$ and the transcription factor T-bet show a significantly higher expression only after mCOL7c-GST/TM immunization (Fig. 3.5 A). The expression of the $T_H2$ cytokine IL4 and the transcription factor GATA3 is not affected among all immunization groups (Fig. 3.5 B). However, IL-10 shows a significantly higher expression only after mCOL7c-GST/TM immunization, whereas FoxP3 is equally expressed among all groups (Fig. 3.5 C). This data show, that the pro-inflammatory $T_H1$ and an IL10 milieu is only inducible after scratching in mCOL7c-GST/TM immunized mice.

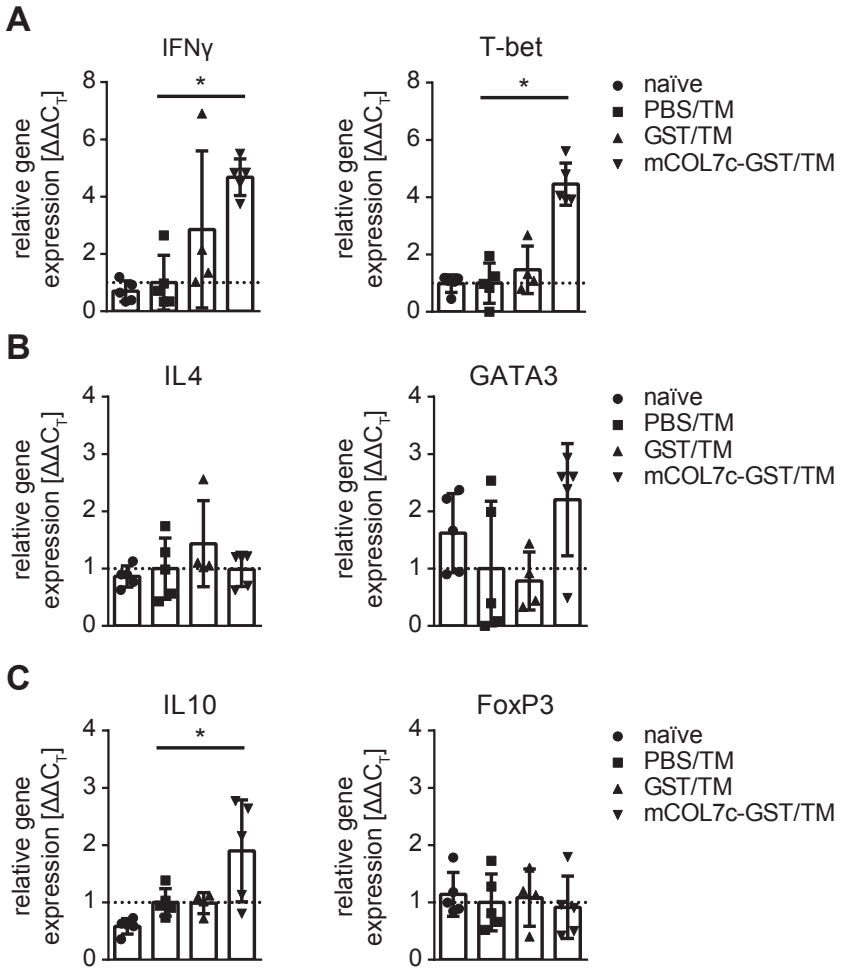


**Figure 3.5: $T_H1$ and IL10 milieu is only reflected after scratching in mCOL7c-GST/TM immunized mice.** SJL/J mice were either naïve or immunized using PBS/TM, GST/TM or mCOL7c-GST/TM. The skin of both ears was scratched 21 days after immunization and 7 days after, skin samples were obtained. mRNA levels were determined using qRT-PCR, adjusted to the $N_F$ and normalized to the mean expression value of the PBS/TM group. Specific cytokines and transcription factors of A) $T_H1$, B) $T_H2$ and C) $T_{reg}$ were evaluated. Dashed line represents mean expression value of the PBS/TM group. n=4-5, data is expressed as means ± SD, * $p<0.05$, Kruskal-Wallis test with Dunnett's post-hoc test.

In summary, scratching induces an immigration of $T_{skin}$ independent from the immunization group and only mCOL7c-GST/TM immunization reflects the milieu found in endogenous wounds. Thus, dermal disruption represents an excellent model to compare the $T_{skin}$ T-lymphocyte receptor$\beta$ repertoire among experimental groups and most important, enables evaluation of a possible auto-antigen based shift in the repertoire of $T_{skin}$ with regard to the control groups PBS/TM and GST/TM.

An elevated pro-inflammatory $T_H1$ milieu is detectable in endogenous woulds and since it is also preserved in scratching-induced wounds, one can speculate, that endogenous presence of the auto-antigen in the skin results in a specific accumulation of $T_{skin}$ in immunization induced EBA. This leads to the hypothesis, that the T-lymphocyte receptor$\beta$ repertoire of $T_{skin}$ is shifted in immunization induced EBA and comprises a different $T_{skin}$ repertoire compared to the one found in the control groups.

## 3.2 The T-lymphocyte receptor$\beta$ repertoire of $T_{skin}$ is unaffected under autoimmune condition

To analyze, if the $T_{skin}$ T-lymphocyte receptor$\beta$ repertoire shifts under autoimmune condition and whether a specific accumulation of $T_{skin}$ is detectable due to the endogenous presence of the auto-antigen mCOL7c, the repertoire of $T_{skin}$ is compared between the immunization groups. For that, the established dermal disruption model is used to trigger $T_{skin}$ immigration among the immunization groups PBS/TM, GST/TM or mCOL7c-GST/TM (according to Fig. 3.6).

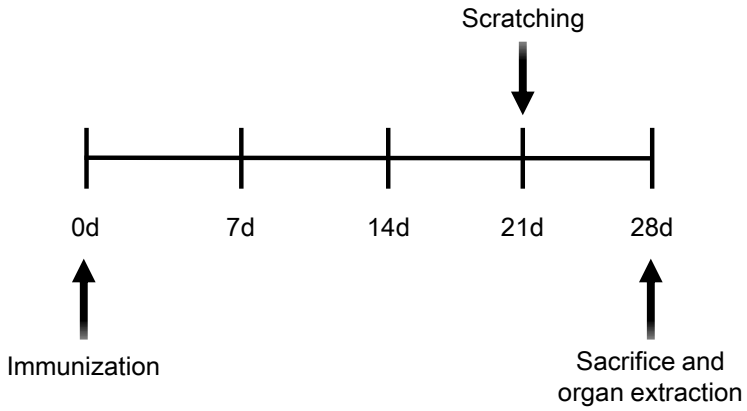


**Figure 3.6: Experimental setup for investigation of the $T_{skin}$ T-lymphocyte receptor$\beta$ repertoire.** SJL/J mice were immunized using PBS/TM, GST/TM or mCOL7c-GST/TM into both hind foot pads. On experimental day 21, the inner side of both ears was scratched. The experiment was terminated on experimental day 28.

### 3.2.1 Identical numbers of T-lymphocyte receptor$\beta$ clonotypes are obtained from $T_{skin}$

The $T_{skin}$ T-lymphocyte receptor$\beta$ repertoire is determined in a fixed number of 40 cryosections, which are obtained from scratched skin. For a comparison of the $T_{skin}$ repertoire among immunization groups, it is essential to use an equal number of T-lymphocytes as starting material. Additionally, skin samples of both ears are used in order to identify possible variations within individual wounds. To test, whether a standardized number of cryosections results in equal $T_{skin}$ numbers and subsequently $T_{skin}$ clonotypes, the dermal volume and the containing T-lymphocyte numbers are analyzed. Analysis of the dermal volumes via a computer based quantification (as described in Chap. 2.2.10.1) results in equal values of $17.8 \times 10^8 \pm 1.9 \times 10^8 \mu m^3$ for PBS/TM, $16.3 \times 10^8 \pm 5.8 \times 10^8 \mu m^3$ for GST/TM and $14.0 \times 10^8 \pm 3.9 \times 10^8 \mu m^3$ for mCOL7c-GST/TM (Fig. 3.7 A). $T_{skin}$

numbers are further calculated based on the isolated volume and cell frequencies shown in Fig. 3.4. As result, equal numbers of $T_{skin}$ between immunization groups with 11.8x$10^5$ ±2.8x$10^5$ $T_{skin}$ cells for PBS/TM, 9.6x$10^5$ ±3.4x$10^5$ $T_{skin}$ cells for GST/TM and 10.0x$10^5$ ±3.5x$10^5$ $T_{skin}$ cells for mCOL7c-GST/TM are extracted (Fig. 3.7 B). Next, the T-lymphocyte receptor$\beta$ repertoire of $T_{skin}$ is identified using a PCR-based approach and subsequent analysis via NGS. A detailed overview of sequencing results and obtained clonotype numbers is depicted in Tab. S1. To avoid any artificial diversity, which could originate from unpredictable PCR errors or unrelated bystander T-lymphocytes, only T-lymphocyte receptor$\beta$ clonotypes with a relative abundance above the median are kept for analysis (described in Chap. 2.2.7.8). Subsequently, this results in 469 ±224 $T_{skin}$ clonotypes for PBS/TM, 944 ±589 for GST/TM and 450 ±242 for mCOL7c-GST/TM with no statistical difference between immunization groups (Fig. 3.7 C). Furthermore, considering the isolated volume, $T_{skin}$ and $T_{skin}$ clonotype numbers, no difference among the left and right skin is detectable. Thus, an equal number of $T_{skin}$ results in an equal number of $T_{skin}$ T-lymphocyte receptor$\beta$ clonotypes, showing that, the repertoire of $T_{skin}$ is comparable among different skin areas and immunization groups.

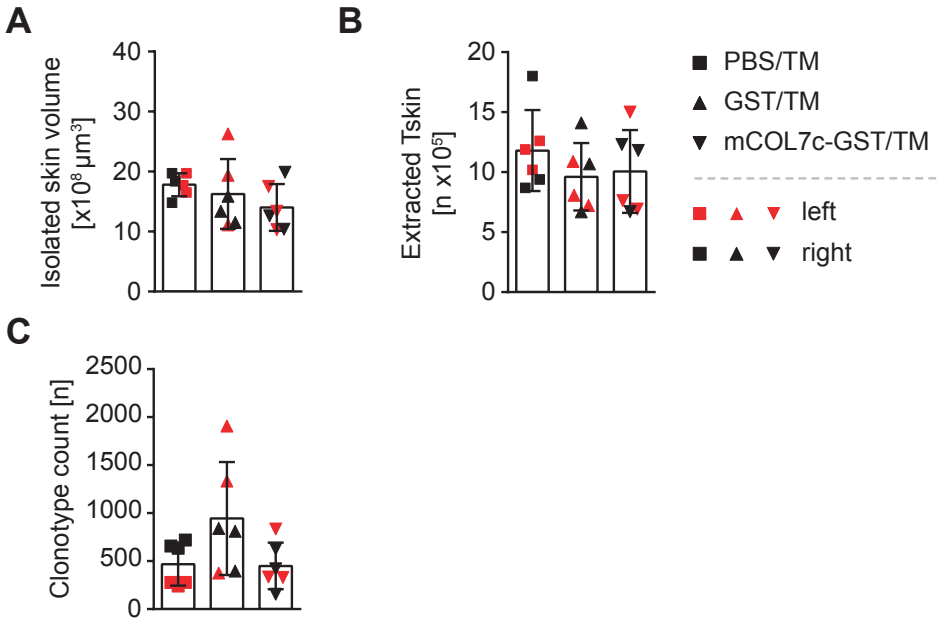


**Figure 3.7: Numbers of extracted $T_{skin}$ are equal and result in an equal number of T-lymphocyte receptor$\beta$ clonotypes.** SJL/J mice were immunized using PBS/TM, GST/TM or mCOL7c-GST/TM into both hind foot pads. The skin of both ears was scratched 21 days after immunization. 7 days after, samples of both ears were obtained and either evaluated as immunohistochemically stained cryosections or the $T_{skin}$ T-lymphocyte receptor$\beta$ repertoire was assessed via NGS. A) Isolated dermal volume per individual skin sample. B) Approximation of totally extracted $T_{skin}$ and C) number of $T_{skin}$ T-lymphocyte receptor$\beta$ clonotypes per individual skin sample. N=3 (number of mice), n=6 (two individual skin lesions per mouse), data is expressed as means ± SD, Kruskal-Wallis test with Dunnett's post-hoc test.

### 3.2.2 $T_{skin}$ T-lymphocyte receptor$\beta$ clonotypes show uniform frequency distribution among immunization groups

After obtaining an equal number of $T_{skin}$ T-lymphocyte receptor$\beta$ clonotypes, a quantitative and qualitative analysis of the $T_{skin}$ repertoire is enabled. First, the frequency distribution of $T_{skin}$ clonotypes is analyzed. Plotting the frequency of each individual clonotype in a decreasing order shows a declining frequency per group (Fig. 3.8 A). The ten most abundant clonotypes exist in frequencies between 7-1%, whereas the remaining ones are present in frequencies $< 1\%$. Surprisingly, no differences are observable among the different immunization groups. To quantify the frequency distribution, the Gini coefficient is calculated for each individual sample, indicating the degree of dispersion (described in Chap. 2.2.7.8.1). Quantification via the Gini coefficient confirms the finding of an equal frequency distribution among all groups with individual values of 0.51 ±0.09 for PBS/TM, 0.54 ±0.09 for GST/TM and 0.46 ±0.06 for mCOL7c-GST/TM (Fig. 3.8 B). In addi-

tion, comparing the frequency distribution between the left and right skin side, also no differences are detectable. Thus, the $T_{skin}$ T-lymphocyte receptor$\beta$ repertoire shows an uniform frequency distribution among immunization groups.

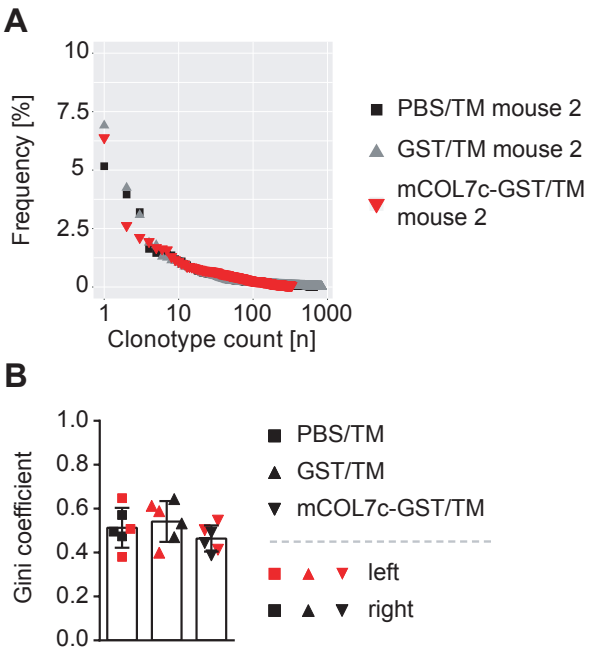


**Figure 3.8: $T_{skin}$ T-lymphocyte receptor$\beta$ clonotypes show uniform frequency distribution.** SJL/J mice were immunized using PBS/TM, GST/TM or mCOL7c-GST/TM into both hind foot pads. The skin of both ears was scratched 21 days after immunization. 7 days after, samples of both ears were obtained and the $T_{skin}$ T-lymphocyte receptor$\beta$ repertoire was analyzed via NGS. A) Frequency of the $T_{skin}$ T-lymphocyte receptor$\beta$ clonotypes alongside the entire repertoire (exemplary depiction of one individual $T_{skin}$ sample per immunization group) and B) quantification of the frequency distribution via the Gini coefficient. N=3, n=6, data is expressed as means ± SD, Kruskal-Wallis test with Dunnett's post-hoc test.

### 3.2.3 $T_{skin}$ T-lymphocyte receptor$\beta$ clonotypes immigrate auto-antigen independent

To analyze, whether identical $T_{skin}$ T-lymphocyte receptor$\beta$ clonotypes accumulate under autoimmune condition, the $T_{skin}$ repertoire is compared among the immunization groups. In an initial analysis, the shared $T_{skin}$ clonotypes are directly compared among individuals and result in mean values of 3 shared clonotypes for PBS/TM, 18 for GST/TM and 8 for mCOL7c-GST/TM (Fig. 3.9 A). Although, no statistical differences among $T_{skin}$ clonotype numbers are detected (Fig. 3.7 C), this analysis only considers absolute numbers and does not correct for different sample sizes among

the analyzed samples. To correct for the sample size, the Jaccard-Index is utilized. The index calculates the overlap of $T_{skin}$ clonotypes between two samples and divides it by the number of clonotypes that exclusively exist in either sample (described in Chap. 2.2.7.8.1). It results in values of 0.008 ±0.004 for PBS/TM, 0.012 ±0.003 for GST/TM and 0.013 ±0.004 for mCOL7c-GST/TM (Fig. 3.9 B). Thereby, GST/TM and mCOL7c-GST/TM immunizations result in a significantly higher similarity compared to PBS/TM. But since the $T_{skin}$ repertoire consists of few clonotypes present in frequencies $> 1\%$, whereas the majority exits in frequencies $< 1\%$, it is necessary to take the individual frequency of each $T_{skin}$ clonotype into account. Therefore, the Morisita-Horn-Index is comprehensively utilized, since it calculates the number of shared $T_{skin}$ clonotypes, likewise the Jaccard-Index does, and integrates their individual frequency (described in Chap. 2.2.7.8.1). This results in values of 0.015 ±0.006 for PBS/TM, 0.031 ±0.008 for GST/TM and 0.025 ±0.006 for mCOL7c-GST/TM, whereby GST/TM and mCOL7c-GST/TM immunizations show a significantly higher similarity compared to PBS/TM (Fig. 3.9 C). The comparison of both peptide based immunization, GST/TM and mCOL7c-GST/TM, results in no significant difference. Compared to the peptide free PBS/TM immunization, a generally higher rate of shared $T_{skin}$ clonotypes exists after peptide immunization. Obviously, under autoimmune condition a specific accumulation of $T_{skin}$ clonotypes is not detectable. Thus, the dermal immigration of $T_{skin}$ T-lymphocyte receptor$\beta$ clonotypes is auto-antigen independent and not affected by the endogenous presence of the auto-antigen mCOL7c in the skin.

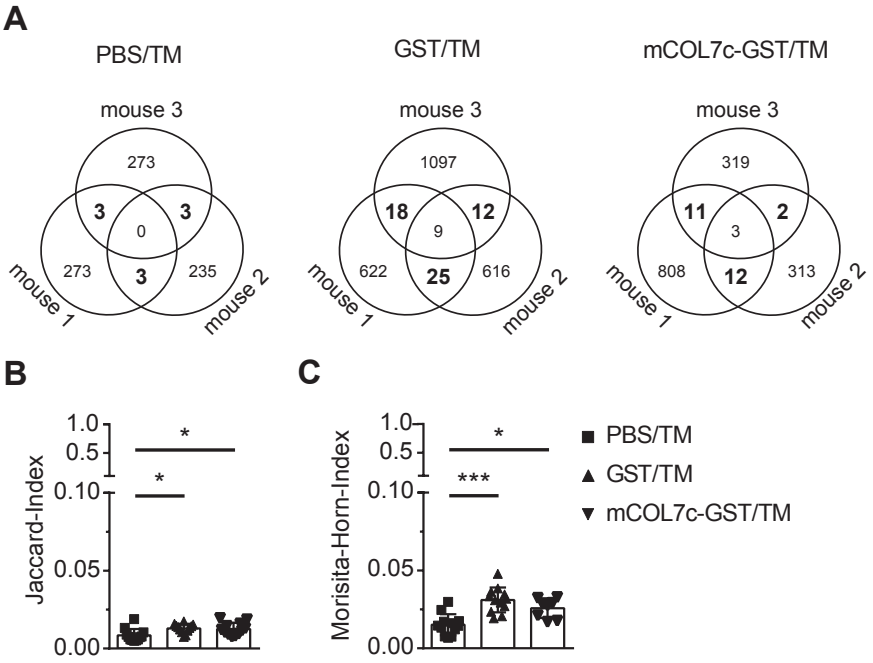


**Figure 3.9: $T_{skin}$ T-lymphocyte receptor$\beta$ clonotypes immigrate auto-antigen independent.** SJL/J mice were immunized using PBS/TM, GST/TM or mCOL7c-GST/TM into both hind foot pads. The skin of both ears was scratched 21 days after immunization. 7 days after, samples of both ears were obtained and the $T_{skin}$ T-lymphocyte receptor$\beta$ repertoire was analyzed via NGS. Similarity of $T_{skin}$ T-lymphocyte receptor$\beta$ clonotypes was assessed among individuals as A) Venn diagram (exemplary depiction of an individual $T_{skin}$ sample per mouse), B) Jaccard-Index and C) Morisita-Horn-Index. N=3, n=9-12, data is expressed as means ± SD,* $p<0.05$, *** $p<0.001$, Kruskal-Wallis test with Dunnett's post-hoc test.

### 3.2.4 The CDR3 region of $T_{skin}$ T-lymphocyte receptor$\beta$ clonotypes does not differ between immunization groups

An equal Morisita-Horn-Index among GST/TM and mCOL7c-GST/TM immunization shows a preferred immigration of $T_{skin}$ T-lymphocyte receptor$\beta$ clonotypes in mice immunized with xeno-antigen GST/TM and auto-antigen mCOL7c-GST/TM compared to mice immunized only with PBS/TM. This indicates that the accumulation of $T_{skin}$ clonotypes is higher after peptide immunization but auto-antigen independent. To take a closer look, whether specific features of T-lymphocyte receptor$\beta$ chain are altered under autoimmune condition, the CDR3 region of $T_{skin}$ clonotypes is analyzed in terms of amino acid length, nucleotide insertions and V-J-segment usage.

#### 3.2.4.1 CDR3 length and nucleotide insertions of $T_{skin}$ clonotypes are not affected under autoimmune condition

In an analysis of the $T_{skin}$ T-lymphocyte receptor$\beta$ CDR3 length, a general extent between 8 and 16 amino acids, with a peak of 12 amino acids is detectable (Fig. 3.10 A). Thereby, distribution of the CDR3 length is identical among immunization groups. Further, the comparison of totally inserted nucleotides into the CDR3 region shows, that the vast majority of $T_{skin}$ clonotypes exhibit a homogeneous insertion of 0-10 nucleotides, independent from the administered immunization (Fig. 3.10 B). Only a minor fraction comprises insertions up to 20 nucleotides. Comparing the general distribution of inserted nucleotides, no significant difference is detectable between immunization groups. Therefore, $T_{skin}$ T-lymphocyte receptor$\beta$ clonotypes are not affected in terms of CDR3 length and nucleotide insertions under autoimmune condition.

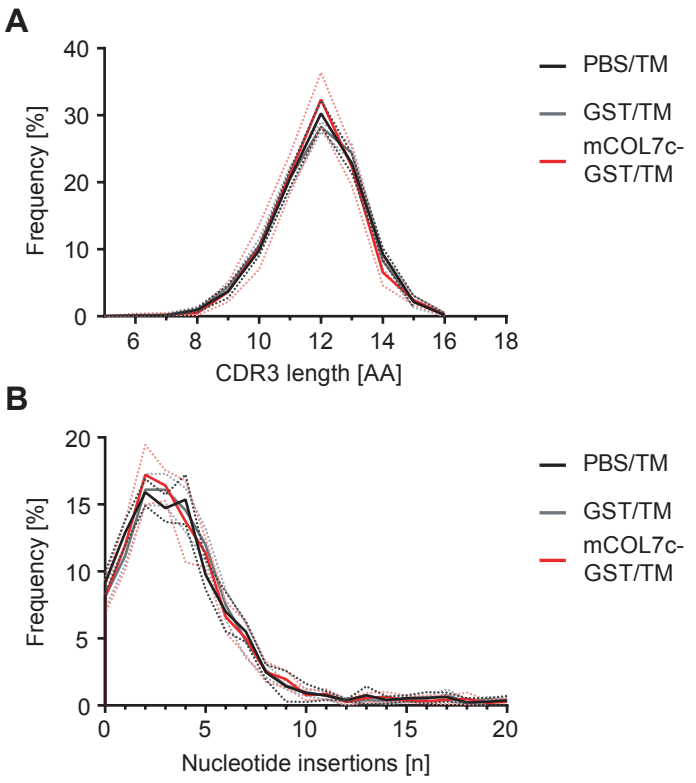


**Figure 3.10: CDR3 length and nucleotide insertions of $T_{skin}$ T-lymphocyte receptor$\beta$ clonotypes are not affected under autoimmune condition.** SJL/J mice were immunized using PBS/TM, GST/TM or mCOL7c-GST/TM into both hind foot pads. The skin of both ears was scratched 21 days after immunization. 7 days after, samples of both ears were obtained and the $T_{skin}$ T-lymphocyte receptor$\beta$ repertoire was analyzed via NGS. A) CDR3 amino acid length and B) CDR3 nucleotide insertions. N=3, n=6, data is expressed as means ± SD (surrounding dashed lines), Kolmogorov-Smirnov test.

#### 3.2.4.2 V- and J-segment usage of $T_{skin}$ clonotypes is not changed under autoimmune condition

To test whether the T-lymphocyte receptor$\beta$ V- and J-segment usage of $T_{skin}$ clonotypes is altered under autoimmune condition, the individual frequency of each V- and J-segment is analyzed for the $T_{skin}$ repertoire. A variety of distinct abundances among different V-segments is detectable (Fig. 3.11 A). Segments like V1, V19 and V26 are most prevalent, V2 to V5 are medium prevalent and V-segments like V20, V23, V24 and V31 are minor prevalent. The V-segments V12-1, V12-2, V13-1, V13-2, V13-3, V14, V15, V16 and V17 are absent due to a genomic deletion in SJL/J mice (Behlke et al., 1986; Jackson and Krangel, 2005). Comparing the individual V-segment frequency among the different immunization groups, no significant differences are detectable. Considering the J-segment usage, likewise the V-segment, a general divergent abundance among different J-segments is observable (Fig. 3.11 B). Thereby J-segments like J2-1 and J2-7 are most frequent, J-segments like J2-3, J2-4 and J2-5 are medium frequent and J-segments like J1-3, J1-4 and J1-5 are less frequent. Assessing J-segment frequencies among immunization groups does not result in significant differences. Thus, the T-lymphocyte receptor$\beta$ V- and J-segment usage of $T_{skin}$ clonotypes is not changed under autoimmune condition.

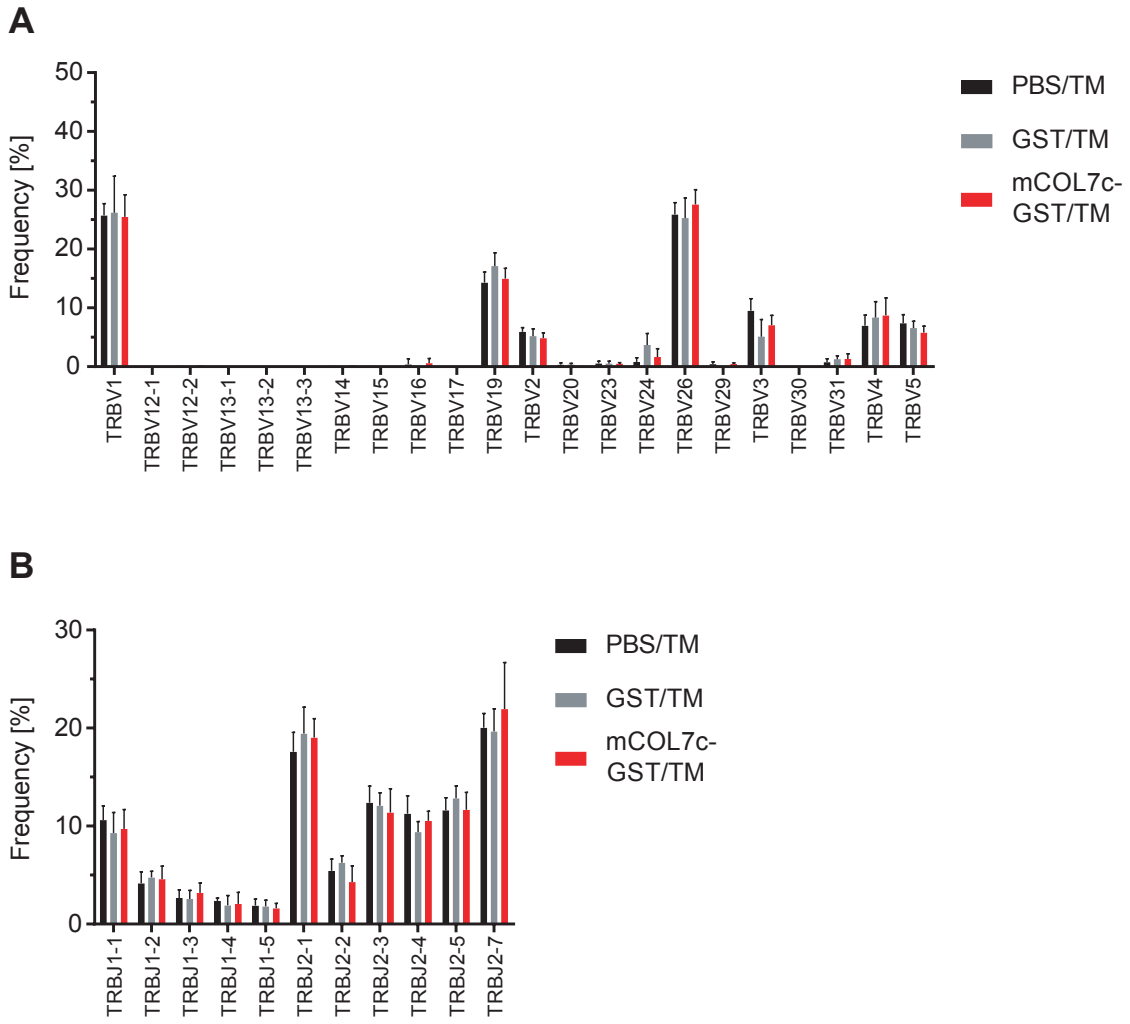


**Figure 3.11: V- and J-segment usage of $T_{skin}$ T-lymphocyte receptor$\beta$ clonotypes is not changed under autoimmune condition.** SJL/J mice were immunized using PBS/TM, GST/TM or mCOL7c-GST/TM into both hind foot pads. The skin of both ears was scratched 21 days after immunization. 7 days after, samples of both ears were obtained and the $T_{skin}$ T-lymphocyte receptor$\beta$ repertoire was analyzed via NGS. Histogram of the $T_{skin}$ T-lymphocyte receptor$\beta$ A) V-segment and B) J-segment usage. N=3, n=6, data is expressed as means ± SD, Kruskal-Wallis test with Dunnett's post-hoc test.

#### 3.2.4.3 Combined V-J-segment usage of $T_{skin}$ clonotypes is not changed under autoimmune condition

To consider the combination of the $T_{skin}$ T-lymphocyte receptor$\beta$ V-J-segments, a principle component analysis (PCA) is conducted. It takes the joined V-J-segment usage into account and therefore might reveal differences among the immunization groups. Analyzing the distribution of an individual skin sample per mouse, a general clustering of immunization groups, but no separation is

detectable (Fig. 3.12). Thus, it can be concluded, that the combined $T_{skin}$ T-lymphocyte receptor$\beta$ V-J-segment usage is not changed under autoimmune condition.

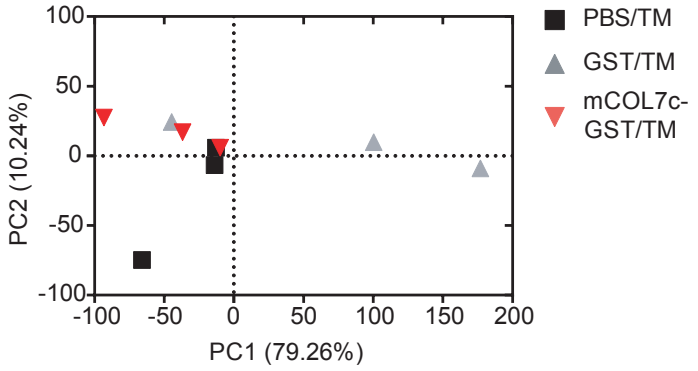


**Figure 3.12: The combined V-J-segment usage of $T_{skin}$ T-lymphocyte receptor$\beta$ clonotypes is not changed under autoimmune condition.** SJL/J mice were immunized using PBS/TM, GST/TM or mCOL7c-GST/TM into both hind foot pads. The skin of both ears was scratched 21 days after immunization. 7 days after, samples of both ears were obtained and the $T_{skin}$ T-lymphocyte receptor$\beta$ repertoire was analyzed via NGS. PCA of the combined $T_{skin}$ T-lymphocyte receptor$\beta$ V-J-segment usage. The principal component axis 1 represents 79.26% and the axis 2 10.24% of the total variance. N=3, n=3.

In summary, T-lymphocyte receptor$\beta$ analysis of skin lesions reveals that the $T_{skin}$ T-lymphocyte receptor$\beta$ repertoire does not fundamental differ between immunization groups. Although, an increased accumulation of $T_{skin}$ T-lymphocyte receptor$\beta$ clonotypes is found for GST/TM and mCOL7c-GST/TM immunizations. This leads to the hypothesis, that the immunization with both peptides induces more frequent clonotypes, which in turn can be found in dermal wounds. This data shows, that the immigration of $T_{skin}$ is a random process and indicates, that the endogenous presence of the auto-antigen in skin does not specifically trigger a $T_{skin}$ clonotype accumulation in experimental EBA.

## 3.3 The $T_{fh}$ T-lymphocyte receptor$\beta$ repertoire reveals a clonotype and V3-segment accumulation under autoimmune condition

$T_{fh}$ display the obligatory T-lymphocyte population, mandatory for EBA induction. In the immunization induced EBA model, $T_{fh}$ are the check point for maturation of auto-reactive B-lymphocytes during germinal center reaction. The detectable IgG deposition at the DEJ indicates, that $T_{fh}$ provide signals for B-lymphocytes specifically in response to the auto-antigen mCOL7c. This leads to the hypothesis, that $T_{fh}$ T-lymphocyte receptor$\beta$ clonotype specifically accumulate in germinal centers in response to the auto-antigen mCOL7c. To identify whether $T_{fh}$ clonotypes accumulate under autoimmune condition, $T_{fh}$ are isolated from germinal centers of draining lymph nodes via laser microdissection. For $T_{fh}$ analysis, the identical mice as used in Chap. 3.2 are utilized.

### 3.3.1 Uniform induction of germinal centers among immunization groups

Prior investigation of the $T_{fh}$ T-lymphocyte receptor$\beta$ repertoire, the question arise, whether germinal centers are uniformly induced in both draining lymph nodes after administration of PBS/TM, GST/TM and mCOL7c-GST/TM into both hind foot pads. Furthermore, PBS/TM immunization induces an unspecific T-lymphocyte activation in lymph nodes, but it is not known, whether this peptide free immunization is capable to induce germinal centers. To test this, cryosections of contralateral lymph nodes are immunohistochemically stained and evaluated. In an overview of representative pictures, an induction of germinal centers is observable as proliferating zones in the cortical lymph node area among all immunization groups (Fig. 3.13 A, representative pictures of both contralateral lymph nodes are depicted in Fig. S2). Magnification of an individual germinal center per immunization group exhibits the prototypic segregation in DZ and LZ (Fig. 3.13 B). Quantifying the relative germinal center area in the cortex of contralateral lymph nodes (described in Chap. 2.2.10.2) results in 17.11% ±2.89% for PBS/TM, 22.72% ±3.59% for GST/TM and 22.59% ±5.69% mCOL7c-GST/TM (Fig. 3.13 C). Comparing individual immunization groups and induction among contralateral lymph nodes, no significant differences are detectable. This demonstrates, that germinal centers are induced by all experimental immunizations and that they are homogeneously formed in contralateral lymph nodes among all immunization groups.

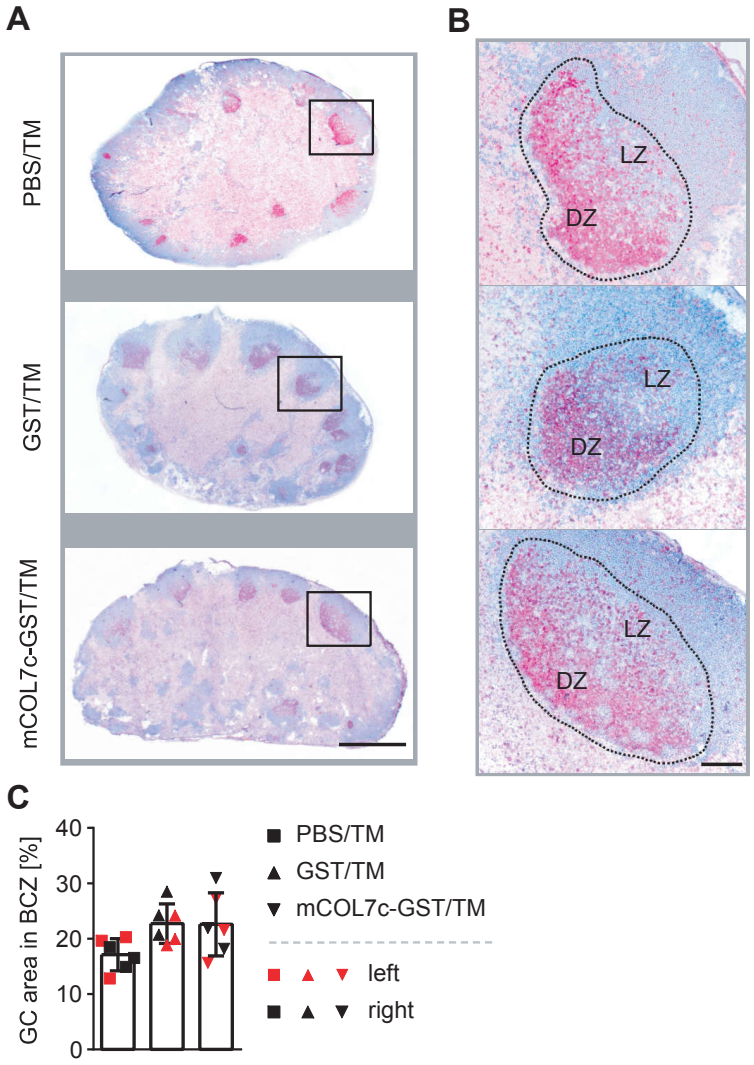


**Figure 3.13: Germinal centers are uniformly induced among immunization groups.** SJL/J mice were immunized using PBS/TM, GST/TM or mCOL7c-GST/TM into both hind foot pads. The skin of both ears was scratched 21 days after immunization. 7 days after, draining lymph nodes were obtained and 12$\mu$m cryosections were stained for proliferating cells (red = Ki-67) and B-lymphocytes (blue = B220). A) A depiction of the entire lymph node (scale bar $\widehat{=}$ 1.000$\mu$m), solid lines indicate area of magnification. B) Magnification of individual germinal centers (scale bar $\widehat{=}$ 100$\mu$m), dashed lines edge individual germinal centers. C) Quantification of the germinal center area within the BCZ. N=3, n=6, DZ = dark zone, LZ = light zone, data is expressed as means ± SD, Kruskal-Wallis test with Dunnett's post-hoc test.

### 3.3.2 Identical numbers of T-lymphocyte receptor$\beta$ clonotypes are obtained from $T_{fh}$

To compare the $T_{fh}$ T-lymphocyte receptor$\beta$ repertoire among different immunization groups, it is necessary to use an equal number of $T_{fh}$ as starting material. To account for variations among drain-

ing lymph nodes, $T_{fh}$ are extracted out of germinal centers from both contralateral lymph nodes. For that, laser microdissection is used to extract and pool individual germinal centers within a fixed volume-range of 4.5x$10^7$ ± 1x$10^7 \mu m^3$. Doing so, identical volumes of 4.1x$10^7$ ±0.2x$10^7$ $\mu m^3$ for PBS/TM, 4.1x$10^7$ ±0.7x$10^7$ $\mu m^3$ for GST/TM and 4.4x$10^7$ ±0.4x$10^7$ $\mu m^3$ for mCOL7c-GST/TM are isolated from contralateral lymph nodes (Fig. 3.14 A). Quantification of the $T_{fh}$ abundance within germinal centers, by computational quantification (as described in Chap. 2.2.10.1), results in equal frequencies of 7.7x$10^3$±0.7x$10^3$ $T_{fh}$ cells per $mm^3$ for PBS/TM, 8.2x$10^3$±0.6x$10^3$ $T_{fh}$ cells per $mm^3$ for GST/TM and 8.5x$10^3$±1.3x$10^3$ $T_{fh}$ cells per $mm^3$ for mCOL7c-GST/TM (Fig. 3.14 B). In addition to counting, $T_{fh}$ are analyzed with regard to their CD4 or CD8 positivity via an IF staining, which showed an exclusive CD4 positivity among $T_{fh}$ (Fig. S3). The extrapolation of extracted $T_{fh}$ numbers results in 3.4x$10^4$ ±0.2x$10^4$ $T_{fh}$ cells for PBS/TM, 3.5x$10^4$ ±0.2x$10^4$ $T_{fh}$ cells for GST/TM and 3.8x$10^4$ ±0.3x$10^4$ $T_{fh}$ cells for mCOL7c-GST/TM, with no significant difference between immunization groups or contralateral lymph nodes (Fig. 3.14 C). Next, individual $T_{fh}$ T-lymphocyte receptor$\beta$ clonotypes are determined via a PCR-based approach and subsequent analysis via NGS. A detailed overview of sequencing results and obtained clonotype numbers is depicted in Tab. S1. Likewise for $T_{skin}$, analysis of $T_{fh}$ T-lymphocyte receptor$\beta$ clonotypes is focused on clonotypes above the median abundance. This results in clonotype numbers of 1201 ±1270 for PBS/TM, 705 ±323 for GST/TM and 1640 ±974 for mCOL7c-GST/TM (Fig. 3.14 D). Considering isolated volumes, $T_{fh}$ frequencies, extracted $T_{fh}$ numbers, as well as $T_{fh}$ T-lymphocyte receptor$\beta$ clonotype numbers between contralateral lymph nodes, no statistical differences are detectable. Thus, the equal number of germinal center extracted $T_{fh}$, results in an equal number of $T_{fh}$ T-lymphocyte receptor$\beta$ clonotypes. This displays, that the $T_{fh}$ repertoire is comparable among contralateral lymph nodes and immunization groups.

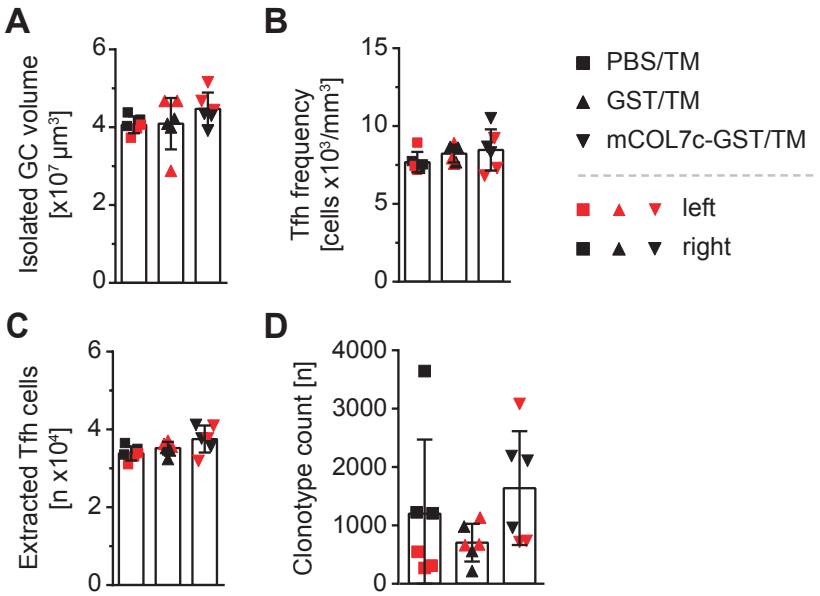


**Figure 3.14: Identical numbers of $T_{fh}$ are extracted from germinal centers and result in an equal number of T-lymphocyte receptor$\beta$ clonotypes.** SJL/J mice were immunized using PBS/TM, GST/TM or mCOL7c-GST/TM into both hind foot pads. The skin of both ears was scratched 21 days after immunization. 7 days after, the draining lymph nodes were obtained and cryosections were immunohistochemically stained. In addition, $T_{fh}$ were extracted out of the lymph nodes via laser microdissection of germinal centers and the $T_{fh}$ T-lymphocyte receptor$\beta$ repertoire was determined using NGS. A) Denoted germinal center volumes were isolated out of contralateral lymph nodes by pooling of individual germinal centers via laser microdissection. B) Quantification of the $T_{fh}$ frequency within germinal centers. C) Extrapolation of the extracted $T_{fh}$ number. D) Quantity of identified $T_{fh}$ T-lymphocyte receptor$\beta$ clonotypes per individual sample. N=3, n=6, data is expressed as means ± SD, Kruskal-Wallis test with Dunnett's post-hoc test.

### 3.3.3 $T_{fh}$ T-lymphocyte receptor$\beta$ repertoire is skewed to high frequency under autoimmune condition

Since identical numbers of $T_{fh}$ T-lymphocyte receptor$\beta$ clonotypes are obtained among immunization groups, the frequency distribution of $T_{fh}$ clonotypes is analyzed. For that, the frequency of each $T_{fh}$ clonotype is plotted in an descending order, revealing that the ten most frequent clonotypes of all immunization groups are present in frequencies of 7.5-1.2%, whereas the remaining clonotypes are present in frequencies $< 1.2\%$ (Fig. 3.15 A). But surprisingly, the top ten clonotypes after mCOL7c-GST/TM immunization are present in a higher frequency compared to PBS/TM and GST/TM. Quantifying this observation via the Gini coefficient results in values of 0.40 ±0.09 for

PBS/TM, 0.45 ±0.10 for GST/TM and 0.56 ±0.07 for mCOL7c-GST/TM (Fig. 3.15 B). Thereby, the mCOL7c-GST/TM immunization results in a significantly higher index compared to PBS/TM. Although, comparing GST/TM to PBS/TM and mCOL7c-GST/TM no difference is detectable. Additionally, comparing the frequency distribution of $T_{fh}$ clonotypes between the left and right lymph node, no difference is detectable in either immunization group. In conclusion, the data show that the injection of the auto-antigen mCOL7c has an impact on the frequency of $T_{fh}$ T-lymphocyte receptor$\beta$ clonotypes. This difference leads to the hypothesis, that identical $T_{fh}$ clonotypes accumulate between individual mice under autoimmune condition.

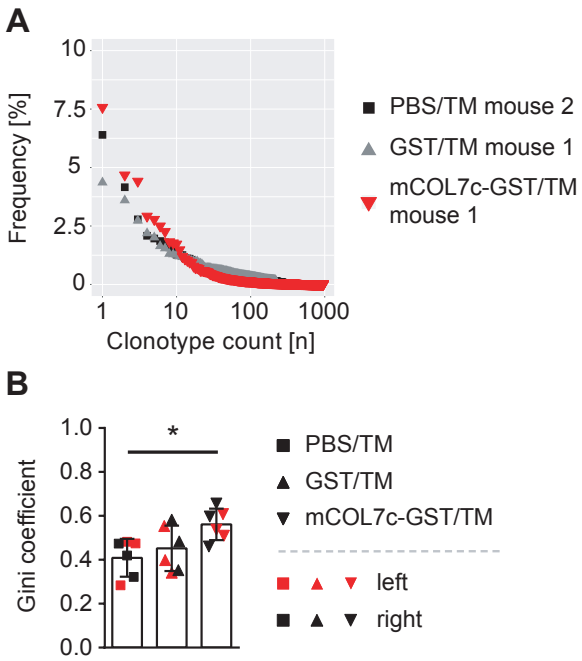


**Figure 3.15: $T_{fh}$ T-lymphocyte receptor$\beta$ repertoire is shifted to high frequent clonotypes in response to the auto-antigen mCOL7c.** SJL/J mice were immunized using PBS/TM, GST/TM or mCOL7c-GST/TM into both hind foot pads. The skin of both ears was scratched 21 days after immunization. 7 days after, $T_{fh}$ were extracted out of the lymph nodes via laser microdissection of germinal centers and the $T_{fh}$ T-lymphocyte receptor$\beta$ repertoire was determined using NGS. A) Frequency of $T_{fh}$ T-lymphocyte receptor$\beta$ clonotypes alongside the entire repertoire (exemplary depiction of one individual $T_{fh}$ sample per immunization group) and B) quantification of the frequency distribution via the Gini coefficient. N=3, n=6, data is expressed as means ± SD, * $p<0.05$, Kruskal-Wallis test with Dunnett's post-hoc test.

### 3.3.4 $T_{fh}$ T-lymphocyte receptor$\beta$ clonotypes accumulate auto-antigen specific in germinal centers

To test whether identical $T_{fh}$ T-lymphocyte receptor$\beta$ clonotypes accumulate between individual mice under autoimmune condition, the $T_{fh}$ repertoire is compared among the immunization groups. In an initial analysis, the shared $T_{fh}$ clonotypes are directly compared among individuals and result in mean values of 4 shared clonotypes for PBS/TM, 12 for GST/TM and 44 for mCOL7c-GST/TM (Fig. 3.16 A). To correct for the sample size, the Jaccard-Index is calculated and results in values of 0.010 $\pm$0.006 for PBS/TM, 0.016 $\pm$0.006 for GST/TM and 0.026 $\pm$0.005 for mCOL7c-GST/TM (Fig. 3.16 B). Thereby, mCOL7c-GST/TM immunization results in a significantly higher index compared to PBS/TM and GST/TM. As described for $T_{skin}$ in Chap. 3.2.3, the uneven distribution of $T_{fh}$ clonotype frequencies make it mandatory to consider the frequency of each individual $T_{fh}$ clonotype, therefore the Morisita-Horn-Index is determined for comprehensive evaluation. This results in values of 0.023 $\pm$0.017 for PBS/TM, 0.050 $\pm$0.019 for GST/TM and 0.080 $\pm$0.020 for mCOL7c-GST/TM (Fig. 3.16 C). As expected from the Gini coefficient, mCOL7c-GST/TM immunization leads to a significantly higher Morisita-Horn-Index compared to PBS/TM and GST/TM. Also the similarity after immunizing with the xeno-antigen GST/TM is significantly higher compared to PBS/TM. Therefore, this data show a $T_{fh}$ clonotype accumulation in response to the xeno-antigen GST, but considerably more remarkable, identical $T_{fh}$ clonotypes accumulate in response to the auto-antigen mCOL7c. Thus, the germinal center reaction among different individuals is orchestrated by accumulating $T_{fh}$ T-lymphocyte receptor$\beta$ clonotypes.

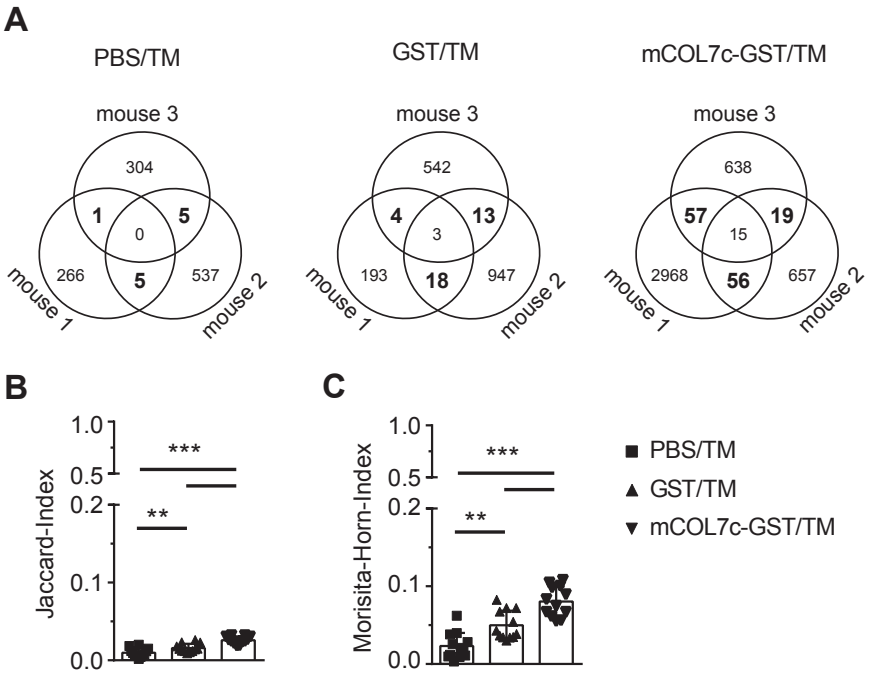


**Figure 3.16: $T_{fh}$ T-lymphocyte receptor$\beta$ clonotypes accumulate auto-antigen specific in germinal centers.** SJL/J mice were immunized using PBS/TM, GST/TM or mCOL7c-GST/TM into both hind foot pads. The skin of both ears was scratched 21 days after immunization. 7 days after, $T_{fh}$ were extracted out of the lymph nodes via laser microdissection of germinal centers and the $T_{fh}$ T-lymphocyte receptor$\beta$ repertoire was determined using NGS. Similarity of $T_{fh}$ T-lymphocyte receptor$\beta$ clonotypes is assessed among individuals as A) Venn diagram (exemplary depiction of an individual $T_{fh}$ sample per mouse), B) Jaccard-Index and C) Morisita-Horn-Index. N=3, n=12, data is expressed as means ± SD, ** $p<0.01$, *** $p<0.001$, One-way ANOVA with Dunnett's post-hoc test.

### 3.3.5 The CDR3 region of $T_{fh}$ T-lymphocyte receptor$\beta$ clonotypes is altered under autoimmune condition

Since $T_{fh}$ T-lymphocyte receptor$\beta$ clonotypes accumulate auto-antigen specific in germinal centers among individuals, it is reasonable to speculate that these differences are also reflected by specific features of the T-lymphocyte receptor$\beta$ CDR3 region. Therefore, the CDR3 region of $T_{fh}$ clonotypes is evaluated in terms of CDR3 amino acid length, nucleotide insertions, V-J-segment usage and number of shared clonotypes.

#### 3.3.5.1 CDR3 length and nucleotide insertions of $T_{fh}$ clonotypes are not changed under autoimmune condition

Analyzing length of the $T_{fh}$ T-lymphocyte receptor$\beta$ CDR3 region results in a homogeneous length of 8-16 amino acids, with a peaking number of 12 amino acids (Fig. 3.17 A). Thereby, no difference in the distribution is detectable among immunization groups. For the number of nucleotide insertions within the CDR3 region, the vast majority harbor 0-10 nucleotide insertions among all immunization groups and only a minor fraction exhibits insertions up to 20 nucleotides (Fig. 3.17 B). Calculating differences in the distribution of nucleotides results in equal insertions among immunization groups. Although $T_{fh}$ T-lymphocyte receptor$\beta$ clonotypes accumulate under autoimmune condition, the CDR3 region of is not changed in terms of length and nucleotide insertions.

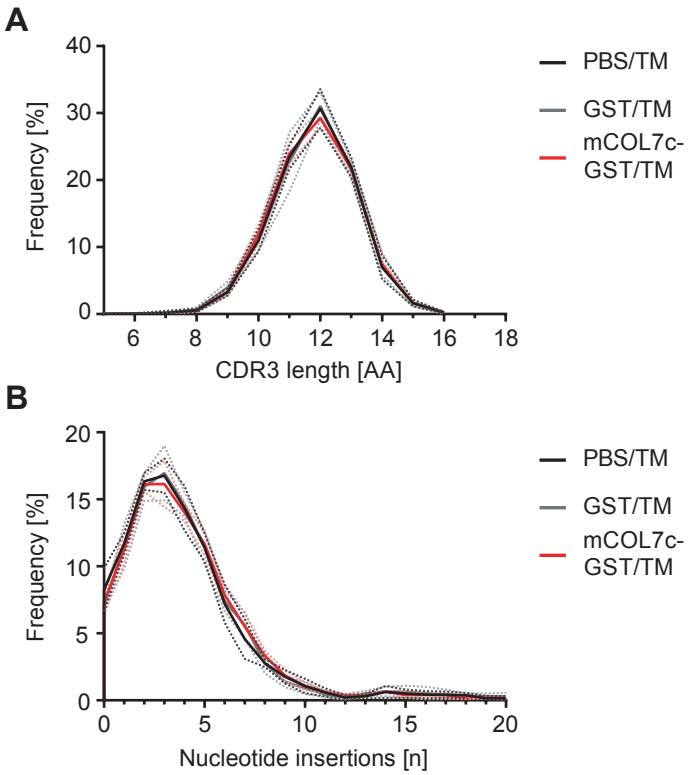


**Figure 3.17: CDR3 length and nucleotide insertions of $T_{fh}$ T-lymphocyte receptor$\beta$ clonotypes are not changed under autoimmune condition.** SJL/J mice were immunized using PBS/TM, GST/TM or mCOL7c-GST/TM into both hind foot pads. The skin of both ears was scratched 21 days after immunization. 7 days after, $T_{fh}$ were extracted out of the lymph nodes via laser microdissection of germinal centers and the $T_{fh}$ T-lymphocyte receptor$\beta$ repertoire was determined using NGS. A) CDR3 amino acid length and B) CDR3 nucleotide insertions. N=3, n=6, data is expressed as means ± SD (surrounding dashed lines), Kolmogorov-Smirnov test.

#### 3.3.5.2 Accumulating $T_{fh}$ clonotypes are characterized by the V3-segment

The accumulation of $T_{fh}$ T-lymphocyte receptor$\beta$ clonotypes under autoimmune condition might also be reflected in a characteristic T-lymphocyte receptor$\beta$ V- and/or J-segment usage. Investigating the general abundance of V-segments shows differences from most prevalent segments like V1, V19 and V26 to medium prevalent like V2, V4 and V5 to low prevalent like V20, V23, V29 and V31 (Fig. 3.18 A). V-segments like V12-1, V12-2, V13-1, V13-2, V13-3, V14, V15, V16 and V17 are absent do to a genomic deletion in SJL/J mice (Behlke et al., 1986; Jackson and Krangel, 2005). Surprisingly, comparing V-segment frequencies among immunization groups, the V3-segment exhibits a significantly higher frequency after mCOL7c-GST/TM immunization compared to PBS/TM and GST/TM. Considering the J-segments, J2-1 and J2-7 are most abundant, J2-3, J2-4 and J2-5 are medium abundant and J1-3, J1-4 and J1-5 are less abundant (Fig. 3.18 B). Also differences among the J-segment usage are detectable. The J2-4-segment, is significantly less abundant in after GST/TM immunization compared to PBS/TM and the J2-5-segment is jointly higher abundant after GST/TM and mCOL7c-GST/TM immunization compared to PBS/TM. Thus, differences in the J-segment usage are only attributable to the xeno-antigen based GST/TM immunization and are not specific for the auto-antigen mCOL7. However, considering differences in the V-segment usage, a characteristic accumulation of the V3-segment is detectable among the $T_{fh}$ clonotypes under autoimmune condition. This data show that in response to the auto-antigen mCOL7c the accumulating $T_{fh}$ T-lymphocyte receptor$\beta$ clonotypes are characterized by the V3-segment.

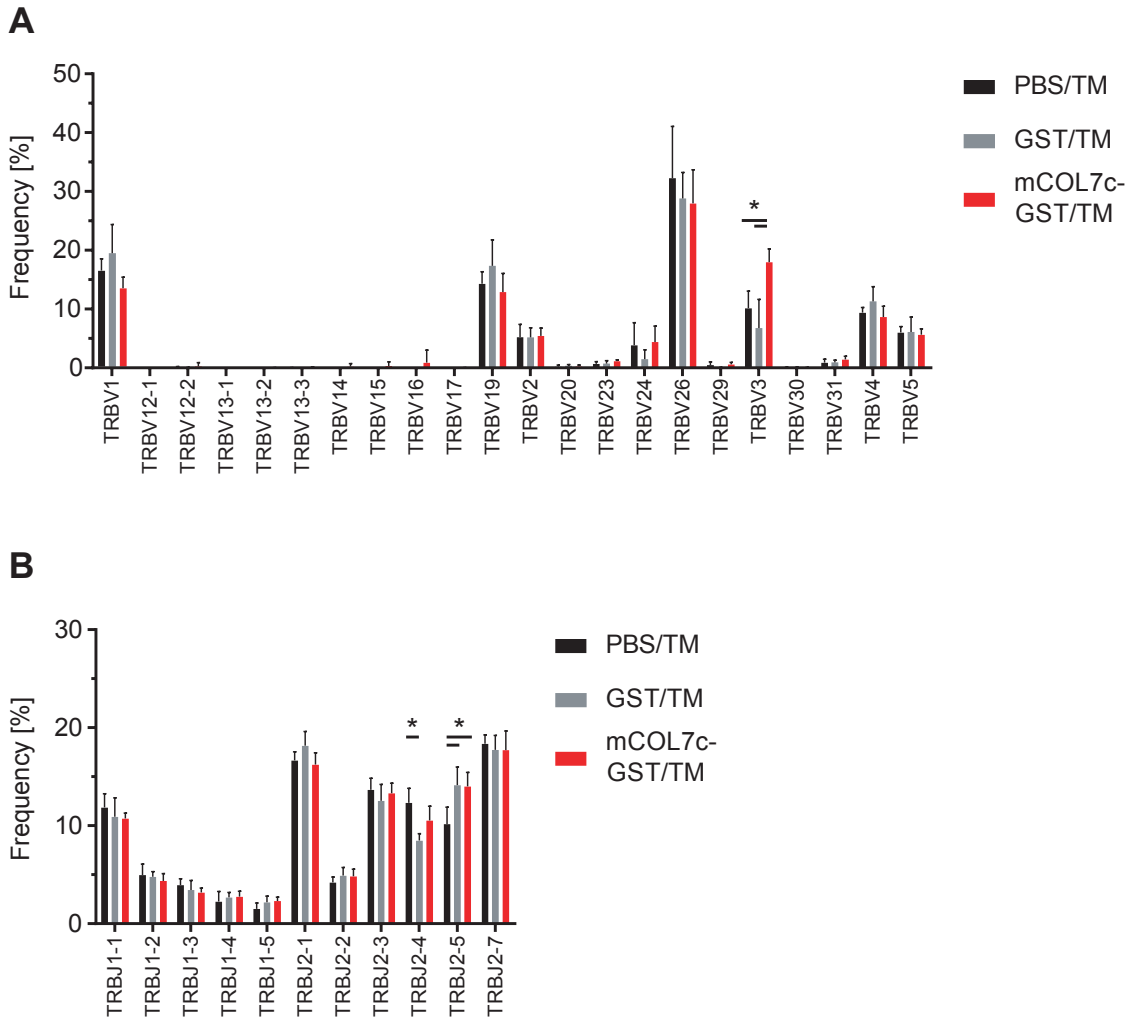


**Figure 3.18: The T-lymphocyte receptor$\beta$ V3-segment is elevated among $T_{fh}$ clonotypes under autoimmune condition.** SJL/J mice were immunized using PBS/TM, GST/TM or mCOL7c-GST/TM into both hind foot pads. The skin of both ears was scratched 21 days after immunization. 7 days after, $T_{fh}$ were extracted out of the lymph nodes via laser microdissection of germinal centers and the $T_{fh}$ T-lymphocyte receptor$\beta$ repertoire was determined using NGS. Histogram of the $T_{fh}$ T-lymphocyte receptor$\beta$ A) V-segment and B) J-segment usage. N=3, n=5-6, data is expressed as means $\pm$ SD, Kruskal-Wallis test with Dunnett's post-hoc test.

#### 3.3.5.3 Combined V-J-segment usage of $T_{fh}$ clonotypes indicates segregation under autoimmune condition

The specific accumulation of the T-lymphocyte receptor$\beta$ V3-segment among $T_{fh}$ clonotypes under autoimmune condition leads to the speculation, that those differences also have an effect on the combined V-J-segment usage. Therefore, the combined usage is assessed via PCA. Analyzing the results, PBS/TM and GST/TM immunization feature a clustering within and among the exper-

imental groups (Fig. 3.19). Interestingly, the joint V-J-segment usage after mCOL7c-GST/TM immunization, leads to a clear separation from the control groups. Certainly within the mCOL7c-GST/TM group, individual samples are segregated from each other by PC1 and also PC2. This leads to the conclusion that the V-J-segment usage is homogeneous in $T_{fh}$ clonotypes after PBS/TM and GST/TM immunization. The segregation after mCOL7c-GST/TM immunization however, indicates a specific and auto-antigen related separation, although each $T_{fh}$ clonotype sample reflects a distinct V-J-segment characteristic.

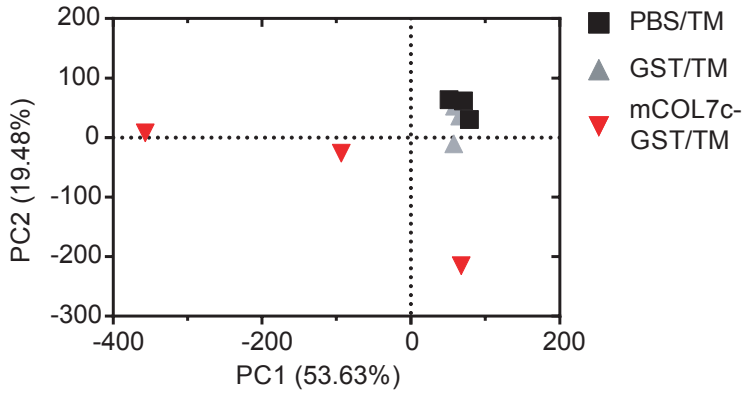


**Figure 3.19: Combined analysis of the $T_{fh}$ V-J-segment usage indicates a segregation under autoimmune condition.** SJL/J mice were immunized using PBS/TM, GST/TM or mCOL7c-GST/TM into both hind foot pads. The skin of both ears was scratched 21 days after immunization. 7 days after, $T_{fh}$ were extracted out of the lymph nodes via laser microdissection of germinal centers and the $T_{fh}$ T-lymphocyte receptor$\beta$ repertoire was determined using NGS. PCA of the combined $T_{fh}$ T-lymphocyte receptor$\beta$ V-J-segment usage. The principal component axis 1 represents 53.63% and the axis 2 19.48% of the total variance. N=3, n=3.

#### 3.3.5.4 Number of shared $T_{fh}$ clonotypes is highest under autoimmune condition

Since $T_{fh}$ T-lymphocyte receptor$\beta$ clonotypes accumulate in response to the auto-antigen mCOL7c in germinal center, the question arise, how many $T_{fh}$ clonotypes are present in one, two or all three analyzed individuals. To address this question, the unique $T_{fh}$ clonotypes per mouse are determined by combining the individual $T_{fh}$ repertoire of both contralateral lymph nodes. Based on this, the sharing count of individual $T_{fh}$ clonotypes in either one, two or three individuals is quantified as described by Madi et al. (2014). Comparing the sharing count of one, PBS/TM exhibits 6445, GST/TM 3681 and mCOL7c-GST/TM 7994 shared $T_{fh}$ clonotypes (Fig. 3.20). The sharing count of two is ascertained as 244 for PBS/TM, 113 for GST/TM and 424 shared $T_{fh}$

clonotypes for mCOL7c-GST/TM. Comparing the sharing count of three, PBS/TM and GST/TM exhibits nearly identical numbers of 18 and 13 shared $T_{fh}$ clonotypes, respectively. Surprisingly, mCOL7c-GST/TM immunization results a 3-5 times higher quantity and exhibit 65 $T_{fh}$ clonotypes to be shared among all three individuals. In a relative consideration, PBS/TM exhibits 96.09%, 3.64% and 0.27%, GST/TM 96.69%, 2.97% and 0.34% and mCOL7c-GST/TM 94.23%, 5.00% and 0.77% for the sharing counts of one, two and three, respectively. Thus, also in relative analysis the frequency of shared $T_{fh}$ clonotypes is highest in response to the auto-antigen mCOL7c. This data show, that in line with the observation of accumulating $T_{fh}$ T-lymphocyte receptor$\beta$ clonotypes, also the number and frequency of $T_{fh}$ clonotypes existing in all analyzed individuals is highest under autoimmune condition.

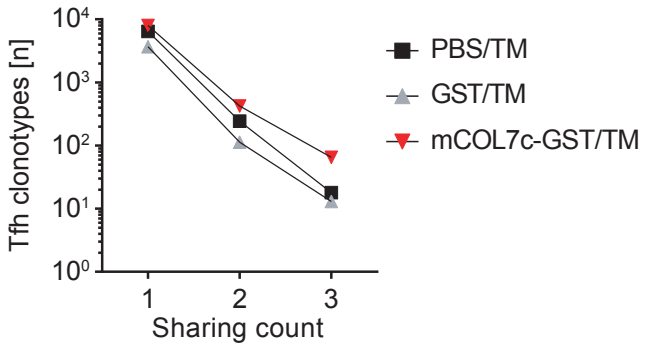


**Figure 3.20: Number of shared $T_{fh}$ T-lymphocyte receptor$\beta$ clonotype is highest in response to the auto-antigen mCOL7c.** SJL/J mice were immunized using PBS/TM, GST/TM or mCOL7c-GST/TM into both hind foot pads. The skin of both ears was scratched 21 days after immunization. 7 days after, $T_{fh}$ were extracted out of the lymph nodes via laser microdissection of germinal centers and the $T_{fh}$ T-lymphocyte receptor$\beta$ repertoire was determined using NGS. Based on the individual $T_{fh}$ repertoire of each draining lymph node, the unique $T_{fh}$ repertoire per mouse was determined and the number of shared $T_{fh}$ clonotypes among individuals was detected as described by Madi et al. (2014). The sharing count reflects the appearance of a $T_{fh}$ clonotype in one, two or three mice. N=3, n=3.

#### 3.3.5.5 Shared $T_{fh}$ clonotypes feature an elevated V3-segment accumulation

To investigate, whether shared $T_{fh}$ T-lymphocyte receptor$\beta$ clonotypes specifically express the T-lymphocyte receptor$\beta$ V3-segment, the V-segment-frequency is evaluated among those clonotypes that are detected among all three individuals (Fig. 3.20). For PBS/TM 16.67% reflect the V3-segment (Fig. 3.21 A), for GST/TM 7.70% (Fig. 3.21 B) and astoundingly, among mCOL7c-GST/TM 33.84% contain the V3-segment (Fig. 3.21 C). Considering the J-segments of $T_{fh}$ clono-

types after mCOL7c-GST/TM immunization, which are shared among three individuals and contain the V3-segment, no homogeneous usage of a J-segment is detectable (Tab. S3). This data show an elevated T-lymphocyte receptor$\beta$ V3-segment frequency after mCOL7c-GST/TM immunization among $T_{fh}$ clonotypes that are shared among all three individual. This strengthens the finding that $T_{fh}$ clonotypes, which contain the V3-segment, specifically accumulate in germinal centers under autoimmune condition.

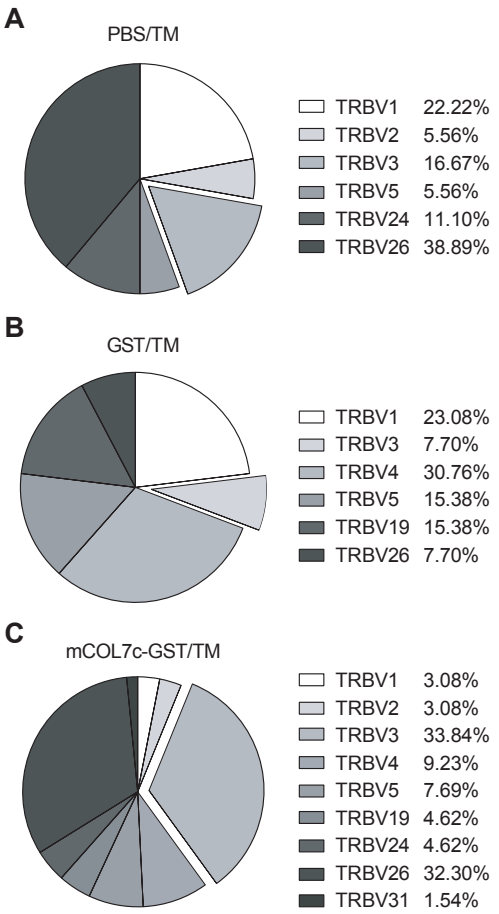


**Figure 3.21: Shared $T_{fh}$ T-lymphocyte receptor$\beta$ clonotypes feature a V3-segment accumulation.** SJL/J mice were immunized using PBS/TM, GST/TM or mCOL7c-GST/TM into both hind foot pads. The skin of both ears was scratched 21 days after immunization. 7 days after, $T_{fh}$ were extracted out of the lymph nodes via laser microdissection of germinal centers and the $T_{fh}$ T-lymphocyte receptor$\beta$ repertoire was determined using NGS. $T_{fh}$ T-lymphocyte receptor$\beta$ clonotypes, shared among three individuals, were analyzed with regard to their T-lymphocyte receptor$\beta$ V-segment usage. Composition of the V-segments found after A) PBS/TM, B) GST/TM and C) mCOL7c-GST/TM immunization. Highlighted section represents the V3-segment usage. N=3, n=3.

In summary, analysis of the $T_{fh}$ T-lymphocyte receptor$\beta$ repertoire reveals an accumulation of $T_{fh}$ clonotypes in response to the auto-antigen mCOL7c. Thereby, the T-lymphocyte receptor$\beta$ V3-segment is generally elevated in response to the auto-antigen and, even more interesting, $T_{fh}$ clonotypes that are shared among three individuals, also feature a V3-segment accumulation. Therefore, it has to be concluded that identical $T_{fh}$ clonotypes accumulate among individual mice in immunization induced EBA, which specifically share the V3-segment.

In conclusion, a diverging picture appears for EBA, whether the T-lymphocyte receptor$\beta$ repertoire of $T_{skin}$ and $T_{fh}$ shifts under autoimmune condition. On the hand, the T-lymphocyte receptor$\beta$ repertoire of $T_{skin}$ is not altered under autoimmune condition and exhibits a potential random process for dermal immigration, which is not triggered by an endogenous presence of the auto-antigen in skin. On the other hand, the T-lymphocyte receptor$\beta$ repertoire of $T_{fh}$ shows clear and specific changes in response to the auto-antigen mCOL7c. Thus, it has to be concluded, that the individual $T_H$ subsets are differently affected in immunization induced EBA and only the repertoire of $T_{fh}$ shifts under autoimmune condition.

## 3.4 Analysis of $T_{fh}$ T-lymphocyte receptor$\beta$ repertoire in contralateral lymph nodes shows high uniformity under autoimmune condition

After having found, that $T_{fh}$ T-lymphocyte receptor$\beta$ clonotypes specifically accumulate in response to the auto-antigen mCOL7c in germinal center between individual mice, the question arise, how $T_{fh}$ clonotypes are distributed within one mouse. In the immunization induced EBA model, the activation of disease mandatory $T_{fh}$ is initiated by administration of mCOL7c-GST/TM into both hind foot pads. Taking advantage of this model, where two activated lymph nodes are present and an uniform induction of germinal centers is achieved (Fig. 3.13 B and Fig. S2), the question arise, if identical $T_{fh}$ T-lymphocyte receptor$\beta$ clonotypes exist among germinal centers of the left and right draining lymph node. It is conceivable that, due to the high diversity, individual $T_{fh}$ clonotypes are only activated in a single lymph node and both contralateral comprise an unique repertoire. On the other hand, it is also possible that a set of identical $T_{fh}$ clonotypes appears in both contralateral lymph nodes. To investigate whether, contralateral lymph nodes harbor an individual or uniform $T_{fh}$ repertoire, samples of Chap. 3.3 are considered and analyzed within individuals. For that, frequency correlation, identity of $T_{fh}$ clonotypes among contralateral lymph nodes and overlap of the most prevalent clonotypes is analyzed. Additionally the data is validated via a phenotypic isolation of $T_{fh}$.

### 3.4.1 $T_{fh}$ T-lymphocyte receptor$\beta$ clonotypes are highly uniform in contralateral lymph nodes under autoimmune condition

To investigate, whether contralateral lymph nodes harbor an individual or uniform $T_{fh}$ T-lymphocyte receptor$\beta$ repertoire, the bilateral frequency of every individual clonotype is plotted in a coordinate system. Next, coherence of $T_{fh}$ clonotype frequency in contralateral lymph nodes is evaluated via a correlation. For PBS/TM no correlation is detectable, with an average correlation coefficient of 0.1784 (Fig. 3.22 A). Analyzing GST/TM, a moderate correlation with an average correlation coefficient of 0.4063 is detectable (Fig. 3.22 B), whereby the individual correlations are highly divers between the mice. However, for mCOL7c-GST/TM a strong correlation of the $T_{fh}$ clonotype frequency in contralateral lymph nodes is detectable with an average correlation coefficient of 0.7591 (Fig. 3.22 C). This leads to the conclusion that a trend towards identical frequencies exists in general after a peptide based immunization, but in response to the auto-antigen mCOL7c it is highest.

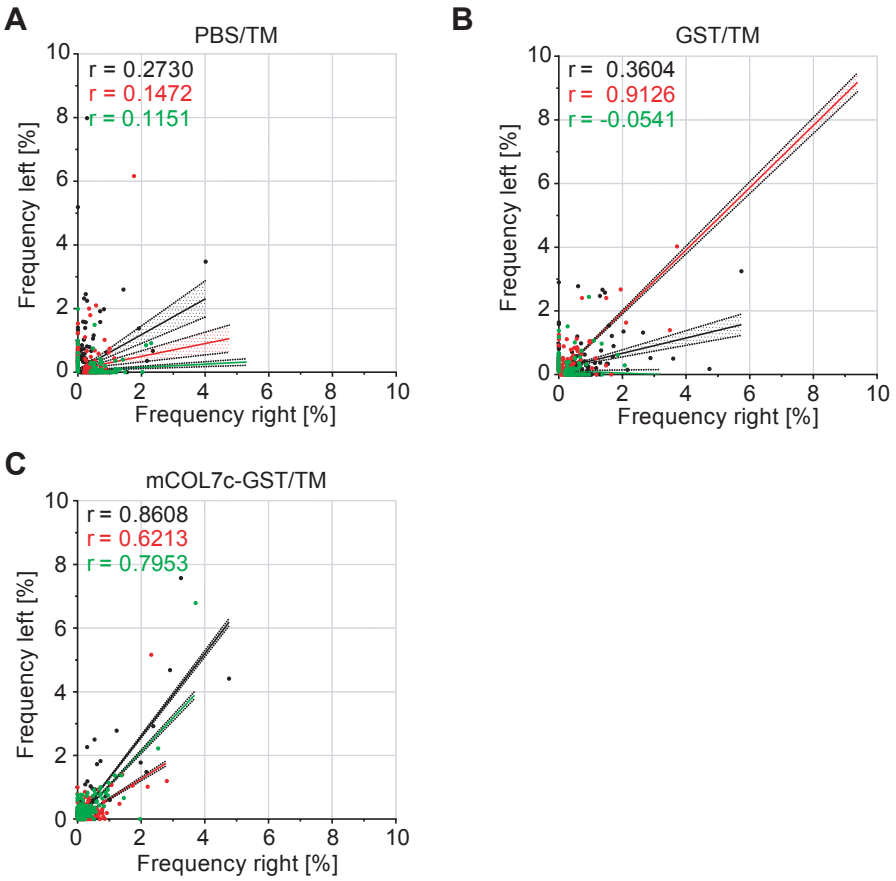


**Figure 3.22: $T_{fh}$ T-lymphocyte receptor$\beta$ repertoire positively correlates in contralateral lymph nodes under autoimmune condition.** SJL/J mice were immunized using PBS/TM, GST/TM or mCOL7c-GST/TM into both hind foot pads. The skin of both ears was scratched 21 days after immunization. 7 days after, $T_{fh}$ were extracted out of the lymph nodes via laser microdissection of germinal centers and the $T_{fh}$ T-lymphocyte receptor$\beta$ repertoire was determined using NGS. Graphs depict the $T_{fh}$ T-lymphocyte receptor$\beta$ clonotype frequencies of the left versus corresponding frequencies of the right lymph node, following A) PBS/TM, B) GST/TM and C) mCOL7c-GST/TM immunization. N=3, n=6, correlation coefficients are denoted as r, calculated linear regression with 95% confidence band is delineated.

To quantify this observation as overlap between contralateral $T_{fh}$ T-lymphocyte receptor$\beta$ clonotypes, the Morisita-Horn-Index of $T_{fh}$ clonotypes among contralateral lymph nodes is calculated. It results in values of 0.18 $\pm$0.05 for PBS/TM and 0.31 $\pm$0.15 for GST/TM, with no differences among both groups (Fig. 3.23). By analysis of the variance, a high standard deviation is observable after GST/TM immunization, which is attributable to the divers correlations. Interestingly, immunizing with mCOL7c-GST/TM results in the highest index of 0.46 $\pm$ 0.07, which is significantly higher compared to PBS/TM. However, compared to the GST/TM significance is not reached. Therefore, this data show, that $T_{fh}$ clonotypes are not only highly uniform in numbers, but also in

frequency and they constitute a highly uniform T-lymphocyte receptor$\beta$ repertoire in contralateral lymph nodes under autoimmune condition. However, also immunization with the xeno-antigen GST/TM shows a highly uniform repertoire among contralateral lymph nodes. Although, the results for GST/TM are more ambiguous compared to mCOL7c-GST/TM, it has to be additionally concluded, that also under non-autoimmune condition an uniform $T_{fh}$ T-lymphocyte receptor$\beta$ repertoire is established among contralateral lymph nodes.

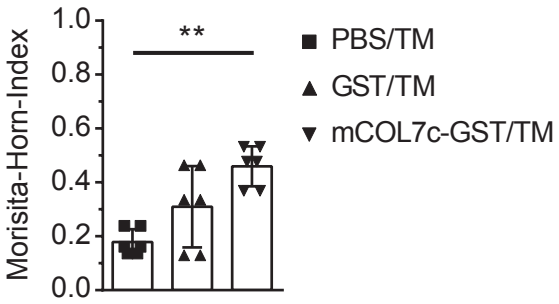


**Figure 3.23: $T_{fh}$ T-lymphocyte receptor$\beta$ repertoire is highly uniform in contralateral lymph nodes.** SJL/J mice were immunized using PBS/TM, GST/TM or mCOL7c-GST/TM into both hind foot pads. The skin of both ears was scratched 21 days after immunization. 7 days after, $T_{fh}$ were extracted out of the lymph nodes via laser microdissection of germinal centers and the $T_{fh}$ T-lymphocyte receptor$\beta$ repertoire was determined using NGS. Similarity of contralateral $T_{fh}$ T-lymphocyte receptor$\beta$ clonotypes was assessed within individuals via the Morisita-Horn-Index. N=3, n=6, data is expressed as means ± SD, ** $p<0.01$, Kruskal-Wallis test with Dunnett's post-hoc test.

### 3.4.2 Most prevalent $T_{fh}$ T-lymphocyte receptor$\beta$ clonotypes are highly identical under autoimmune condition

Taking a closer look at the most prevalent $T_{fh}$ T-lymphocyte receptor$\beta$ clonotypes the question arise, whether especially these are identical among contralateral lymph nodes. Therefore, the overlap of the 20 most prevalent clonotypes is analyzed as described by Textor et al. (2018). In this analysis, the 20 most prevalent $T_{fh}$ clonotypes are exemplarily depicted from the left lymph node. Further, it is ascertained, whether these clonotypes appear within the entire $T_{fh}$ repertoire of the right lymph node. For PBS/TM 10 (Fig. 3.24 A), for GST/TM 13 (Fig. 3.24 B) and for mCOL7c-GST/TM 19 (Fig. 3.24 C) $T_{fh}$ clonotypes are detectable among the $T_{fh}$ clonotypes of the contralateral lymph node. Thus, a general trend towards a high overlap among the most prevalent $T_{fh}$ T-lymphocyte receptor$\beta$ clonotypes is detectable under autoimmune condition.

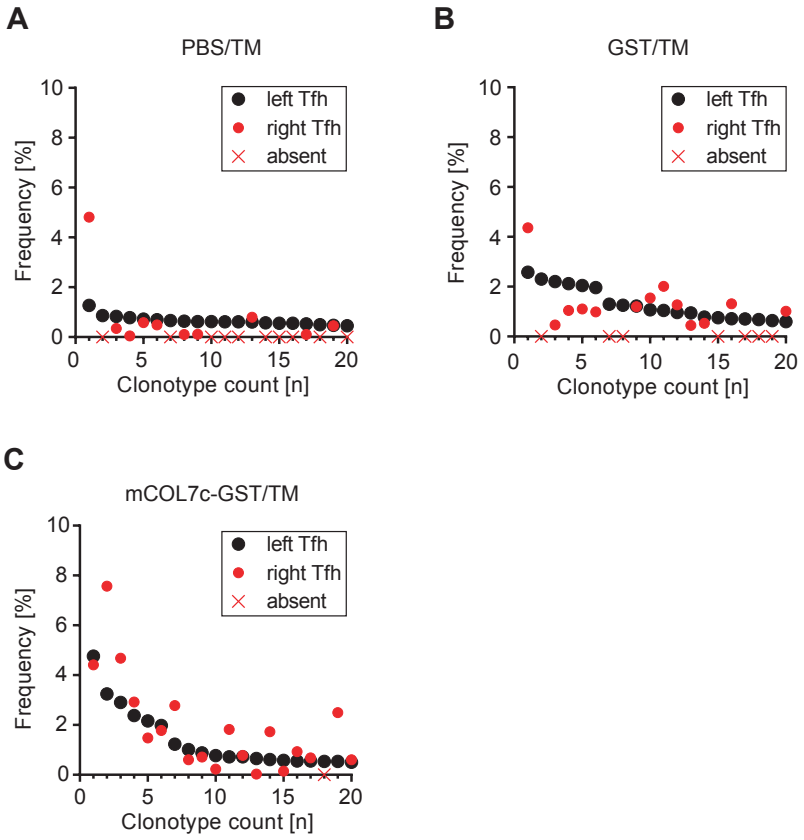


**Figure 3.24: In response to the auto-antigen mCOL7c the most prevalent $T_{fh}$ T-lymphocyte receptor$\beta$ clonotypes are highly identical.** SJL/J mice were immunized using PBS/TM, GST/TM or mCOL7c-GST/TM into both hind foot pads. The skin of both ears was scratched 21 days after immunization. 7 days after, $T_{fh}$ were extracted out of the lymph nodes via laser microdissection of germinal centers and the $T_{fh}$ T-lymphocyte receptor$\beta$ repertoire was determined using NGS. Frequencies of the 20 most prevalent $T_{fh}$ T-lymphocyte receptor$\beta$ clonotypes of the left draining lymph node were plotted in a descending order. If the exact clonotype is also present among the entire $T_{fh}$ clonotypes of the right lymph node, its frequency was additionally plotted. Representative depiction of the overlapping $T_{fh}$ clonotypes after A) PBS/TM, B) GST/TM and C) mCOL7c-GST/TM immunization. N= 1, n=2

To quantify the observed trend towards a high overlap among most prevalent clonotypes, the intersection of the 20 most prevalent $T_{fh}$ T-lymphocyte receptor$\beta$ clonotypes among the entire contralateral $T_{fh}$ repertoire is calculated. This results in an overlap of 59.2% ±18.8% for PBS/TM, 71.7% ±19.4% for GST/TM and 94.2% ±4.9% for mCOL7c-GST/TM (Fig. 3.25). Comparing mCOL7c-GST/TM against PBS/TM results in a significantly higher overlap. The difference between mCOL7c-GST/TM and GST/TM trends towards a significantly higher overlap. This data strengthens the result, that in response to the auto-antigen mCOL7c especially the most prevalent

$T_{fh}$ T-lymphocyte receptor$\beta$ clonotypes are shared among contralateral lymph nodes.

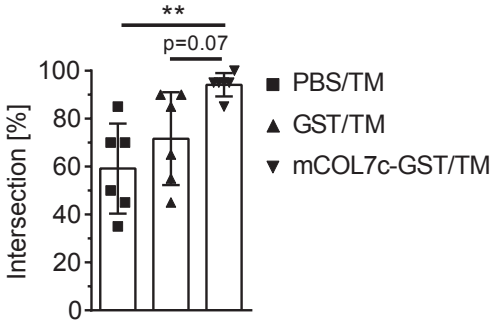


**Figure 3.25: Most prevalent contralateral $T_{fh}$ T-lymphocyte receptor$\beta$ clonotypes are highly identical under autoimmune condition.** SJL/J mice were immunized using PBS/TM, GST/TM or mCOL7c-GST/TM into both hind foot pads. The skin of both ears was scratched 21 days after immunization. 7 days after, $T_{fh}$ were extracted out of the lymph nodes via laser microdissection of germinal centers and the $T_{fh}$ T-lymphocyte receptor$\beta$ repertoire was determined using NGS. Intersection of the 20 most prevalent $T_{fh}$ T-lymphocyte receptor$\beta$ clonotypes among the entire contralateral $T_{fh}$ repertoire is depicted. N=3, n=6, data is expressed as means ± SD, ** $p<0.01$, Kruskal-Wallis test with Dunnett's post-hoc test.

### 3.4.3 Phenotypic isolation of $T_{fh}$ verifies positive correlation and uniformity of the $T_{fh}$ T-lymphocyte receptor$\beta$ repertoire

The observation of a correlating and highly uniform $T_{fh}$ T-lymphocyte receptor$\beta$ repertoire is based on the isolation of $T_{fh}$ by their localization within germinal centers and pooling via laser microdissection. Using this method, the extraction of germinal centers is methodically restricted to a certain region of the lymph node. Thereby, being limited to a restricted area for germinal center mediated $T_{fh}$ extraction results in the question, whether a location-independent isolation of $T_{fh}$ validates the correlation and uniformity among the $T_{fh}$ clonotypes in contralateral lymph nodes. For that, an independent experiment is conducted, in which a phenotypic isolation of $T_{fh}$ via Fluorescence-activated cell sorting (FACS) is established. After the anatomic structure of both lymph node is resolved, the identification of $T_{fh}$ is achieved via detection of the $T_{fh}$-specific surface-proteins CD4, CxCR5 and PD-1 (Fig. 3.26 A) (Baumjohann et al., 2013). The analysis of cellular frequencies results in uniform values of 17.9% ±2.8% for $CD4^+$ and 2.2% ±0.1% for $T_{fh}$ among contralateral lymph nodes (Fig. 3.26 B). $T_{fh}$ are isolated via FACS and an uniform cell number of $4.6x10^4$ ±$0.6x10^4$ $T_{fh}$ cells is obtained (Fig. 3.26 C). Determination of individual $T_{fh}$ T-lymphocyte receptor$\beta$ clonotypes results in 5781 ±868 clonotypes (Fig. 3.26 D), a detailed overview

of sequencing results and obtained clonotype numbers is depicted in Tab. S2. Consideration of the $T_{fh}$ clonotype frequency in contralateral lymph nodes results in a strong correlation with an average correlation coefficient of 0.8388 (Fig. 3.26 E) and a complete overlap of the 20 most prevalent $T_{fh}$ clonotypes (Fig. 3.26 F). To quantify, whether contralateral lymph nodes harbor an uniform $T_{fh}$ repertoire, the Morisita-Horn-Index is calculated and results in a value of $0.71 \pm 0.11$ (Fig. 3.26 G). Thus, the results obtained by phenotypic isolation of $T_{fh}$ verify the positive correlation and high uniformity of the $T_{fh}$ T-lymphocyte receptor$\beta$ clonotypes in contralateral lymph nodes.

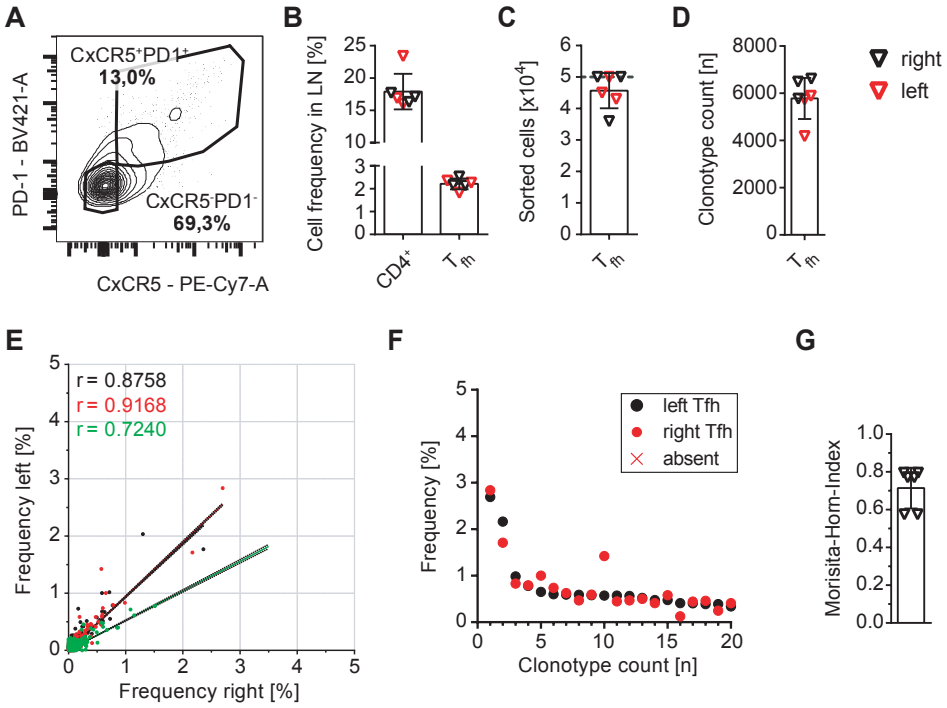


**Figure 3.26: Phenotypic isolation of $T_{fh}$ verifies the uniformity of the contralateral $T_{fh}$ T-lymphocyte receptor$\beta$ clonotypes.** In an independent experiment SJL/J mice were immunized using mCOL7c-GST/TM into both hind foot pads. The skin of both ears was scratched 21 days after immunization. 7 days after, the draining lymph nodes were extracted and $T_{fh}$ were identified using FACS via A) gating for $CD4^+$ and $CxCR5^+$, $PD\text{-}1^+$ co-expressing cells (entire gating is depicted in Fig. S4). The frequency of B) $CD4^+$ and $T_{fh}$ cells was assessed and C) up to $5x10^4$ $T_{fh}$ were sorted. The $T_{fh}$ T-lymphocyte receptor$\beta$ repertoire of sorted $T_{fh}$ cells was determined via NGS. D) Quantity of identified $T_{fh}$ T-lymphocyte receptor$\beta$ clonotypes per individual sample. E) Correlation of $T_{fh}$ clonotypes from contralateral lymph nodes. F) Overlap of 20 most prevalent $T_{fh}$ clonotypes was evaluated and is representatively depicted. G) Similarity of $T_{fh}$ clonotypes is assessed within individuals via the Morisita-Horn-Index. N=3, n=6, data is expressed as means $\pm$ SD, correlation coefficients are denoted as r, calculated linear regression with 95% confidence band is delineated.

In summary, analysis of the $T_{fh}$ T-lymphocyte receptor$\beta$ clonotypes in an individual result in a highly uniform $T_{fh}$ repertoire within contralateral lymph nodes under autoimmune condition. Thereby, the frequency of $T_{fh}$ clonotypes positively correlates and specifically the most prevalent are shared among the contralateral lymph nodes of an individual. However, a similar picture is also observable using a xeno-antigen based GST/TM immunization. This leads to the conclusion, that draining lymph nodes comprise an uniform $T_{fh}$ repertoire after a peptide immunization, but the uniformity is highest in response to the auto-antigen mCOL7c. Therefore, this data strongly suggests an active exchange of $T_{fh}$ clonotypes among contralateral lymph nodes, since the overall high diversity of the T-lymphocyte repertoire makes a parallel and independent activation of identical $T_{fh}$ clonotypes extremely unlikely. Thus, the uniform $T_{fh}$ repertoire could be explained by a migration of $T_{fh}$.

### 3.4.4 Uniformity of the $T_{fh}$ T-lymphocyte receptor$\beta$ repertoire is initiated early and segregates at late time points

The data obtained from day 28 shows a highly uniform $T_{fh}$ T-lymphocyte receptor$\beta$ repertoire in contralateral lymph nodes at the time point of disease onset. This raises the question, whether the uniform $T_{fh}$ repertoire also exists before and after disease induction. To investigate this, the contralateral $T_{fh}$ repertoire is analyzed during EBA progression. As time points, 14, 28 and 49 days after immunization are selected. These reflect a pre-diseased time point with circulating auto-antibodies (14d), the time point of regular diseases manifestation (28d) and a chronic time point (49d) (Sitaru et al., 2006; Hammers et al., 2011; Tiburzy et al., 2013).

#### 3.4.4.1 Uniformity of the $T_{fh}$ T-lymphocyte receptor$\beta$ repertoire synchronizes during onset and segregates during chronic EBA manifestation

For analysis, whether the uniform $T_{fh}$ T-lymphocyte receptor$\beta$ repertoire also exists before and after disease induction, similarity of $T_{fh}$ clonotypes among contralateral lymph nodes is analyzed via the Morisita-Horn-Index 14, 28 and 49 days after immunization. Initially 14 days after mCOL7c-GST/TM immunization, the index results in significantly higher values of 0.35 $\pm$0.08 compared to PBS/TM with values of 0.18 $\pm$0.05 (Fig. 3.27). Ongoing to the time point of regular disease induction, 28 days after mCOL7c-GST/TM immunization, uniformity peaks with a maximum index of 0.46 $\pm$0.07, which is significantly higher compared to PBS/TM, but not different compared to the 14 day time point. Interestingly, during chronic manifestation 49 day after mCOL7c-GST/TM immunization, the index declines to values of 0.24 $\pm$0.08, resulting in a significantly lower uniformity compared to 28 days and no statistical difference compared to PBS/TM. This leads to the

conclusion, that the pre-diseased uniformity is equal to the time point of induction, reaches the maximum at disease onset and declines to control levels during chronic manifestation.

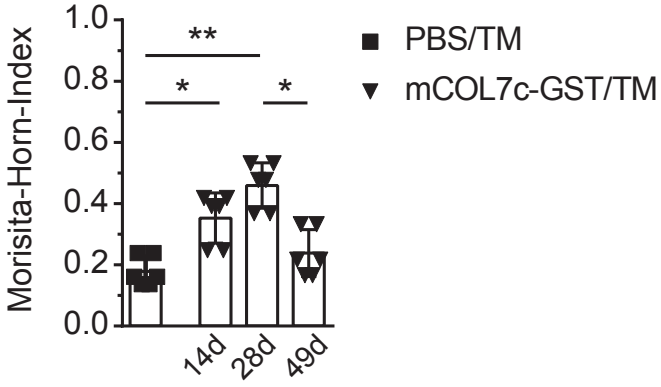


**Figure 3.27: Identity of $T_{fh}$ T-lymphocyte receptor$\beta$ repertoire synchronizes during onset and segregates during chronic establishment.** SJL/J mice were immunized using PBS/TM, GST/TM or mCOL7c-GST/TM into both hind foot pads. The skin of both ears was scratched 7 days prior end of the experiment. 7 days after, on experimental days 14, 28 or 49, $T_{fh}$ were extracted out of the lymph nodes via laser microdissection of germinal centers and the $T_{fh}$ T-lymphocyte receptor$\beta$ repertoire was determined using NGS. Similarity of contralateral $T_{fh}$ T-lymphocyte receptor$\beta$ clonotypes was assessed within individuals via the Morisita-Horn-Index. N=3, n=6, data is expressed as means ± SD, * $p<0.05$, ** $p<0.01$, Kruskal-Wallis test with Dunnett's post-hoc test.

#### 3.4.4.2 Most prevalent $T_{fh}$ T-lymphocyte receptor$\beta$ clonotypes are maintained in an individual during EBA

Since the uniformity of $T_{fh}$ T-lymphocyte receptor$\beta$ clonotypes synchronizes during onset and segregates during chronic EBA manifestation, the question arise, whether $T_{fh}$ clonotypes, that are presents at the pre-diseased time point, are maintained in an individual during chronic EBA manifestation. Therefore, the $T_{fh}$ repertoire is analyzed within an individual at two consecutive time points and the persistence of individual $T_{fh}$ clonotypes is assessed. For this, experimental samples acquired by Ellebrecht et al. (2016), where an individual draining lymph node was surgically removed prior disease onset at experimental day 15 after mCOL7c-GST/TM immunization and the contralateral during chronic disease manifestation 71 days after immunization, are analyzed with regard to the persistence of $T_{fh}$ clonotypes. Initially, to consider whether $T_{fh}$ clonotypes are maintained, the 20 most prevalent $T_{fh}$ clonotypes found on experimental day 15 are exemplarily depicted and compared to experimental day 71 (Fig. 3.28 A). Thereby, 16 $T_{fh}$ clonotypes are

maintained in an individual during chronic EBA development. Interestingly, in the vice versa consideration only 5 of the most prevalent $T_{fh}$ clonotypes found on experimental day 71 are also present at experimental day 15 (Fig. 3.28 B). Quantifying the intersection among most prevalent $T_{fh}$ clonotypes of both time points results in a significantly higher frequency of 71.3% ±16.5% considering experimental day 15 within experimental day 71, compared to 22.5% ±8.7% considering experimental day 71 within experimental day 15 (Fig. 3.28 C). By comparing the intersection of the entire $T_{fh}$ repertoire, equal values of 14.3% ±3.2% for experimental day 15 within experimental day 71 and 9.5% ±2.3% for experimental day 71 within experimental day 15 are revealed. Therefore, it has to be concluded, that the most prevalent $T_{fh}$ T-lymphocyte receptor$\beta$ clonotypes, present in germinal centers prior disease onset, are maintained in an individual during chronic disease manifestation.

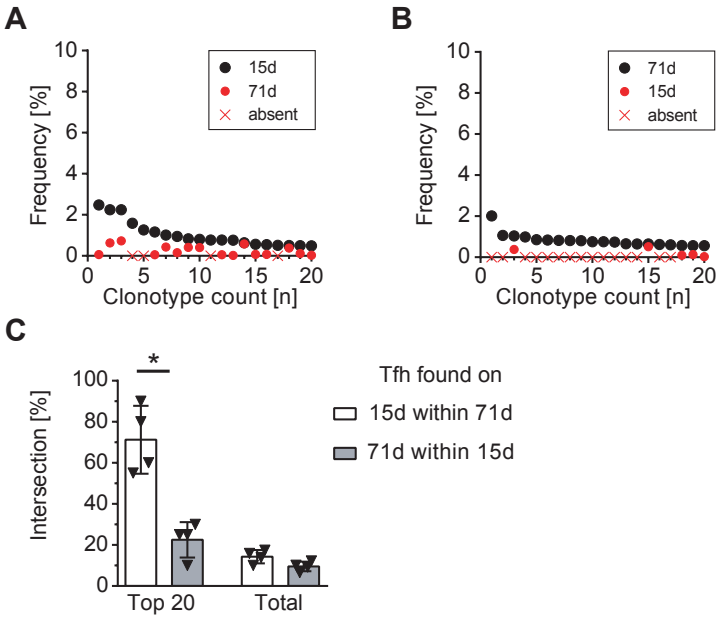


**Figure 3.28: Most prevalent $T_{fh}$ T-lymphocyte receptor$\beta$ clonotypes are maintained in an individual during chronic EBA establishment.** SJL/J mice were immunized using mCOL7c-GST/TM into both hind foot pads. An individual draining lymph node was surgically removed on experimental day 15, the contralateral on experimental day 71 (Ellebrecht et al., 2016). $T_{fh}$ were extracted via laser microdissection of germinal centers and the $T_{fh}$ T-lymphocyte receptor$\beta$ repertoire was determined using NGS. Frequency of the most prevalent $T_{fh}$ T-lymphocyte receptor$\beta$ clonotypes was plotted in a descending order. If the exact $T_{fh}$ clonotype was also present among the entire $T_{fh}$ clonotypes of the contralateral lymph node, its frequency was additionally plotted. One representative example of the 20 most prevalent $T_{fh}$ clonotypes found on A) experimental day 15 within experimental day 71 and B) experimental day 71 within experimental day 15. C) Intersection of the 20 most frequent $T_{fh}$ clonotypes and the entire repertoire among the contralateral lymph nodes. N=4, n=4, data is expressed as means ± SD, * $p<0.05$, Mann-Whitney U-test.

In conclusion, analysis of $T_{fh}$ within individuals reveals a highly uniform $T_{fh}$ T-lymphocyte receptor$\beta$ repertoire in germinal centers of contralateral lymph nodes under autoimmune condition. Thereby, not only the uniformity is highly similar, also the frequency of $T_{fh}$ clonotypes correlates among contralateral lymph nodes and specifically the most prevalent are shared. Furthermore, this uniformity of the $T_{fh}$ repertoire is initiated at early time points and segregates during chronic establishment of EBA, whereby the most prevalent clonotypes are maintained over time. However, consideration of the xeno-antigen GST, which shows comparable results regarding the contralateral $T_{fh}$ repertoire, indicates that this process is not only restricted to autoimmune condition, rather the constitution of uniformity is a peptide based process.

## 3.5 Appearance of $T_{fh}$ T-lymphocyte receptor$\beta$ clonotypes in the skin is centered to most prevalent clonotypes and emerges auto-antigen independent

The analysis of $T_{fh}$ T-lymphocyte receptor$\beta$ clonotypes within an individual shows a highly uniform $T_{fh}$ repertoire. Furthermore, it is shown, that the uniformity is initiated early and segregates during chronic establishment of EBA. The likeliest explanation for this observation is a migration of $T_{fh}$ between contralateral lymph nodes and since both contralateral popliteal lymph nodes are not directly connected via lymphatic vessels (Zhang et al., 2013), the migration is presumably taking place via the blood stream. Thus it is imaginable that during immunization induced EBA, migrating $T_{fh}$ pass a site of dermal inflammation and immigrate into dermal wounds. This raises the question, whether the T-lymphocyte receptor$\beta$ repertoire of $T_{fh}$ and $T_{skin}$ is identical and if a specific accumulation is detectable in response to the auto-antigen mCOL7c. To investigate this, samples used in Chap. 3.2 and 3.3 are analyzed with regard to an identical T-lymphocyte receptor$\beta$ repertoire within individuals. For that, correlation of T-lymphocyte receptor$\beta$ clonotype frequencies among $T_{fh}$ and $T_{skin}$, the uniformity of clonotypes and overlap of most prevalent clonotypes is analyzed.

### 3.5.1 Auto-antigen independent localization of $T_{fh}$ T-lymphocyte receptor$\beta$ clonotypes in the skin

To initially analyze, whether identical T-lymphocyte receptor$\beta$ clonotypes are detectable among $T_{fh}$ and $T_{skin}$, the frequency of each clonotype in both compartments is depicted in a coordinate system and the connection is evaluated via a correlation. Analyzing PBS/TM results in no correlation with a mean correlation coefficient of -0.2582 (Fig. 3.29 A). For GST/TM immunization, no correlation with a mean correlation coefficient of 0.0607 (Fig. 3.29 B) and likewise, mCOL7c-GST/TM exhibits no correlation with a mean correlation coefficient of 0.0946 (Fig. 3.29 C). Thus, it has to be concluded that some $T_{fh}$ T-lymphocyte receptor$\beta$ clonotypes are present in the skin, but the frequency of those clonotypes does not correlate between both compartments.

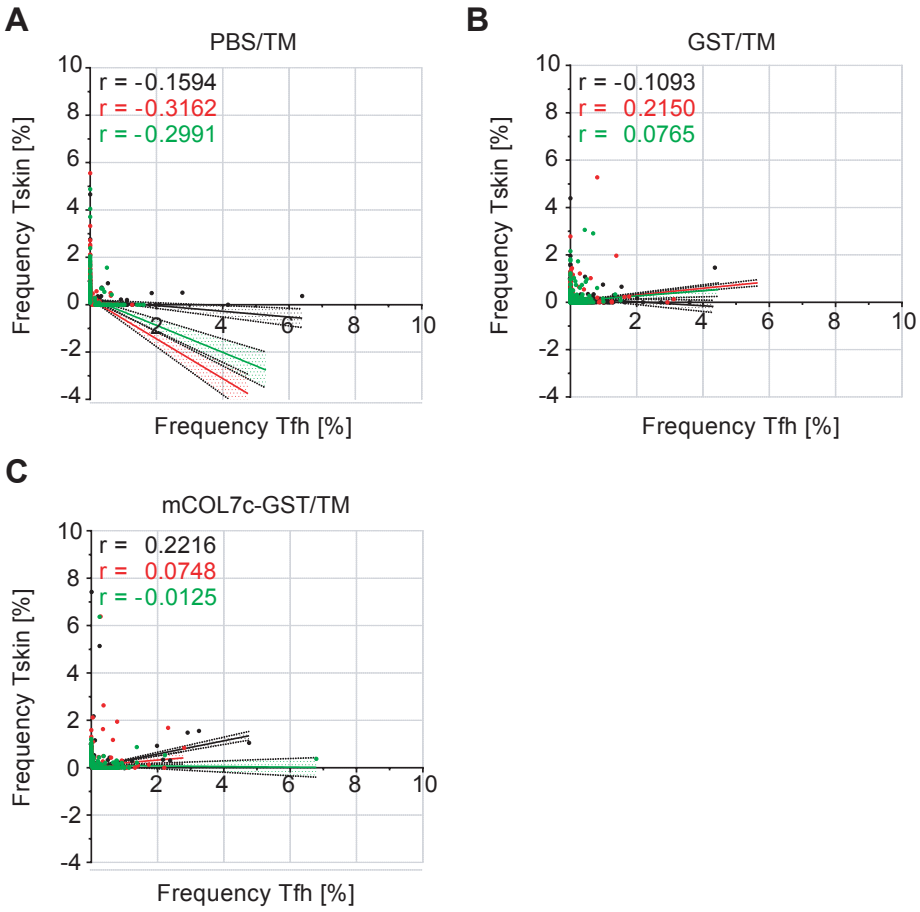


**Figure 3.29: Frequency of $T_{fh}$ T-lymphocyte receptor$\beta$ clonotypes and $T_{skin}$ clonotypes does not correlate.** SJL/J mice were immunized using PBS/TM, GST/TM or mCOL7c-GST/TM into both hind foot pads. The skin of both ears was scratched 21 days after immunization. 7 days after, samples of both ears were obtained and the $T_{skin}$ T-lymphocyte receptor$\beta$ repertoire was analyzed via NGS. Parallel, $T_{fh}$ were extracted out of the lymph nodes via laser microdissection of germinal centers and the $T_{fh}$ T-lymphocyte receptor$\beta$ repertoire was determined using NGS. Graphs depict the T-lymphocyte receptor$\beta$ clonotype-frequencies of $T_{fh}$ (x-axis) and $T_{skin}$ (y-axis) after A) PBS/TM, B) GST/TM and C) mCOL7c-GST/TM immunization (exemplary depiction of the comparison between $T_{fh}$ clonotypes from the left LN and $T_{skin}$ clonotypes for the left). N=3, n=6, correlation coefficients are denoted as r, calculated linear regression with 95% confidence band is delineated.

To quantify the presence of $T_{fh}$ T-lymphocyte receptor$\beta$ clonotypes in skin, the Morisita-Horn-Index among both compartments is calculated within individuals. This results in values of 0.04 $\pm$0.02 for PBS/TM, 0.13 $\pm$0.04 for GST/TM and 0.14 $\pm$0.04 for mCOL7c-GST/TM (Fig. 3.30). Comparison among immunization groups results in significantly higher values after GST/TM and mCOL7c-GST/TM immunization compared to PBS/TM. However, no statistical difference is de-

tectable among GST/TM and mCOL7c-GST/TM. Thus, it has to be concluded, that $T_{fh}$ T-lymphocyte receptor$\beta$ clonotypes do not specifically accumulate in the skin.

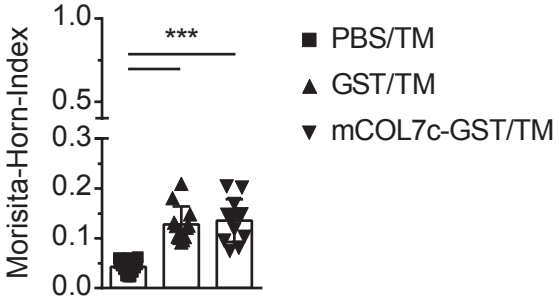


**Figure 3.30: $T_{fh}$ T-lymphocyte receptor$\beta$ clonotypes localize auto-antigen independent in the skin.** SJL/J mice were immunized using PBS/TM, GST/TM or mCOL7c-GST/TM into both hind foot pads. The skin of both ears was scratched 21 days after immunization. 7 days after, samples of both ears were obtained and the $T_{skin}$ T-lymphocyte receptor$\beta$ repertoire was analyzed via NGS. Parallel, $T_{fh}$ were extracted out of the lymph nodes via laser microdissection of germinal centers and the $T_{fh}$ T-lymphocyte receptor$\beta$ repertoire was determined using NGS. Similarity of $T_{fh}$ and $T_{skin}$ T-lymphocyte receptor$\beta$ clonotypes is depicted as Morisita-Horn-Index. N=3, n=12, data is expressed as means ± SD, *** $p<0.001$, One-way ANOVA with Dunnett's post-hoc test.

Additionally, also the T-lymphocyte receptor$\beta$ V- and J-segment usage are assessed for the $T_{fh}$ T-lymphocyte receptor$\beta$ clonotypes found in the skin. Thereby it is evaluated, whether the characteristic V3-segment accumulation of $T_{fh}$ clonotypes (Fig. 3.18 A) is also reflected by the $T_{fh}$ clonotypes that are present in the skin. However, neither the specific V3-segment accumulation, nor a general auto-antigen related V- or J-segment usage is detectable (Fig. 3.31). This demonstrates, that although some $T_{fh}$ clonotypes are detectable in the skin, their dermal location is independent from the auto-antigen mCOL7c.

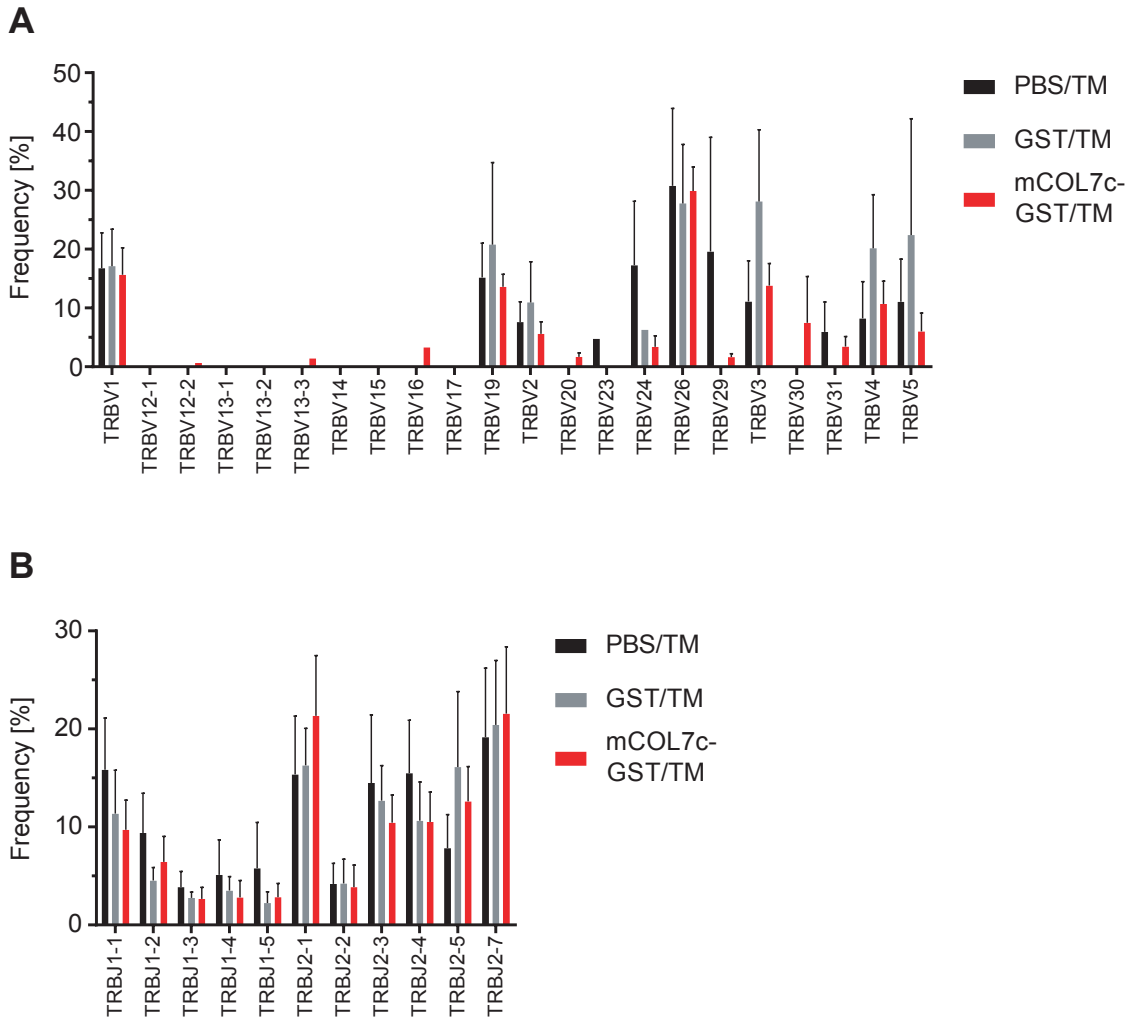


**Figure 3.31: V- and J-segment usage of $T_{fh}$ T-lymphocyte receptor$\beta$ clonotpyes found in skin is not changed under autoimmune condition.** SJL/J mice were immunized using PBS/TM, GST/TM or mCOL7c-GST/TM into both hind foot pads. The skin of both ears was scratched 21 days after immunization. 7 days after, samples of both ears were obtained and the T-lymphocyte receptor$\beta$ repertoire of $T_{skin}$ was analyzed via NGS. Parallel, $T_{fh}$ were extracted via laser microdissection of germinal centers and the T-lymphocyte receptor$\beta$ repertoire was determined using NGS. Histogram depicts the T-lymphocyte receptor$\beta$ A) V-segment and B) J-segment usage of the $T_{fh}$ T-lymphocyte receptor$\beta$ clonotpyes found in the skin. N=3, n=12, data is expressed as means ± SD, Kruskal-Wallis test with Dunnett's post-hoc test.

### 3.5.2 Most prevalent $T_{fh}$ T-lymphocyte receptor$\beta$ clonotypes appear in the skin

Since it is shown, that the most prevalent $T_{fh}$ T-lymphocyte receptor$\beta$ clonotypes are highly identical in response to the auto-antigen mCOL7c (Fig. 3.25), the question arise, whether the most prevalent $T_{fh}$ clonotypes specifically immigrate in the skin. To answer this question it is ascer-

tained, whether the 20 most prevalent $T_{fh}$ T-lymphocyte receptor$\beta$ clonotypes are detectable in the skin. Analyzing the different experimental groups, for PBS/TM 2 (Fig. 3.32 A), for GST/TM 8 (Fig. 3.32 B) and for mCOL7c-GST/TM 11 $T_{fh}$ clonotypes are present in the skin (Fig. 3.32 C). Thus, a general trend towards high frequent $T_{fh}$ T-lymphocyte receptor$\beta$ clonotypes, which immigrate into the skin is detectable under autoimmune condition.

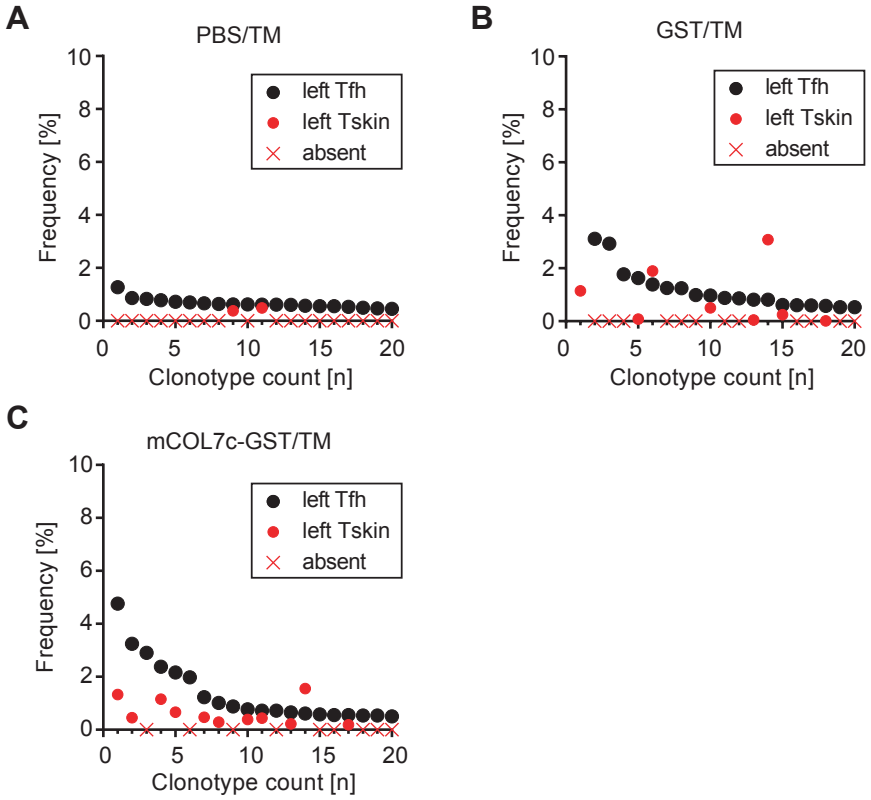


**Figure 3.32: High frequent $T_{fh}$ clonotypes immigrate into the skin under autoimmune condition.** SJL/J mice were immunized using PBS/TM, GST/TM or mCOL7c-GST/TM into both hind foot pads. The skin of both ears was scratched 21 days after immunization. 7 days after, samples of both ears were obtained and the $T_{skin}$ T-lymphocyte receptor$\beta$ repertoire was analyzed via NGS. Parallel, $T_{fh}$ were extracted out of the lymph nodes via laser microdissection of germinal centers and the $T_{fh}$ T-lymphocyte receptor$\beta$ repertoire was determined using NGS. Frequency of the 20 most prevalent $T_{fh}$ clonotypes was plotted in a descending order. If the exact clonotype was also present among the entire $T_{skin}$ clonotypes, its frequency was additionally plotted. Representative depiction after A) PBS/TM, B) GST/TM and C) mCOL7c-GST/TM immunization (exemplary depiction of the comparison between one $T_{fh}$ sample of the left lymph node and one $T_{skin}$ sample of the left skin). N= 1, n=2.

To quantify the presence of $T_{fh}$ T-lymphocyte receptor$\beta$ clonotypes in the skin, intersection of

the 20 most prevalent $T_{fh}$ clonotypes and the entire $T_{skin}$ repertoire or the intersection of both entire repertoires is calculated. For PBS/TM this results in values of 12.92% ±10.76%, for GST/TM in 43.33% ±13.37% and for mCOL7c-GST/TM in 48.18% ±11.89% for the 20 most prevalent $T_{fh}$ clonotypes (Fig. 3.33). For the entire repertoires, the intersection results in values of 3.58% ±2.16% for PBS/TM, 9.43% ±4.77% for GST/TM and 4.51% ±2.45% for mCOL7c-GST/TM. By comparison of the 20 most prevalent clonotypes after PBS/TM immunization to the entire repertoire, no difference is detectable. However for GST/TM and mCOL7c-GST/TM immunization, the intersection of the 20 most prevalent clonotypes is significantly higher compared to their entire repertoire. Comparison among immunization groups results a significantly higher intersection of the 20 most prevalent clonotypes after GST/TM and mCOL7c-GST/TM immunization compared to PBS/TM. Therefore it has to be concluded, that the appearance of $T_{fh}$ T-lymphocyte receptor$\beta$ clonotypes in the skin is centered to most prevalent $T_{fh}$ clonotypes. However, this process is auto-antigen independent.

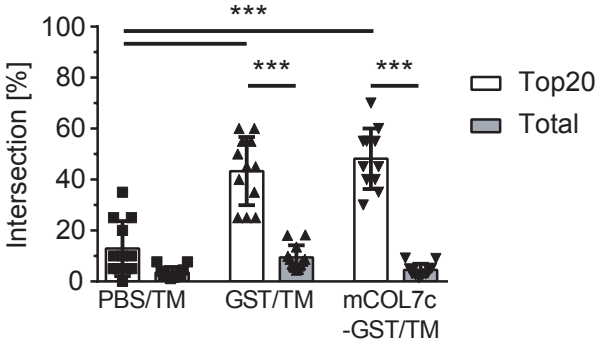


**Figure 3.33: Appearance of $T_{fh}$ T-lymphocyte receptor$\beta$ clonotypes in the skin is centered to most prevalent clonotypes and emerges auto-antigen independent.** SJL/J mice were immunized using PBS/TM, GST/TM or mCOL7c-GST/TM into both hind foot pads. The skin of both ears was scratched 21 days after immunization. 7 days after, samples of both ears were obtained and the $T_{skin}$ T-lymphocyte receptor$\beta$ repertoire was analyzed via NGS. $T_{fh}$ were extracted out of the lymph nodes via laser microdissection of germinal centers and the $T_{fh}$ T-lymphocyte receptor$\beta$ repertoire was determined using NGS. Intersection of the $T_{fh}$ and $T_{skin}$ T-lymphocyte receptor$\beta$ clonotypes is depicted. Thereby, the intersection was calculated among the 20 most prevalent $T_{fh}$ clonotypes and the entire $T_{skin}$ repertoire or among both entire repertoires. N=3, n=12, data is expressed as means ± SD, *** $p<0.001$, One-way ANOVA with Dunnett's post-hoc test.

In summary, analysis of the $T_{fh}$ T-lymphocyte receptor$\beta$ clonotypes among $T_{skin}$ clonotypes reveals a general presence of $T_{fh}$ clonotypes in the skin, which is certainly less distinct as the

highly uniform $T_{fh}$ repertoire in contralateral lymph nodes. Thereby, clonotype frequencies do not correlate and the dermal location of $T_{fh}$ clonotypes is independent from the auto-antigen mCOL7c. Additionally it could be shown, that the overlap between $T_{fh}$ and $T_{skin}$ clonotypes is centered to the most prevalent $T_{fh}$ clonotypes. Addressing the question, whether the T-lymphocyte receptor$\beta$ repertoire of $T_{fh}$ and $T_{skin}$ is identical in an individual, this data show that clonotypes found at high frequency in germinal centers are also present in the skin and demonstrates, that the $T_{fh}$ and $T_{skin}$ T-lymphocyte receptor$\beta$ repertoires are not completely independent.

## 3.6 Summary of results

The results obtained in this dissertation show, that $T_{skin}$ T-lymphocyte receptor$\beta$ clonotypes migrate randomly into dermal EBA wounds and do not specifically accumulate in response to the endogenous presence of auto-antigen mCOL7c in the skin. In contrast, for $T_{fh}$ clonotypes, a specific accumulation in germinal centers of the draining lymph nodes could be shown under autoimmune condition. Thereby, the V3-segment is generally elevated in response to the auto-antigen mCOL7c and also specifically among the $T_{fh}$ clonotypes, that are shared among all analyzed individuals. Surprisingly, also a highly uniform $T_{fh}$ repertoire within individual mice could be identified in germinal centers of contralateral lymph nodes, which is constituted early and segregates during chronic establishment of EBA. Additionally, $T_{fh}$ clonotypes are also found in dermal wounds, however they do not specifically exhibit the V3-segment and rather immigrate randomly into the skin.

# 4 Discussion

The present study provides for the first time a detailed insight in the T-lymphocyte receptor$\beta$ repertoire of skin immigrating T-lymphocytes ($T_{skin}$) and $T_{fh}$ in immunization induced EBA by demonstrating, that:

I. the T-lymphocyte receptor$\beta$ repertoire of $T_{skin}$ is not dominated by accumulating clonotypes under autoimmune condition.

II. identical $T_{fh}$ T-lymphocyte receptor$\beta$ clonotypes accumulate in germinal centers under autoimmune condition and specifically share the V3-segment.

II. in response to the auto-antigen mCOL7c, a highly uniform $T_{fh}$ T-lymphocyte receptor$\beta$ repertoire is constituted in germinal centers within individual mice. Thereby, uniformity is initiated at early time points and segregates during chronic disease establishment.

IV. $T_{fh}$ T-lymphocyte receptor$\beta$ clonotypes, found at high frequency in germinal centers, are also present in the skin. Thereby, they immigrate auto-antigen independent.

The following chapters will discuss these findings and their implications for general understanding of the $T_{skin}$ and $T_{fh}$ T-lymphocyte receptor$\beta$ repertoire and specifically for immunization induced EBA.

## 4.1 The T-lymphocyte receptor$\beta$ repertoire of $T_{skin}$ is not affected, whereas the repertoire of $T_{fh}$ shifts under autoimmune condition

Disease development in experimental EBA can be dived into two consecutive steps: (I) the $T_{fh}$-mediated induction-phase and (II) the $T_{skin}$-mediated effector-phase. To answer, whether $T_{fh}$ or $T_{skin}$ accumulate disease-specific in immunization induced EBA, their T-lymphocyte receptor$\beta$ repertoire was analyzed with regard to shifts under autoimmune condition.

### 4.1.1 Dermal disruption leads to immunization independent immigration of $T_{skin}$

Prior analysis of the $T_{skin}$ T-lymphocyte receptor$\beta$ repertoire, it was aimed to develop a model to investigate the $T_{skin}$ repertoire in immunization induced EBA with regard to control groups. For that the situation in endogenous wounds was investigated and scratching as a trigger for an immunization independent $T_{skin}$ immigration was evaluated.

#### 4.1.1.1 $T_H1$ milieu is constituted in endogenous wounds

For establishment of a $T_{skin}$ immigration model, the situation in endogenous wounds was initially assessed by induction of EBA via immunization using mCOL7c-GST/TM (Sitaru et al., 2006). Thereby, a general thickening and infiltration of neutrophils was restricted to the auto-antigen based immunization (Fig. 3.3 A). This correlates with the observation, that PBS/TM does not result in dermal wounds (Iwata et al., 2013), whereas administration of the auto-antigen mCOL7c results in dermal wounds and neutrophil immigration (Hammers et al., 2011). For $CD4^+$ and $CD8^+$ T-lymphocytes an analogous situation was observable, whereby $CD4^+$ T-lymphocytes predominantly immigrate. This is in accordance with the observation of a general dermal T-lymphocyte immigration during effector-phase in the experimental EBA model (Bieber et al., 2016) and also in humans a T-lymphocyte immigration was generally shown for dermal blistering disease (Hussein et al., 2007).

For $T_{skin}$ cytokines and transcription factors, an elevated IFN$\gamma$ and T-bet expression (Fig. 3.3 C) was found in endogenous wounds, leading to the conclusion of a $T_H1$ immigration. This fits well to a previously reported elevated expression of the chemokine-receptor CxCR3 (Maass, 2015), which is expressed in $T_H1$, and an elevated expression of its ligand CxCL9 (Bieber et al., 2017b) and thus, strengthening the finding of a $T_H1$ immigration into endogenous EBA wounds. In contrast for $T_H2$, neither an elevated IL4, nor GATA3 expression (Fig. 3.3 C) were detectable in endogenous EBA wounds. For the immunization induced EBA model, a $T_H2$ mediated IL4 milieu was found to be disease preventive during the induction-phase (Hammers et al., 2011). This could also apply for the effector-phase, where an exceeding $T_H1$ mediated pro-inflammatory IFN$\gamma$ milieu might be necessary for the development of wounds and an anti-inflammatory $T_H2$ milieu might be preventive. Although an elevated expression of IL10 (Fig. 3.3 C) was found in EBA wounds. But, the unchanged expression of FoxP3 (Fig. 3.3 C) suggests no elevated $T_{reg}$ presence in EBA wounds and leads to the conclusion, that the IL10 is not primarily derived from $T_{reg}$. However, for $T_{reg}$ it its known, that FoxP3 is not constitutively expressed (Ziegler, 2006). Therefore, it might be possible, that the mRNA based detection via qPCR fails to detect FoxP3, although the protein might be present.

In a further experiment, the cellularity of dermal $T_{skin}$ could be addressed. Therefore, a flow cytometry based analysis could be used to specifically detect individual $T_H$ subsets in the skin based on protein level. This holds the possibility, that beside the already known $T_{skin}$ subsets in experimental EBA, $T_H1$, $T_H2$ and $T_{reg}$, also additional subsets are revealed. Thereby, it is possible,

that also $T_H17$ might be identified to immigrate into EBA wounds, since $T_H17$ are already known to play a role during wound progression in EBA related diseases (Arakawa et al., 2011).

#### 4.1.1.2 Scratching induces an immunization independent $T_{skin}$ immigration and reflects the $T_H1$ milieu of endogenous wounds

In this study, it could be shown, that dermal disruption via scratching leads to an immunization independent immigration of $T_{skin}$ in all experimental groups (Fig. 3.4), whereby the immigrating $T_{skin}$ reflect the $T_H1$ milieu of endogenous wounds (Fig. 3.5).

Cellular analysis 7 days after scratching showed an immunization independent dermal immigration of $CD4^+$ T-lymphocytes in uniform frequencies (Fig. 3.4 B). This immigration can be attributed to disruption of the skin, since all experimental groups contain equal frequencies compared to the naïve control group. Also in general, dermal disruption was described to result in an inflammatory recruitment of lymphocytes (Homey et al., 2006). Furthermore, the expression of cytokines and transcription factors in scratched skin (Fig. 3.5) reflects the situation found in endogenous wounds (Fig. 3.3 C). This might be attributable to the fact, that only under autoimmune condition T-lymphocytes emerge, that are specific for mCOL7c. Then these $T_{skin}$ are possibly retained in the skin and accumulate, due to the dermal presence of the auto-antigen (McLachlan and Jenkins, 2007). In contrast for the other immunization groups, where a lack of their specific antigen might lead to a high turnover rate, preventing an accumulation. Thus, it has been shown, that scratching results in an immunization independent immigration of $T_{skin}$ and reflects the situation in endogenous wounds. Therefore, the dermal disruption model enables an excellent assessment of the $T_{skin}$ T-lymphocyte receptor$\beta$ repertoire under autoimmune condition and a simultaneous comparison to control groups.

### 4.1.2 An uniform number of T-lymphocyte receptor$\beta$ clonotypes was found for $T_{skin}$ and $T_{fh}$

After establishment of the dermal disruption model, the $T_{skin}$ and $T_{fh}$ T-lymphocyte receptor$\beta$ repertoires were assessed in immunization induced EBA and are jointly discussed in the following.

For determination of the T-lymphocyte receptor$\beta$ repertoire, it is important to utilize an equal number of $T_{skin}$ and $T_{fh}$ as starting material. Since the frequency of $T_{skin}$ was shown to be equal among immunization groups after scratching (Fig. 3.4 B), the isolation of an identical dermal volume (Fig. 3.7 A) resulted consequently in an equal number of $T_{skin}$ (Fig. 3.7 B). The equivalent picture

was also true for $T_{fh}$. Here the equally microdissected volume of germinal centers (Fig. 3.14 A) and the equal frequency of $T_{fh}$ within germinal centers (Fig. 3.14 B) resulted in an equal number of extracted $T_{fh}$ (Fig. 3.14 C). Thereby, the identified $T_{fh}$ frequencies within germinal centers (Fig. 3.14 B) are comparable to already published data in the literature (Banczyk et al., 2014). This standardization was obligatory, since an unequal number of $T_{skin}$ or $T_{fh}$ for T-lymphocyte receptor$\beta$ repertoire analysis might lead to a divergent number of clonotypes and subsequently a divergent diversity among the analyzed repertoires (Laydon et al., 2015; Oakes et al., 2017a). Thus, the standardization represents an important point for comparability among samples (Rosati et al., 2017) and provided a basis for the quantitative and qualitative T-lymphocyte receptor$\beta$ repertoire analysis.

Based on the equal cellular numbers, an equal number of T-lymphocyte receptor$\beta$ clonotypes was detected for $T_{skin}$ (Fig. 3.7 C) and $T_{fh}$ (Fig. 3.14 D) via NGS. Thereby, the GST/TM immunization for the $T_{skin}$ and both, PBS/TM and mCOL7c-GST/TM immunizations for $T_{fh}$ showed an elevated variability, although not resulting in significant differences. Since all samples were treated equally and resulted in technically comparable sequencing parameter (Tab. S1), a specific reason for this variability is not known. However, such a variability was also observed in comparable studies (Fähnrich et al., 2018; Textor et al., 2018). Specifically addressing the number of obtained $T_{skin}$ clonotypes, already published data reports clonotype-numbers in the same scale and, in turn, comprises also a variation in numbers (Harden et al., 2015).

In summary, the equal numbers of extracted cells established a basis for uniform T-lymphocyte receptor$\beta$ clonotypes numbers among the analyzed experimental groups and enabled a comparative analysis of the $T_{skin}$ and $T_{fh}$ repertoire.

### 4.1.3 Only $T_{fh}$ T-lymphocyte receptor$\beta$ clonotypes are present at higher frequency under autoimmune condition

In the subsequent analysis, the frequency distribution of $T_{skin}$ (Fig. 3.8 A) and $T_{fh}$ (Fig. 3.15 A) T-lymphocyte receptor$\beta$ clonotypes revealed that some exist in high frequencies, whereas the majority is only present in low frequencies. Such a frequency distribution is also observable among T-lymphocyte receptor$\beta$ clonotypes of naïve individuals and leads to an increased rate of expanded clonotypes after immunization (Fähnrich et al., 2018). An expansion of individual clonotypes was also reported for *in vitro* (Oakes et al., 2017b) and *in vivo* (Kirsch et al., 2015) analysis and in-

dicates an antigen-specific expansion of T-lymphocyte receptor$\beta$ clonotypes (Pogorelyy et al., 2018).

Quantification of the frequency distribution via the Gini coefficient among $T_{skin}$ T-lymphocyte receptor$\beta$ clonotypes (Fig. 3.8 B) and $T_{fh}$ clonotypes (Fig. 3.15 B) results in nearly identical values. This shows, that the expansion among different $T_H$ subsets is equal among all induced immunological condition. In analysis of the Gini coefficient within the different $T_H$ subsets, also no expansion is detectable among $T_{skin}$ clonotypes. However, for the $T_{fh}$ clonotypes, a specific expansion after mCOL7c-GST/TM immunization is detectable in comparison against PBS/TM (Fig. 3.15 B). This difference might be explainable by the observation, that although some T-lymphocyte clonotypes are shared between the $T_{skin}$ and $T_{fh}$ repertoire (Fig. 3.30), the majority is different between both compartments. Thus, the T-lymphocyte clonotypes which differ between $T_{skin}$ and $T_{fh}$ have to be considered in terms of their different T-lymphocyte receptor signaling strengths (Tubo et al., 2013; Tubo and Jenkins, 2014). Whereas $T_{skin}$ are restricted to a low to medium signaling strength, the differentiation towards $T_{fh}$ demands a high to very high signaling strength. Since it was additionally shown, that a higher T-lymphocyte receptor stimulation results in a higher expansion rate (Jenkins et al., 1991), one could speculate, that specifically the higher signaling strength of $T_{fh}$ results in an accumulation in germinal centers. Thereby, the accumulation of $T_{fh}$ clonotypes in germinal centers might be restricted to the auto-antigen based mCOL7c-GST/TM immunization, since the specificity of auto-reactive clonotypes, which bypass the negative selection, is presumably very high and therefore leads to the highest expansion rate. However, also T-lymphocyte clonotypes were detectable, which are shared between the $T_{skin}$ and $T_{fh}$ repertoire (Fig. 3.30), therefore a different T-lymphocyte receptor signaling strengths does not completely explain the increases expansion of $T_{fh}$ clonotypes. As an additional factor, also the availability of the antigen might play a role. Since the $T_{fh}$ clonotypes were extracted out of the lymph nodes, which directly drain the site of injection, it can be speculated, that considerably more antigen is available for $T_{fh}$ expansion compared to the peripheral skin side, where $T_{skin}$ were extracted from.

However, the frequency of individual clonotypes does not permit a statement about possible accumulation of T-lymphocyte receptor$\beta$ clonotypes under autoimmune condition. For that, a comparative analysis of the clonotype uniformity is necessary, which exceeds the capability of the Gini coefficient. Therefore in the following, the detection of accumulating T-lymphocyte receptor$\beta$ clonotypes via the Morisita-Horn-Index is discussed.

### 4.1.4 A shift in the T-lymphocyte receptor$\beta$ repertoire in experimental EBA exists only for $T_{fh}$

To identify, whether the $T_{skin}$ and $T_{fh}$ T-lymphocyte receptor$\beta$ clonotypes accumulate under autoimmune condition, both repertoires were analyzed with regard to accumulation of identical clonotypes and shared CDR3 features. Thereby, this dissertation showed a divergent picture for $T_{skin}$, which immigrate auto-antigen unspecific into the skin (Fig. 3.9 C) and $T_{fh}$, which show a specific accumulation of identical clonotypes under autoimmune condition (Fig. 3.16 C). To identify the T-lymphocyte receptor$\beta$ clonotype accumulation, the Morisita-Horn-Index was calculated. As described in Chap. 2.2.7.8, this index corrects for sample size and incorporates the individual clonotype frequency. Furthermore, it is a widely published method to detect similarities and accumulation among T-lymphocyte receptor$\beta$ repertoires (Hindley et al., 2011; Niu et al., 2015).

#### 4.1.4.1 $T_{skin}$ T-lymphocyte receptor$\beta$ clonotypes accumulate auto-antigen unspecific

For $T_{skin}$ T-lymphocyte receptor$\beta$ clonotypes, GST/TM and mCOL7c-GST/TM immunizations resulted in an equal dermal immigration (Fig. 3.9 C), which leads to the conclusion of an auto-antigen independent process. Additionally, the unaltered T-lymphocyte receptor$\beta$ CDR3 region of $T_{skin}$ clonotypes, described in Chap. 3.2.4, strengthens the finding of an auto-antigen independent immigration into the skin. This is an unexpected finding, since the constitution of a dermal pro-inflammatory $T_H1$ milieu was only detectable after mCOL7c-GST/TM immunization (Fig. 3.5 A) and suggested that $T_{skin}$ clonotypes are specifically retained by dermal presence of the auto-antigen (discussed in Chap. 4.1.1.2). However, such a retention is not detectable, which rather indicates, that the immigration of $T_{skin}$ clonotypes is a random process, not triggered by endogenous presence of the auto-antigen in skin. Transferring this results to the endogenous situation of experimental EBA, where $T_{skin}$ immigrate and express cytokines (Fig. 3.3), analysis of the T-lymphocyte receptor$\beta$ repertoire deducts the high rate of immigrating $T_{skin}$ to be a bystander process during EBA pathogenesis. A possible explanation for this observation might be provided by Ghani et al. (2009). They found, that antigen-specific T-lymphocytes function a pioneers and constitute a milieu for antigen-unspecific T-lymphocyte immigration. Thus, it might be possible, that during early EBA wounds auto-antigen specific $T_{skin}$ clonotypes immigrate into the skin and by a strong $T_H1$ mediated IFN$\gamma$ expression (Fig. 3.3 C) unspecific recruitment of further $T_{skin}$ occurs (Issekutz et al., 1988). Therefore, the time point of examination might contribute to the finding of an auto-antigen unspecific $T_{skin}$ clonotype accumulation. In this regard, in further experiments the time point for examination of the $T_{skin}$ repertoire should be adapted. Thereby, two possible

alteration are imaginable: (I) following Ghani et al. (2009), the time point for examination should be earlier after scratching or (II) the chronic induction of wounds under autoimmune condition (Fig. S1) imply the possibility, that an auto-antigen specific accumulation of the $T_{skin}$ clonotypes is only observable at late time points. Thereby, a selection process in response to the endogenous presence of the auto-antigen in skin might select mCOL7c-specific $T_{skin}$ clonotypes from the by-stander immigrating and thus, leads to a specific accumulation and/or proliferation over course of the disease (Reinhardt et al., 2003). Therefore, since $T_{fh}$ clonotypes feature an accumulation of the T-lymphocyte receptor$\beta$ V3-segment (Fig. 3.18 A), it is reasonable to speculate, that an auto-antigen specific presence of $T_{skin}$ clonotype at early or late time points is also represented by an increased V3-segment usage.

In summary, the $T_{skin}$ T-lymphocyte receptor$\beta$ repertoire is unchanged under autoimmune condition and suggest, that the role of $T_{skin}$ during the effector-phase of EBA is auto-antigen unspecific and restricted to provision of cytokines.

#### 4.1.4.2 $T_{fh}$ T-lymphocyte receptor$\beta$ clonotypes accumulate auto-antigen specific in germinal centers

For $T_{fh}$, a clear accumulation of T-lymphocyte receptor$\beta$ clonotypes in germinal centers (Fig. 3.16 C), a generally elevated T-lymphocyte receptor$\beta$ V3-segment usage (Fig. 3.18 A) and a specific accumulation of the V3-segment among the clonotypes shared between three individuals (Fig. 3.21) was shown in this dissertation. These findings clearly show, that $T_{fh}$ clonotypes specifically accumulate under autoimmune condition in immunization induced EBA. Furthermore, by directly comparing the accumulation, $T_{fh}$ clonotypes (Fig. 3.16 C) exhibit a 4 times higher Morisita-Horn-Index compared to $T_{skin}$ clonotypes (Fig. 3.9 C). This shows, that the set of $T_{fh}$ clonotypes, which is recruited into germinal centers, is substantially more identical compared to $T_{skin}$ clonotypes.

These finding are highly interesting and show for the first time a direct association of the T-lymphocyte receptor$\beta$ repertoire to experimental EBA. However, these findings are also in contrast to already publish literature, showing that the majority of T-lymphocytes in the draining lymph nodes are directed against the xeno-antigen GST and a specific response to the auto-antigen mCOL7c is hardly detectable (Tiburzy et al., 2013). Such a GST specific response is also detectable in this data (Fig. 3.16 C), which clearly exceed the unspecific activation via PBS/TM and verifies the previous observation by Tiburzy et al. (2013). Although, the picture of an auto-antigen-specific response directed against mCOL7c differs. Whereas, Tiburzy et al. (2013) were unable to detect

a response specifically against mCOL7c by comparing the rate of GST and mCOL7c-GST specific T-lymphocytes via restimulation, this dissertation shows a clear difference in accumulating $T_{fh}$ clonotypes between GST/TM and mCOL7c-GST/TM immunizations (Fig. 3.16 C). One possible explanation for this difference might be the divergent experimental setup. Whereas the immunization using GST/TM and mCOL7c-GST/TM were identically among both studies, the extraction of T-lymphocytes and the way of analysis was different. Tiburzy et al. (2013) unspecifically extracted T-lymphocytes out of the draining lymph nodes, restimmulated them *in vitro* and analyzed CD154 emergence, which displays antigen-specific activation (Frentsch et al., 2005). In contrast, the analysis in this study was narrowed to $T_{fh}$, which where specifically extracted out of germinal centers via laser microdissection. Thereby, laser microdissection was shown to be a precise tool for defined extraction out of primary tissues and allows a specific analysis of $T_{fh}$, which are located *in vivo* in germinal centers (Fend et al., 1999; Kalies et al., 2008). Thus, the data generated by Tiburzy et al. (2013) has to be considered in the context of total $CD4^+$ T-lymphocytes, which implies, that T-lymphocyte subsets with divergent T-lymphocyte receptor signaling strengths are analyzed in parallel. In contrast, this study was specifically focused on $T_{fh}$, which only account for 2.2% of the total $CD4^+$ T-lymphocytes (Fig. 3.26 B). In this light, it might be possible, that in the study of Tiburzy et al. (2013), T-lymphocyte subsets with a divergent T-lymphocyte receptor signaling strength are triggered and since the precursor frequency of auto-antigen specific T-lymphocytes is low, a specific response to mCOL7c might not exceed the unspecifically triggered background of GST specific T-lymphocytes. In fact, the similar picture can be seen by analysis of the $T_{skin}$ repertoire that also contains subsets of divergent T-lymphocyte receptor signaling strengths (Fig. 3.9 C) and also shows no difference in response to mCOL7c. In contrast, focusing on $T_{fh}$ which are localized in germinal centers, restricts the activated T-lymphocytes to clonotypes with the highest signaling strength to the antigen (Tubo et al., 2013; Cho et al., 2017). Since auto-reactive clonotypes, which bypass the negative selection, are presumably highly specific for the auto-antigen, the differentiation of particular mCOL7c-specific T-lymphocytes towards $T_{fh}$ is highly likely. In addition to that, also during immigration into the cortical BCZ, $T_{fh}$ are selected for antigen specificity (Crotty, 2014), which could further narrow the $T_{fh}$ T-lymphocyte receptor$\beta$ repertoire towards mCOL7c specificity. An additional mechanism, which might facilitates the detection of differences, specifically among the $T_{fh}$ T-lymphocyte receptor$\beta$ repertoire, is displayed by the pro-inflammatory IFN$\gamma$ milieu, which was shown to be necessary for disease induction (Hammers et al., 2011). It was shown by Lee et al. (2012), that IFN$\gamma$ leads to an accumulation of $T_{fh}$ and could be directly linked to the induction of pathology in a murine lupus erythematosus model. Therefore, it is reasonable

to speculate that specifically the focus on $T_{fh}$ revealed the auto-antigen specific accumulation of T-lymphocyte receptor$\beta$ clonotypes in experimental EBA.

Compared to the accumulation of $T_{fh}$ T-lymphocyte receptor$\beta$ clonotypes, which was detected by comparative examination of the hyper-variable CDR3 region, analysis of the T-lymphocyte receptor$\beta$ V- and J-segment displays a comparison of genetically encoded characteristics. Thereby, in this dissertation an elevated usage of the V3-segment (Fig. 3.18 A) was found for $T_{fh}$ clonotypes under autoimmune condition. Although the usage of the J-segment was unchanged among $T_{fh}$ clonotypes (Fig. 3.18 B), an auto-antigen related segregation is also indicated by the combined V-J-segment usage (Fig. 3.19). Even more interesting, not only the number of $T_{fh}$ clonotypes shared among three individuals is highest under autoimmune condition (Fig. 3.20), especially also the V3-segment among these $T_{fh}$ clonotypes is highest (Fig. 3.21), although in the general consideration it is only the second most abundant (Fig. 3.18 A). This shows, that not only the general $T_{fh}$ repertoire contains an elevated V3-segment usage, also clonotypes that are present among all analyzed individuals share this identical characteristic. In the literature such clonotypes are referred to as public clonotypes (Woodsworth et al., 2013), which are in contrast to the private clonotypes, present among individuals. Thereby, in a study by Madi et al. (2014) public clonotypes were associated with self-reactivity and autoimmunity. Therefore, finding such an elevated usage of the T-lymphocyte receptor$\beta$ V3-segment among public clonotypes leads to the hypothesis of a direct disease association between experimental EBA and the T-lymphocyte receptor$\beta$ V3-segment. Thus, it is imaginable, that an antibody-mediated depletion of T-lymphocytes sharing the V3-segment might specifically prevent the germinal center mediated maturation of auto-reactive B-lymphocytes and leads to a decreased or abolished production of auto-antibodies in immunization induced EBA. Subsequently, a lowered or disabled auto-antibody production might diminish clinical symptoms of EBA. Therefore, it would be of highest interest to analyze the effect for the pathogenic development of immunization induced EBA by specifically depleting T-lymphocytes expressing the T-lymphocyte receptor$\beta$ V3-segment.

In summary, the T-lymphocyte receptor$\beta$ repertoire of $T_{fh}$ is shifted under autoimmune condition, revealing an accumulation of identical $T_{fh}$ clonotypes specifically sharing the V3-segment. This shows, that $T_{fh}$ migrate auto-antigen specific into germinal centers during the induction-phase of EBA and also demonstrates, that $T_{fh}$ clonotypes share an EBA-specific shift. Thus, one could speculate, that an intervention, specifically targeting the T-lymphocyte receptor$\beta$ V3-segment at-

tenuates the disease severity in experimental EBA.

As delineated in this dissertation, shifts in the T-lymphocyte receptor$\beta$ repertoire in immunization induced EBA are compartment specific. Likewise in other skin related autoimmune diseases, a shift under autoimmune condition is not detectable for $T_{skin}$ (Harden et al., 2015; Brunner et al., 2017). However, as described for lupus erythematosus (Kita et al., 1995), also auto-antigen specific accumulation is known under autoimmune condition and could also be shown for the $T_{fh}$ repertoire. The leads to overall conclusion that the T-lymphocyte receptor$\beta$ repertoire in immunization induced EBA is shifted, but the side of examination matters for detection.

#### 4.1.4.3 Consideration of further experimental analysis of the T-lymphocyte receptor$\beta$ repertoire in experimental EBA

For further investigation of the T-lymphocyte receptor$\beta$ repertoire in experimental EBA, two promising directions can be pursued: (I) detailed analysis of auto-antigen specificity and (II) experimental expansion to the EBA model of Iwata et al. (2013).

The first direction for further analysis of the T-lymphocyte receptor$\beta$ repertoire in experimental EBA is the association of auto-antigen specificity for the identified accumulating $T_{fh}$ clonotypes via peptide MHC class II tetramers (Altman et al., 1996). MHC class II tetramers are artificially generated MHC class II complexes, which have bound a defined part of a desired antigen. Furthermore, the peptide MHC class II tetramers are soluble and can be designed to contain a defined fluorochrome (Nepom, 2012). Thus, by incubation of unspecifically isolated T-lymphocytes, binding of such a peptide MHC class II tetramer facilitates not only the labeling of individual cells, most importantly, an identification of single T-lymphocytes, which recognize the auto-antigen loaded MHC class II via the CDR3 antigen binding site of the T-lymphocyte receptor can be achieved (Huang et al., 2016). Having such a technique for the auto-antigen mCOL7c, two interesting possibilities arise: (I) validation of identified clonotypes and (II) screening for epitope specificity. In an initial experiment, it would be interesting to validate the identified public $T_{fh}$ clonotypes, which are shared among all three immunized individuals (Tab. S3). For that, the experimental setup for the phenotypic isolation of $T_{fh}$ (Fig. S4) could be adapted. In this way, the peptide MHC class II tetramer-recognizing $T_{fh}$ could be isolated and subsequently the T-lymphocyte receptor$\beta$ repertoire of these auto-antigen specific $T_{fh}$ could be sequenced. Such a validation, would not only directly demonstrate the auto-antigen specificity, it would also point towards the general existence of mCOL7c specific public clonotypes, likewise in other autoimmune animal mod-

els (Menezes et al., 2007). In a secondary experiment, different parts of the mCOL7c auto-antigen could be loaded into peptide MHC class II tetramers and an association towards the specificity of $T_{fh}$ clonotypes for different epitops could be achieved (Nepom, 2012). Based on association of the epitope specificity, it is also imaginable to interfere into the activation of auto-reactive T-lymphocytes. Thereby, the application of soluble peptide MHC class II tetramers could capture auto-reactive T-lymphocytes and prevent their activation (Yuan et al., 2004) or an antibody-mediated blocking of specific epitopes within the MHC class II at the surface of endogenous APCs might also prevent activation of auto-reactive T-lymphocytes (Wraith et al., 1992).

The second direction for further investigation of the T-lymphocyte receptor$\beta$ repertoire in experimental EBA is displayed by the additionally published model for experimental EBA, which was developed by Iwata et al. (2013). Likewise the model by Sitaru et al. (2006), the model of Iwata et al. (2013) is based on the application of a peptide derived from the NC1 domain of the murine COL7, but uses the von-Willebrand-factor A like domain 2 (vWFA2). It would be interesting to analyze the T-lymphocyte receptor$\beta$ repertoire in this model with regard to $T_{fh}$ repertoire under autoimmune condition. For such an analysis, two differences between both model have to be considered: (I) Iwata et al. (2013) utilize a murine C57BL/6 background, in which the H2s MHC class II was introduced and (II) the administered antigen vWFA2 is not linked to GST. Since SJL/J mice contain a genomic deletion within the T-lymphocyte receptor$\beta$ V-segment locus (Behlke et al., 1986; Jackson and Krangel, 2005), the number of V-segments in the C57BL/6 background is higher and the lack of GST makes this control group unnecessary. Thus, results in model by Iwata et al. (2013) might be different from the results obtained in the dissertation. Therefore, of special interest would be the usage of the V3-segment. One could speculate, that the identical disease phenotype of the model by Iwata et al. (2013) also shows a V3-segment association, however, the different murine background and the application of a distinct antigen make also an association of no or a different V-segment possible.

## 4.2 $T_{fh}$ T-lymphocyte receptor$\beta$ clonotypes are highly uniform in contralateral lymph nodes of an individual

In the EBA model by Sitaru et al. (2006), immunization is carried out by a parallel injection into both foot pads, which leads to an uniform induction of germinal centers within contralateral lymph nodes (Fig. 3.13 C and Fig. S2). Since in this dissertation, a specific accumulation of $T_{fh}$ T-lymphocyte receptor$\beta$ clonotypes was found under autoimmune condition, the question

was addressed, whether the $T_{fh}$ repertoire is identical among contralateral lymph nodes within individuals. When comparing the individual $T_{fh}$ clonotypes among contralateral lymph nodes, this dissertation revealed, that frequencies of clonotypes correlate in contralateral lymph nodes (Fig. 3.22) and a highly uniform repertoire is formed under autoimmune condition (Fig. 3.23). Furthermore, specifically the most prevalent $T_{fh}$ clonotypes are shared between contralateral lymph nodes of an individual (Fig. 3.25). Therefore, this data show, that draining lymph node harbor a highly uniform $T_{fh}$ repertoire under autoimmune condition, which exist bilaterally.

### 4.2.1 Migration of $T_{fh}$ might establish uniformity of the contralateral T-lymphocyte receptor$\beta$ repertoire

When investigating the uniformity of the contralateral $T_{fh}$ T-lymphocyte receptor$\beta$ repertoire within an individual (Fig. 3.23), it was found to exceed uniformity of the $T_{fh}$ repertoire between individuals up to 5 times (Fig. 3.16 C) and the repertoire of $T_{skin}$ up to 20 times (Fig. 3.9 C). This demonstrates, that the $T_{fh}$ repertoire among contralateral lymph nodes in an individual is highly identical and dramatically exceed the identity found among mice. An explanation of the high uniformity among contralateral lymph nodes might be a random upcoming of identical $T_{fh}$ clonotypes in similar frequencies by chance. Since the identical antigen is injected in both foot pads and subsequently T-lymphocytes in both contralateral lymph nodes are activated by the identical antigen, a parallel activation of identical $T_{fh}$ clonotypes is imaginable. Also the correlating frequencies are explainable in the situation of a parallel activation. Since identical T-lymphocyte receptor$\beta$ clonotypes comprise an equal specificity to the antigen loaded MHC class II complex, an equal expansion rate is conceivable (Jenkins et al., 1991). However, this assumption neglects the tremendous diversity of the T-lymphocyte receptor repertoire (Zarnitsyna et al., 2013; Lythe et al., 2016) and assumes a nearly equal repertoire between contralateral lymph nodes prior immunization, which was shown to be only in the range of 10% identity (Textor et al., 2018). Therefore, a different explanation for this observation, considering the tremendous diversity and initial low identity, might be a migratory behavior of $T_{fh}$. This could display the underlying mechanism for the highly uniform $T_{fh}$ T-lymphocyte receptor$\beta$ repertoire among contralateral lymph nodes. For $T_{fh}$ it is known that, they are able to migrate between germinal centers within a lymph node (Shulman et al., 2013), are able to leave lymphatic organs and circulate in the blood stream (Ueno, 2016; Ma and Phan, 2017) and are also known to be specifically elevated in skin related autoimmune diseases (Choi et al., 2015; Wang et al., 2017). Transferring this to the experimental EBA model, it deducts the hypothesis, that during the germinal center reaction, $T_{fh}$ emigrate out of the draining lymph

node and since the contralateral popliteal lymph nodes are not directly connected via lymphatic vessels (Zhang et al., 2013), they circulate via the blood stream until immigration into the opposing lymph node and re-localization in a germinal center. Thereby, this hypothesis is supported by results of the phenotypic $T_{fh}$ isolation obtained in the dissertation. For the phenotypic isolation of $T_{fh}$, the anatomical structure of the lymph node was resolved. Therefore, by isolation of $T_{fh}$ via FACS (Fig. 3.26), a random assortment of $T_{fh}$ was obtained, in which $T_{fh}$ from germinal centers of the entire lymph node were combined. By comparison of these $T_{fh}$ T-lymphocyte receptor$\beta$ clonotypes, the overall highest correlation (Fig. 3.26 D) and uniformity (Fig. 3.26 F) was observable. This demonstrates, that nearly the entirety of $T_{fh}$ among contralateral lymph nodes is not only build up by identical T-lymphocyte receptor$\beta$ clonotypes, they also exists in correlating frequencies. This makes a parallel emergence nearly impossible and further strengthens the hypothesis of an active cross talk of contralateral lymph nodes via migrating $T_{fh}$.

### 4.2.2 Availability of the antigen might determine the the uniformity of the contralateral $T_{fh}$ T-lymphocyte receptor$\beta$ repertoire

The hypothesis, that the uniformity of the $T_{fh}$ T-lymphocyte receptor$\beta$ repertoire is constituted via a migratory cross talk between contralateral lymph nodes also implies, that after all immunizations an uniform repertoire has to be established. However, investigating the correlation of individual $T_{fh}$ clonotype frequencies (Fig. 3.22) and uniformity of the contralateral $T_{fh}$ repertoires (Fig. 3.23) three stages of uniformity are revealed. Thereby, PBS/TM shows the lowest frequency correlation and uniformity, GST/TM shows medium levels and mCOL7c-GST/TM shows the highest levels. This separation in three stages is also observable, by specifically focusing on the most prevalent clonotypes (Fig. 3.25). This shows, that this observation is not only present for the entire repertoire, but also for the most prevalent clonotypes. Given, that the cross talk between contralateral lymph nodes is equal among immunization groups, it has to be assumed, that $T_{fh}$ are mechanistically retained in germinal centers. Since $T_{fh}$ are selected for antigen specificity during migration into germinal centers (Crotty, 2014), one could speculate, that the presentation of the identical antigen among the contralateral lymph nodes results in a cellular capturing. Thus, in terms of PBS/TM, where no specific antigen was injected, no capturing occurs and subsequently results in the lowest uniformity. In the case of GST/TM and mCOL7c-GST/TM, where $T_{fh}$ can be captured by the identical antigen, the uniformity is higher compared to PBS/TM. However, although not being significantly different, the variable GST/TM results show the second highest, whereas mCOL7c-GST/TM results in the highest uniformity (Fig. 3.23). Considering, that no statistical difference is

detectable among GST/TM and mCOL7c-GST/TM and both antigens were administered equimolar (Tab. 2.9), it might be possible, that availability of the peptides differ between mice at the time point of examination. In case of the GST/TM, two mice show a correlation coefficient and an uniformity comparable to PBS/TM, whereas the remaining is comparable to mCOL7c-GST/TM. Thus, it might be possible, that the xeno-antigen GST is depleted over time, which leads to a decreased capturing rate and results in a reduced uniformity of the $T_{fh}$ repertoire in contralateral lymph nodes. In contrast, the endogenous presence of the auto-antigen, might sustain capturing at the time point of examination, keeping the uniformity at highest level.

To test, this capturing hypothesis, uniformity of the $T_{fh}$ T-lymphocyte receptor$\beta$ repertoire was followed at defined disease stages over time. Thereby, it was found, that the pre-diseased uniformity is equal to the time point of induction, reaches the maximum at disease onset and declines to control levels during chronic manifestation (Fig. 3.27). 14 days after immunization, were auto-antibodies are detectable in the blood and deposit at the DEJ (Hammers et al., 2011), the rate of capturing is identical to the time point of disease onset 28 day after immunization (Hammers et al., 2011). This demonstrates on the one hand, that uniformity of the $T_{fh}$ repertoire is already established prior disease onset and on the other hand, expectably $T_{fh}$ are captured, since the auto-antigen was administered bilaterally. But in this experiment, the interesting finding concerns the time point 49 days after immunization. For that time point, an unspecific activation of bystander B-lymphocytes is reported (Tiburzy et al., 2013) and since B-lymphocytes are only activated unspecifically, an auto-antigen driven germinal center reaction can be excluded. This implies, that also an auto-antigen specific capturing of $T_{fh}$ is lacking 49 days after mCOL7c-GST/TM immunization. And indeed, the uniformity of the $T_{fh}$ repertoire among contralateral lymph nodes decreased to PBS/TM control level (Fig. 3.27). This particular finding strengthens the hypothesis, that the availability of the antigen mediates capturing of migrating $T_{fh}$ T-lymphocyte receptor$\beta$ clonotypes in contralateral lymph nodes.

Applying this hypothesis to the analysis of the $T_{fh}$ T-lymphocyte receptor$\beta$ repertoire within one mouse, which was analyzed at two consecutive time points in Chap. 3.4.4.2, no connection between the early and chronic late time point should exist. However, the results of this dissertation shown, that $T_{fh}$ clonotypes, which are most prevalent at early time points in germinal centers are also present at late time points (Fig. 3.28). This demonstrates, independent from the antigen-specific capturing, that dominant $T_{fh}$ clonotypes of a pre-diseased time point are present in germinal cen-

ters. This observation might be attributable to an establishment of a $T_{fh}$ memory compartment (Hale and Ahmed, 2015) of potentially auto-antigen-specific $T_{fh}$. For such memory $T_{fh}$ it could be shown, that the characteristic CxCR5 surface expression is maintained long lasting (Choi et al., 2013) and that those memory $T_{fh}$ are recalled to immune reactions (Liu et al., 2012). Therefore, it might be possible, that auto-antigen-specific memory $T_{fh}$ are constantly and quickly recalled into the immune response and since they retained the $T_{fh}$ phenotype, they specifically search for their antigen in germinal centers.

Taken together findings of the $T_{fh}$ T-lymphocyte receptor$\beta$ repertoire analysis among contralateral lymph nodes in an individual show, that the repertoire of $T_{fh}$ is highly uniform among germinal centers of the left and right draining lymph node. Thereby, it could be shown, that this uniformity is highest in response to the auto-antigen at the time point of EBA onset. In relation with the finding, that the T-lymphocyte receptor$\beta$ V3-segment is elevated under autoimmune condition, the hypothesis of a direct disease association between experimental EBA and the V3-segment is further strengthened and demonstrates, that a synchronized T-lymphocyte receptor$\beta$ repertoire of $T_{fh}$ displays a promising intervention target. However, the formation of this uniformity is not exclusively auto-antigen related and rather a general immunological process, which might be triggered by migration of $T_{fh}$ and an antigen mediated capturing in germinal centers, as long as the antigen is available. An interesting experiment, to confirm, that $T_{fh}$ are captured in germinal centers during migration, would be the modulation of administered antigens. By administering two divergent antigens, the antigen-specific capturing for immigration into germinal centers would differ in contralateral lymph nodes. It is imaginable, that due to this experimental adaptation the emergence of uniformity among the contralateral $T_{fh}$ T-lymphocyte receptor$\beta$ repertoire is prevented. In such an experiment it has to be expected, that the uniformity would only reach the PBS/TM control level, which would confirm that capturing only occurs if the specific antigen is available.

## 4.3 $T_{fh}$ T-lymphocyte receptor$\beta$ clonotypes localize auto-antigen independent in the skin

This dissertation suggests a migration to be the underlying mechanism, for constitution of the highly uniform $T_{fh}$ T-lymphocyte receptor$\beta$ repertoire among contralateral lymph nodes. For $T_{fh}$ it is known, that they circulate in the blood stream (Ueno, 2016; Ma and Phan, 2017), are elevated in skin related autoimmune diseases (Choi et al., 2015; Wang et al., 2017) and for systemic sclerosis, a dermal immigration of $T_{fh}$-like cells was found (Taylor et al., 2018). Based on this, it is reasonable

to speculate, that a migration of $T_{fh}$ is not only restricted to lymphatic organs, one could also speculate, that in immunization induced EBA $T_{fh}$ are able to migrate in dermal wounds. Therefore the $T_{fh}$ repertoire was compared to the repertoire of $T_{skin}$ and the question was addressed, whether $T_{fh}$ clonotypes are also present in the skin.

### 4.3.1 Most prevalent $T_{fh}$ T-lymphocyte receptor$\beta$ clonotypes are present in the skin

When comparing the T-lymphocyte receptor$\beta$ repertoire of $T_{fh}$ to $T_{skin}$, no frequency-correlation was detectable in either immunization group (Fig. 3.29) and although an overlap between both repertoires exist, the overlap is constituted auto-antigen unspecific after peptide immunization (Fig. 3.30). Also the overlapping clonotypes do neither feature the specific T-lymphocyte receptor$\beta$ V3-segment accumulation of $T_{fh}$, nor a general accumulation of a V- or J-segment (Fig. 3.31). With regard to the previous findings, that the $T_{skin}$ repertoire is not affected under autoimmune condition (Fig. 3.9 C) and no elevated V3-segment usage could be found for $T_{skin}$ (Fig. 3.11 A), it is reasonable, that no elevated presence of $T_{fh}$ clonotypes was detectable in the skin. This demonstrates, that although $T_{fh}$ clonotypes are present among the $T_{skin}$ clonotypes, the immigration of those is triggered by an antigen-unspecific effect, likewise discussed for $T_{skin}$ in Chap. 4.1.4.1.

However, focusing specifically on the most prevalent $T_{fh}$ T-lymphocyte receptor$\beta$ clonotypes, it could be shown, that after GST/TM and mCOL7c-GST/TM immunization especially the most prevalent clonotypes can be found in the skin (Fig. 3.33). For PBS/TM however, such an elevated appearance is not detectable. This observation might also be attributable to the uniformity of the contralateral $T_{fh}$ repertoire, which is discussed in Chap. 4.2. Via the bilateral administration of the identical antigen, specifically the most prevalent $T_{fh}$ clonotypes are shared between contralateral lymph nodes of an individual (Fig. 3.25) and the uniformity of the contralateral $T_{fh}$ repertoire is higher in response to peptide antigens (Fig. 3.23). Thus, the most prevalent $T_{fh}$ clonotypes probably emigrate at the highest rate out of the lymph nodes and therefore, it is most likely, that these are also present among the $T_{skin}$ clonotypes. This shows, that this process is most likely based on the $T_{fh}$ frequencies in the lymph nodes and suggests a cross talk between the activated lymph nodes and the skin.

### 4.3.2 Identical $T_{fh}$ and $T_{skin}$ T-lymphocyte receptor$\beta$ clonotypes might be derived for a common clonal origin

As discussed, the presence of $T_{fh}$ T-lymphocyte receptor$\beta$ clonotypes among the repertoire of $T_{skin}$ might be attributable to an immigration of $T_{fh}$ into the skin. However, a phenotypic verification, whether $T_{fh}$ cells are present in the skin has not been analyzed in this study. An alternative explanation for the presence of $T_{fh}$ clonotypes among the $T_{skin}$ clonotypes might also be, that both are derived from a common clonal origin. Thereby, for the skin immigrating $T_H1$ and germinal center $T_{fh}$ a transitional stage between both subtypes is described in the literature (Nakayamada et al., 2011; Oestreich and Weinmann, 2012). Thus, in accordance to the strong $T_H1$ phenotype in the skin after mCOL7c-GST/TM immunization and, at least, the partial elevated IFN$\gamma$ expression after GST/TM immunization (Fig. 3.5 A), the observed auto-antigen unspecific overlap might also be attributable to the parallel emergence of $T_H1$ and $T_{fh}$ form a common clonal origin.

# 5 Supplemental data

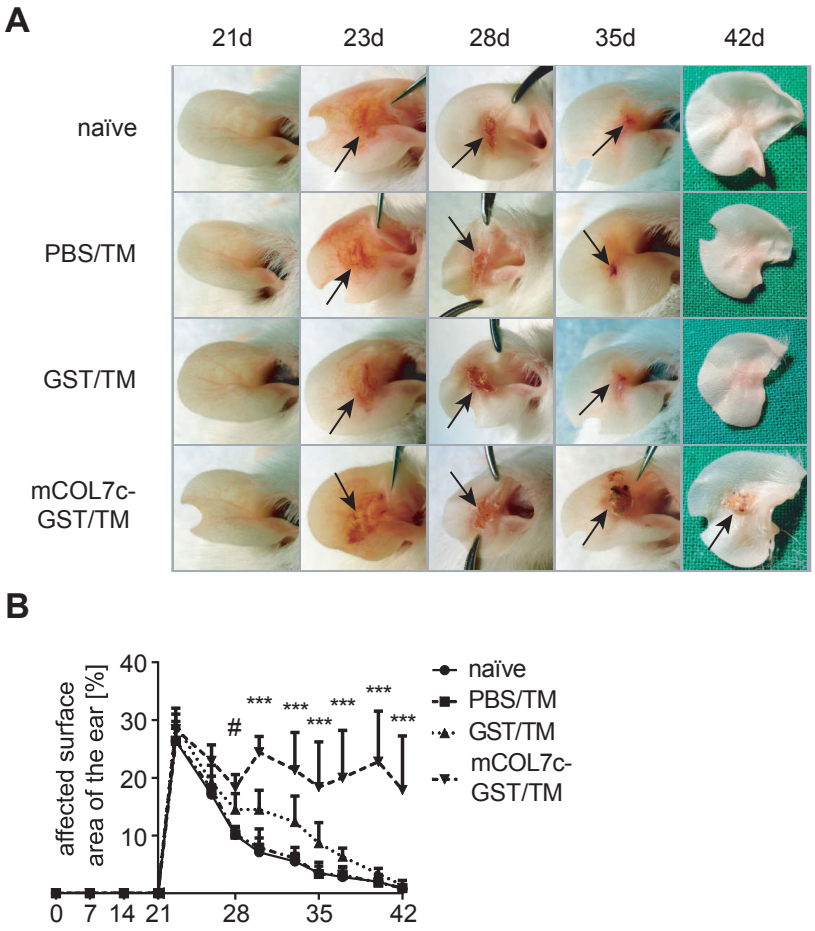


**Figure S1: Scratching triggers chronic wound formation in immunization induced EBA.** SJL/J mice were either naïve or immunized using PBS/TM, GST/TM or mCOL7c-GST/TM into both hind foot pads. On experimental day 21, the inner side of both ears was scratched. The affected ear area was evaluated progressively, prior scratching in weekly iterations and iterations of 2-3 days after scratching. The experiment ran until experimental day 42. A) Representative images of ears on experimental day 21, 23, 28, 35 and 42. Arrows point at dermal wounds. B) Percentage of the affected ear surface area over time (significance represents the comparison of mCOL7c-GST/TM against the different experimental groups, # mCOL7c-GST/TM against GST/TM is not significant, mCOL7c-GST/TM against naïve and PBS/TM = ***). n=5-6, data is expressed as means ± SD, *** $p<0.001$, Two-Way ANOVA with Dunnett's post-hoc test.

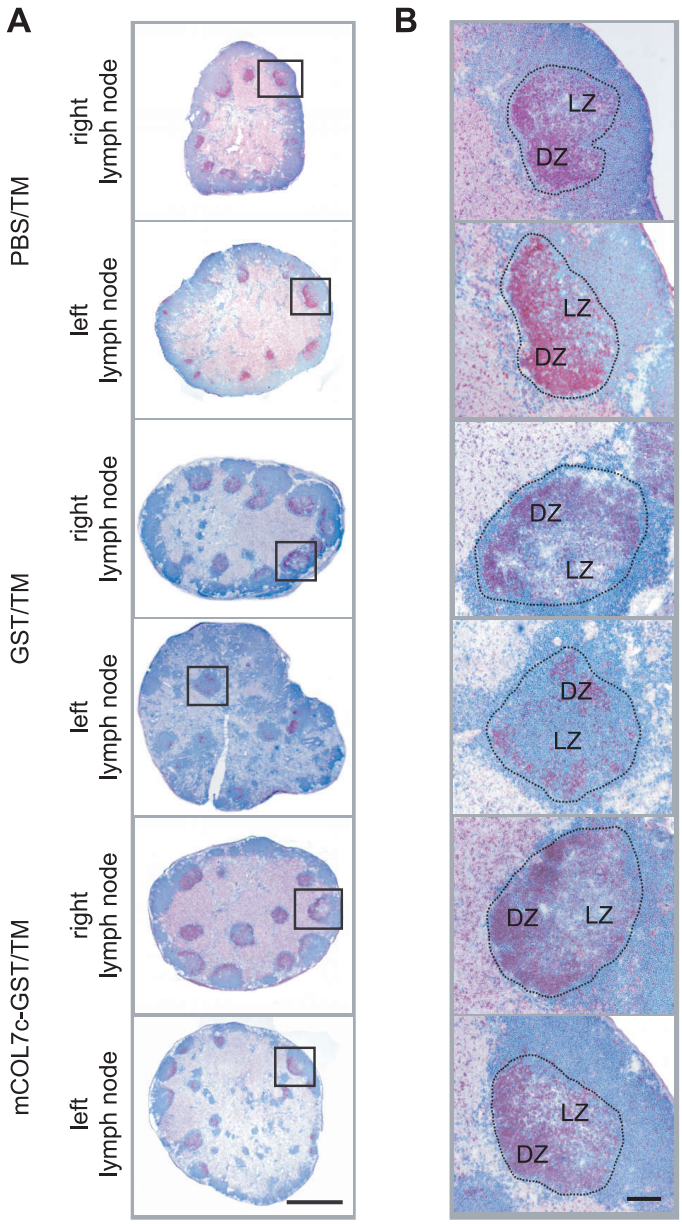


**Figure S2: Germinal centers are homogeneously induced in opposing draining lymph nodes.** SJL/J mice were immunized using PBS/TM, GST/TM or mCOL7c-GST/TM into both hind foot pads. The skin of both ears was scratched 21 days after immunization. 7 days after, draining lymph nodes were obtained and 12$\mu$m cryosections were stained for proliferating cells (red = Ki-67) and B-lymphocytes (blue = B220). A) A depiction of contralateral lymph nodes of an individual mouse per immunization group (scale bar $\widehat{=}$ 1.000$\mu$m), solid lines indicate area of magnification. B) Magnification of an individual germinal center exhibits the prototypic segregation in DZ and LZ (scale bar $\widehat{=}$ 100$\mu$m), dashed lines edge the GC. DZ=dark zone, LZ=light zone.

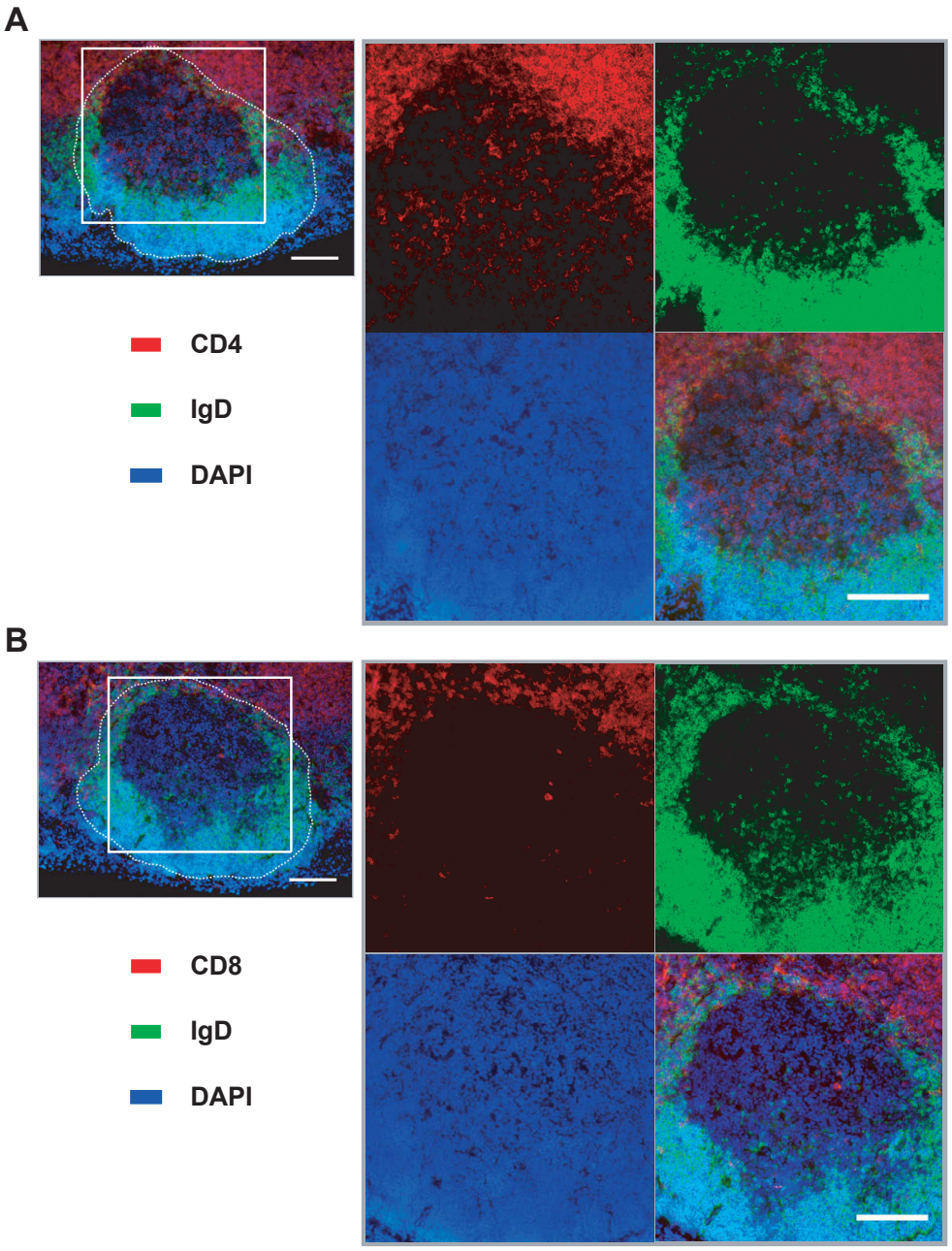


**Figure S3: Only CD4$^+$ T-lymphocytes are detectable in germinal center.** SJL/J mice were immunized using mCOL7c-GST/TM into both hind foot pads. The skin of both ears was scratched 21 days after immunization. 7 days after, draining lymph nodes were obtained and serial 12$\mu$m cryosections were stained for CD4 (red) or CD8 (red) and IgD (green), nuclei were counter-stained using DAPI (blue). Germinal centers were identified as rounded IgD$^+$ areas, with a distinct IgD$^-$ center. Immunofluorescence staining for A) CD4$^+$ T-lymphocytes and B) CD8$^+$ T-lymphocytes within the identical germinal center. Scale bar $\widehat{=}$ 100$\mu$m.

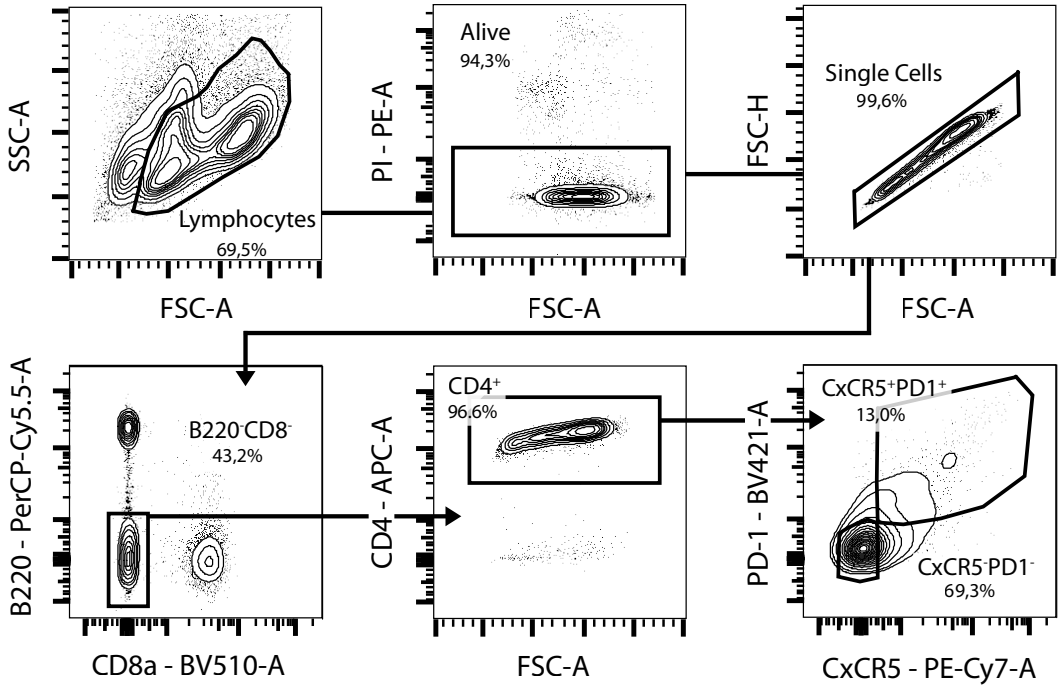


**Figure S4: Gating-strategy for phenotypic isolation of $T_{fh}$ via FACS.** SJL/J mice were immunized using mCOL7c-GST/TM into both hind foot pads. The skin of both ears was scratched 21 days after immunization. 7 days after, both draining lymph nodes were obtained. Subsequently, $4x10^6$ cells were isolated and incubated with anti-CD16/CD32 mAbs. Fluorescence labeled mAbs against B220, CD8, CD4, CxCR5 and PD-1 were used in established concentrations for surface staining. Cellular viability was considered by adding Propidium iodide prior evaluation. Viable single cells were gated for $B220^-/CD8a^-/CD4^+$. $T_{fh}$ were further identified as $CxCR5^+/PD\text{-}1^+$ (Baumjohann et al., 2013). $T_{fh}$-sorting was conducted using the FACS LSR III platform.

**Table S1: Summary of T-lymphocyte receptor$\beta$ clonotypes obtained by laser microdissection**

| | mouse | comp. | days post imm. | volume [x$10^7 \mu m^3$] | isolated T-lymphocytes [x$10^4$] | raw reads [n x$10^6$] | TCR$\beta$ sequences [n x$10^6$] | Annotated TCR$\beta$ clonotypes [n] | TCR$\beta$ clonotypes > median [n] |
|---|---|---|---|---|---|---|---|---|---|
| **mCOL7c-GST/TM** | 1 | Skin left | 28 | 123.0 | 69.2 | 0.59 | 0.17 | 1669 | 834 |
| | | GC left | | 4.68 | 3.19 | 2.08 | 0.95 | 6269 | 3096 |
| | | Skin right | | 103.0 | 67.1 | 1.86 | 0.82 | 310 | 155 |
| | | GC right | | 4.34 | 3.77 | 2.04 | 1.42 | 1919 | 958 |
| | 2 | Skin left | | 104.0 | 76.3 | 1.62 | 0.40 | 662 | 330 |
| | | GC left | | 5.16 | 3.77 | 2.30 | 1.08 | 1503 | 747 |
| | | Skin right | | 175.0 | 118.0 | 1.75 | 0.93 | 1263 | 626 |
| | | GC right | | 3.91 | 4.12 | 1.99 | 1.16 | 4378 | 2187 |
| | 3 | Skin left | | 199.0 | 150.0 | 1.62 | 0.44 | 670 | 335 |
| | | GC left | | 4.44 | 4.10 | 1.56 | 1.00 | 1467 | 729 |
| | | Skin right | | 134.0 | 123.0 | 1.88 | 0.86 | 840 | 420 |
| | | GC right | | 4.29 | 3.57 | 2.04 | 1.21 | 4250 | 2122 |

| | mouse | comp. | days post imm. | volume [x$10^7 \mu m^3$] | isolated T-lymphocytes [x$10^4$] | raw reads [n x$10^6$] | TCR$\beta$ sequences [n x$10^6$] | Annotated TCR$\beta$ clonotypes [n] | TCR$\beta$ clonotypes > median [n] |
|---|---|---|---|---|---|---|---|---|---|
| **mCOL7c-GST/TM** | 1 | GC left | 14 | 4.26 | 3.62 | 2.32 | 0.70 | 1625 | 808 |
| | | GC right | | 4.51 | 3.85 | 1.96 | 1.04 | 3033 | 1514 |
| | 2 | GC left | | 4.63 | 3.69 | 2.19 | 1.02 | 2321 | 1159 |
| | | GC right | | 4.52 | 3.63 | 2.45 | 1.16 | 1672 | 835 |
| | 3 | GC left | | 4.29 | 3.59 | 2.09 | 0.60 | 2851 | 1422 |
| | | GC right | | 4.68 | 3.87 | 2.26 | 0.55 | 2287 | 1141 |
| **mCOL7c-GST/TM** | 1 | GC left | 49 | 4.32 | 3.67 | 1.95 | 0.67 | 2408 | 1204 |
| | | GC right | | 4.23 | 3.59 | 2.37 | 0.2 | 1033 | 514 |
| | 2 | GC left | | 4.15 | 3.62 | 1.96 | 0.47 | 2060 | 1028 |
| | | GC right | | 4.64 | 3.93 | 2.09 | 0.56 | 644 | 322 |
| | 3 | GC left | | 4.16 | 3.54 | 1.63 | 0.31 | 954 | 474 |
| | | GC right | | 3.75 | 3.36 | 2.28 | 0.24 | 394 | 197 |

| | mouse | comp. | days post imm. | volume [x$10^7 \mu m^3$] | isolated T-lymphocytes [x$10^4$] | raw reads [n x$10^6$] | TCR$\beta$ sequences [n x$10^6$] | Annotated TCR$\beta$ clonotypes [n] | TCR$\beta$ clonotypes > median [n] |
|---|---|---|---|---|---|---|---|---|---|
| mCOL7c-GST/TM | 1 | GC left | 15 | 3.91 | 3.24 | 2.03 | 0.34 | 2219 | 1103 |
| | | GC right | 71 | 4.48 | 3.11 | 1.63 | 0.79 | 3821 | 1898 |
| | 2 | GC left | 15 | 3.98 | 3.13 | 1.84 | 0.60 | 1375 | 686 |
| | | GC right | 71 | 4.51 | 3.43 | 2.03 | 1.30 | 3680 | 1836 |
| | 3 | GC left | 15 | 3.99 | 3.00 | 1.77 | 0.85 | 2064 | 1032 |
| | | GC right | 71 | 4.18 | 3.04 | 1.77 | 0.85 | 2064 | 1032 |
| | 4 | GC left | 15 | 4.04 | 3.30 | 2.03 | 0.91 | 723 | 361 |
| | | GC right | 71 | 4.29 | 3.54 | 1.70 | 0.43 | 820 | 410 |

| | mouse | comp. | days post imm. | volume [x$10^7 \mu m^3$] | isolated T-lymphocytes [x$10^4$] | raw reads [n x$10^6$] | TCR$\beta$ sequences [n x$10^6$] | Annotated TCR$\beta$ clonotypes [n] | TCR$\beta$ clonotypes > median [n] |
|---|---|---|---|---|---|---|---|---|---|
| **GST/TM** | 1 | Skin left | 28 | 134 | 72.3 | 1.59 | 0.22 | 757 | 375 |
| | | GC left | | 4.68 | 3.56 | 1.74 | 0.86 | 1348 | 674 |
| | | Skin right | | 111 | 66.9 | 1.97 | 1.06 | 792 | 396 |
| | | GC right | | 4.22 | 3.24 | 1.70 | 0.61 | 439 | 218 |
| | 2 | Skin left | | 159 | 109.0 | 1.24 | 0.49 | 3903 | 1907 |
| | | GC left | | 2.88 | 3.63 | 1.87 | 1.24 | 1328 | 662 |
| | | Skin right | | 263 | 141.0 | 1.62 | 1.48 | 1680 | 840 |
| | | GC right | | 4.09 | 3.53 | 2.27 | 0.64 | 1974 | 981 |
| | 3 | Skin left | | 115 | 80.7 | 1.53 | 0.40 | 2725 | 1355 |
| | | GC left | | 4.68 | 3.71 | 1.59 | 0.45 | 2275 | 1136 |
| | | Skin right | | 194 | 107.0 | 1.71 | 1.55 | 1623 | 811 |
| | | GC right | | 3.99 | 3.46 | 1.71 | 1.03 | 1125 | 562 |

| | mouse | comp. | days post imm. | volume [x$10^7 \mu m^3$] | isolated T-lymphocytes [x$10^4$] | raw reads [n x$10^6$] | TCR$\beta$ sequences [n x$10^6$] | Annotated TCR$\beta$ clonotypes [n] | TCR$\beta$ clonotypes > median [n] |
|---|---|---|---|---|---|---|---|---|---|
| **PBS/TM** | 1 | Skin left | 28 | 197 | 119.0 | 2.31 | 0.56 | 558 | 279 |
| | | GC left | | 3.97 | 3.31 | 2.10 | 0.97 | 545 | 272 |
| | | Skin right | | 165 | 86.9 | 1.61 | 1.31 | 1440 | 720 |
| | | GC right | | 4.38 | 3.65 | 1.96 | 0.59 | 2455 | 1226 |
| | 2 | Skin left | | 148 | 102.0 | 2.15 | 0.75 | 483 | 241 |
| | | GC left | | 3.73 | 3.11 | 2.26 | 0.72 | 1091 | 547 |
| | | Skin right | | 197 | 180.0 | 1.81 | 1.49 | 1271 | 635 |
| | | GC right | | 4.20 | 3.50 | 1.61 | 0.45 | 2427 | 1207 |
| | 3 | Skin left | | 184 | 126.0 | 2.31 | 0.88 | 559 | 279 |
| | | GC left | | 4.06 | 3.39 | 2.35 | 0.63 | 623 | 310 |
| | | Skin right | | 177 | 94.0 | 1.63 | 1.27 | 1316 | 658 |
| | | GC right | | 4.03 | 3.36 | 1.63 | 1.45 | 7329 | 3646 |

**Table S2: Summary of T-lymphocyte receptor$\beta$ clonotypes obtained by FACS**

| | mouse | comp. | days post imm. | isolated $T_{fh}$ cells [n x$10^4$] | raw reads [n x$10^6$] | TCR$\beta$ sequences [n x$10^6$] | Annotated TCR$\beta$ clonotypes [n] | TCR$\beta$ clonotypes > median [n] |
|---|---|---|---|---|---|---|---|---|
| **mCOL7c-GST/TM** | 1 | Tfh left | 28 | 4.3 | 2.02 | 1.68 | 11522 | 5744 |
| | | Tfh right | | 5.0 | 2.23 | 1.76 | 13418 | 6615 |
| | 2 | Tfh left | | 4.5 | 2.04 | 1.68 | 11942 | 5891 |
| | | Tfh right | | 3.6 | 2.12 | 1.89 | 12988 | 6489 |
| | 3 | Tfh left | | 5.0 | 1.83 | 1.43 | 8420 | 4181 |
| | | Tfh right | | 5.0 | 2.42 | 2.17 | 11579 | 5768 |

**Table S3: CDR3 amino acid composition of $T_{fh}$ T-lymphocyte receptor$\beta$ clonotypes that are shared among three individuals and contain the V3-segment**

| # | CDR3 [AA] | TRBV | TRBJ |
|---|---|---|---|
| 1 | ASSFRQDTQY | V3 | J2-5 |
| 2 | ASSFRQYEQY | V3 | J2-7 |
| 3 | ASSLALGGQNTLY | V3 | J2-4 |
| 4 | ASSLARDAEQF | V3 | J2-1 |
| 5 | ASSLARDERLF | V3 | J1-4 |
| 6 | ASSLGENTLY | V3 | J2-4 |
| 7 | ASSLGRANTEVF | V3 | J1-1 |
| 8 | ASSLKSQNTLY | V3 | J2-4 |
| 9 | ASSLLDNYEQY | V3 | J2-7 |
| 10 | ASSLRQDTQY | V3 | J2-5 |
| 11 | ASSLRQYEQY | V3 | J2-7 |
| 12 | ASSLRSAETLY | V3 | J2-3 |
| 13 | ASSLRSQNTLY | V3 | J2-4 |
| 14 | ASSLRTGGAETLY | V3 | J2-3 |
| 15 | ASSLVRDAEQF | V3 | J2-1 |
| 16 | ASSPDRANTEVF | V3 | J1-1 |
| 17 | ASSPRAETLY | V3 | J2-3 |
| 18 | ASSPRQDTQY | V3 | J2-5 |
| 19 | ASSSDRGQDTQY | V3 | J2-5 |

# 6 Bibliography

Abbas, A. K., Lichtman, A. H., Pillai, S., and Preceded by: Abbas, A. K. (2017). *Cellular and molecular immunology*. Elsevier, 9th edition.

Altman, J. D., Moss, P. A., Goulder, P. J., Barouch, D. H., McHeyzer-Williams, M. G., Bell, J. I., McMichael, A. J., and Davis, M. M. (1996). Phenotypic analysis of antigen-specific T lymphocytes. *Science*, 274(5284):94–6.

Arakawa, M., Dainichi, T., Ishii, N., Hamada, T., Karashima, T., Nakama, T., Yasumoto, S., Tsuruta, D., and Hashimoto, T. (2011). Lesional Th17 cells and regulatory T cells in bullous pemphigoid. *Experimental Dermatology*, 20(12):1022–1024.

Bagwell, C. B. and Adams, E. G. (1993). Fluorescence spectral overlap compensation for any number of flow cytometry parameters. *Annals of the New York Academy of Sciences*, 677:167–84.

Banczyk, D., Kalies, K., Nachbar, L., Bergmann, L., Schmidt, P., Bode, U., Teegen, B., Steven, P., Lange, T., Textor, J., Ludwig, R. J., Stöcker, W., König, P., Bell, E., and Westermann, J. (2014). Activated CD4 + T cells enter the splenic T-cell zone and induce autoantibody-producing germinal centers through bystander activation. *European Journal of Immunology*, 44(1):93–102.

Baumjohann, D., Baumjohann, D., and Ansel, K. M. (2013). Identification of T follicular helper (Tfh) cells by flow cytometry. *Protocol Exchange*, 6:1–14.

Behlke, M. A., Chou, H. S., Huppi, K., and Loh, D. Y. (1986). Murine T-cell receptor mutants with deletions of beta-chain variable region genes. *Proceedings of the National Academy of Sciences*, 83(3):767–771.

Benichou, J., Ben-Hamo, R., Louzoun, Y., and Efroni, S. (2012). Rep-Seq: uncovering the immunological repertoire through next-generation sequencing. *Immunology*, 135(3):183–191.

Bennett, B., Check, I. J., Olsen, M. R., and Hunter, R. L. (1992). A comparison of commercially available adjuvants for use in research. *Journal of Immunological Methods*, 153(1-2):31–40.

Best, K., Oakes, T., Heather, J. M., Shawe-Taylor, J., and Chain, B. (2015). Computational analysis of stochastic heterogeneity in PCR amplification efficiency revealed by single molecule barcoding. *Scientific Reports*, 5:14629.

Bieber, K., Koga, H., and Nishie, W. (2017a). In vitro and in vivo models to investigate the pathomechanisms and novel treatments for pemphigoid diseases. *Experimental Dermatology*, 26(12):1163–1170.

Bieber, K., Sun, S., Witte, M., Kasprick, A., Beltsiou, F., Behnen, M., Laskay, T., Schulze, F. S., Pipi, E., Reichhelm, N., Pagel, R., Zillikens, D., Schmidt, E., Sparwasser, T., Kalies, K., and Ludwig, R. J. (2017b). Regulatory T Cells Suppress Inflammation and Blistering in B. *Frontiers in Immunology*, 8:1628.

Bieber, K., Witte, M., Sun, S., Hundt, J. E., Kalies, K., Dräger, S., Kasprick, A., Twelkmeyer, T., Manz, R. A., König, P., Köhl, J., Zillikens, D., and Ludwig, R. J. (2016). T cells mediate autoantibody-induced cutaneous inflammation and blistering in epidermolysis bullosa acquisita. *Scientific Reports*, 6(1):38357.

Birkholz, K., Hofmann, C., Hoyer, S., Schulz, B., Harrer, T., Kämpgen, E., Schuler, G., Dörrie, J., and Schaft, N. (2009). A fast and robust method to clone and functionally validate T-cell receptors. *Journal of Immunological Methods*, 346(1-2):45–54.

Bolotin, D. A., Shugay, M., Mamedov, I. Z., Putintseva, E. V., Turchaninova, M. A., Zvyagin, I. V., Britanova, O. V., and Chudakov, D. M. (2013). MiTCR: software for T-cell receptor sequencing data analysis. *Nature Methods*, 10(9):813–814.

Bosc, N., Folch, G., Ginestoux, C., Giudicelli, V., and Lefranc, M.-P. (2005a). IMGT overview: the mouse T cell receptor alpha TRA genes. Technical report, IMGT, the international ImMunoGeneTics information system.

Bosc, N., Folch, G., Ginestoux, C., Giudicelli, V., and Lefranc, M.-P. (2005b). IMGT overview: the mouse T cell receptor beta TRB genes. Technical report, IMGT, the international ImMunoGeneTics information system.

Brunner, P. M., Emerson, R. O., Tipton, C., Garcet, S., Khattri, S., Coats, I., Krueger, J. G., and Guttman-Yassky, E. (2017). Nonlesional atopic dermatitis skin shares similar T-cell clones with lesional tissues. *Allergy*, 72(12):2017–2025.

Calis, J. J. and Rosenberg, B. R. (2014). Characterizing immune repertoires by high throughput sequencing: strategies and applications. *Trends in Immunology*, 35(12):581–590.

Ceccarelli, F., Agmon-Levin, N., and Perricone, C. (2016). Genetic Factors of Autoimmune Diseases. *Journal of Immunology Research*, 2016:3476023.

Chen, W., Jin, W., Hardegen, N., Lei, K.-j., Li, L., Marinos, N., McGrady, G., and Wahl, S. M. (2003). Conversion of Peripheral CD4+CD25 Naive T Cells to CD4+CD25+ Regulatory T Cells by TGF-$\beta$ Induction of Transcription Factor Foxp3. *Journal of Experimental Medicine*, 198(12):1875–1886.

Chiriac, M., Roesler, J., Sindrilaru, A., Scharffetter-Kochanek, K., Zillikens, D., and Sitaru, C. (2007). NADPH oxidase is required for neutrophil-dependent autoantibody-induced tissue damage. *Journal of Pathology*, 212(1):56–65.

Cho, Y.-L., Flossdorf, M., Kretschmer, L., Höfer, T., Busch, D. H., Buchholz, V. R., Huseby, E., Way, S., Jenkins, M., Hodgkin, P., and et Al. (2017). TCR Signal Quality Modulates Fate Decisions of Single CD4 + T Cells in a Probabilistic Manner. *Cell Reports*, 20(4):806–818.

Choi, J.-Y., Ho, J. H.-e., Pasoto, S. G., Bunin, V., Kim, S. T., Carrasco, S., Borba, E. F., Gonçalves, C. R., Costa, P. R., Kallas, E. G., Bonfa, E., and Craft, J. (2015). Circulating Follicular Helper-Like T Cells in Systemic Lupus Erythematosus: Association With Disease Activity. *Arthritis & Rheumatology*, 67(4):988–999.

Choi, Y. S., Yang, J. A., Yusuf, I., Johnston, R. J., Greenbaum, J., Peters, B., and Crotty, S. (2013). Bcl6 Expressing Follicular Helper CD4 T Cells Are Fate Committed Early and Have the Capacity To Form Memory. *Journal of Immunology*, 190(8):4014–4026.

Ciupe, S. M., Devlin, B. H., Markert, M. L., and Kepler, T. B. (2013). Quantification of total T-cell receptor diversity by flow cytometry and spectratyping. *BMC Immunology*, 14(1):35.

Clemente, M. J., Przychodzen, B., Jerez, A., Dienes, B. E., Afable, M. G., Husseinzadeh, H., Rajala, H. L. M., Wlodarski, M. W., Mustjoki, S., and Maciejewski, J. P. (2013). Deep sequencing of the T-cell receptor repertoire in CD8+ T-large granular lymphocyte leukemia identifies signature landscapes. *Blood*, 122(25):4077–85.

Coffman, R. L. and Weissman, I. L. (1981). B220: a B cell-specific member of th T200 glycoprotein family. *Nature*, 289(5799):681–3.

Crotty, S. (2014). T follicular helper cell differentiation, function, and roles in disease. *Immunity*, 41(4):529–42.

D'Agostino, R. and Pearson, E. S. (1973). Tests for Departure from Normality. Empirical Results for the Distributions of b 2 and b 1. *Biometrika*, 60(3):613.

Dash, P., Fiore-Gartland, A. J., Hertz, T., Wang, G. C., Sharma, S., Souquette, A., Crawford, J. C., Clemens, E. B., Nguyen, T. H. O., Kedzierska, K., La Gruta, N. L., Bradley, P., and Thomas, P. G. (2017). Quantifiable predictive features define epitope-specific T cell receptor repertoires. *Nature*, 547(7661):89–93.

Dempsey, L. A. (2011). Keys to $\beta$-selection. *Nature Immunology*, 12:816.

Dornmair, K., Goebels, N., Weltzien, H.-U., Wekerle, H., and Hohlfeld, R. (2003). T-cell-mediated autoimmunity: novel techniques to characterize autoreactive T-cell receptors. *American Journal of Pathology*, 163(4):1215–26.

Dunnett, C. W. (1955). A Multiple Comparison Procedure for Comparing Several Treatments with a Control. *Journal of the American Statistical Association*, 50(272):1096.

Ellebrecht, C. T., Srinivas, G., Bieber, K., Banczyk, D., Kalies, K., Künzel, S., Hammers, C. M., Baines, J. F., Zillikens, D., Ludwig, R. J., and Westermann, J. (2016). Skin microbiota-associated inflammation precedes autoantibody induced tissue damage in experimental epidermolysis bullosa acquisita. *Journal of Autoimmunity*, 68:14–22.

Epperson, D. E., Nakamura, R., Sauntharajah, Y., Melenhorst, J., and Barrett, A. (2001). Oligoclonal T cell expansion in myelodysplastic syndrome: evidence for an autoimmune process. *Leukemia Research*, 25(12):1075–1083.

Ewing, B. and Green, P. (1998). Base-calling of automated sequencer traces using phred. II. Error probabilities. *Genome Research*, 8(3):186–194.

Fähnrich, A., Klein, S., Sergé, A., Nyhoegen, C., Kombrink, S., Möller, S., Keller, K., Westermann, J., and Kalies, K. (2018). CD154 Costimulation Shifts the Local T-Cell Receptor Repertoire Not Only During Thymic Selection but Also During Peripheral T-Dependent Humoral Immune Responses. *Frontiers in Immunology*, 9:1019.

Fähnrich, A., Krebbel, M., Decker, N., Leucker, M., Lange, F. D., Kalies, K., and Möller, S. (2017). ClonoCalc and ClonoPlot: immune repertoire analysis from raw files to publication figures with graphical user interface. *BMC Bioinformatics*, 18(1):164.

Farrar, J. D., Ouyang, W., Löhning, M., Assenmacher, M., Radbruch, A., Kanagawa, O., and Murphy, K. M. (2001). An instructive component in T helper cell type 2 (Th2) development mediated by GATA-3. *Journal of Experimental Medicine*, 193(5):643–50.

Fend, F., Emmert-Buck, M. R., Chuaqui, R., Cole, K., Lee, J., Liotta, L. A., and Raffeld, M. (1999). Immuno-LCM: Laser Capture Microdissection of Immunostained Frozen Sections for mRNA Analysis. *American Journal of Pathology*, 154(1):61–66.

Frentsch, M., Arbach, O., Kirchhoff, D., Moewes, B., Worm, M., Rothe, M., Scheffold, A., and Thiel, A. (2005). Direct access to CD4+ T cells specific for defined antigens according to CD154 expression. *Nature Medicine*, 11(10):1118–1124.

Friedl, P. and Gunzer, M. (2001). Interaction of T cells with APCs: the serial encounter model. *Trends in Immunology*, 22(4):187–191.

Fuller, C. W., Middendorf, L. R., Benner, S. A., Church, G. M., Harris, T., Huang, X., Jovanovich, S. B., Nelson, J. R., Schloss, J. A., Schwartz, D. C., and Vezenov, D. V. (2009). The challenges of sequencing by synthesis. *Nature Biotechnology*, 27(11):1013–1023.

Gastwirth, J. L. (1971). A General Definition of the Lorenz Curve. *Econometrica*, 39(6):1037.

Gerdes, J., Li, L., Schlueter, C., Duchrow, M., Wohlenberg, C., Gerlach, C., Stahmer, I., Kloth, S., Brandt, E., and Flad, H. D. (1991). Immunobiochemical and molecular biologic characterization of the cell proliferation-associated nuclear antigen that is defined by monoclonal antibody Ki-67. *American Journal of Pathology*, 138(4):867–73.

Ghani, S., Feuerer, M., Doebis, C., Lauer, U., Loddenkemper, C., Huehn, J., Hamann, A., and Syrbe, U. (2009). T cells as pioneers: antigen-specific T cells condition inflamed sites for high-rate antigen-non-specific effector cell recruitment. *Immunology*, 128(1 Suppl):e870–80.

Gilfillan, S., Dierich, A., Lemeur, M., Benoist, C., and Mathis, D. (1993). Mice lacking TdT: mature animals with an immature lymphocyte repertoire. *Science*, 261(5125):1175–8.

Gimmi, C. D., Freeman, G. J., Gribben, J. G., Gray, G., and Nadler, L. M. (1993). Human T-cell clonal anergy is induced by antigen presentation in the absence of B7 costimulation. *Proceedings of the National Academy of Sciences of the United States of America*, 90(14):6586–90.

Gini, C. (1912). Variabilità e Mutabilità, contributo allo studio delle distribuzioni e realizioni statiche. *Studi Economico-Giuridici della R. Università di Cagliari*, 3.

Giudicelli, V., Chaume, D., and Lefranc, M.-P. P. (2005). IMGT/GENE-DB: a comprehensive database for human and mouse immunoglobulin and T cell receptor genes. *Nucleic Acids Research*, 33:D256–61.

Gong, C., Linderman, J. J., and Kirschner, D. (2014). Harnessing the heterogeneity of T cell differentiation fate to fine-tune generation of effector and memory T cells. *Frontiers in Immunology*, 5:57.

Grant, C. R., Liberal, R., Mieli-Vergani, G., Vergani, D., and Longhi, M. S. (2015). Regulatory T-cells in autoimmune diseases: Challenges, controversies and—yet—unanswered questions. *Autoimmunity Reviews*, 14(2):105–116.

Groom, J. R. and Luster, A. D. (2011). CXCR3 in T cell function. *Experimental Cell Research*, 317(5):620–31.

Grubbs, F. E. (1950). Sample Criteria for Testing Outlying Observations. *Annals of Mathematical Statistics*, 21(1):27–58.

Haegert, D. G., Cowan, T., Murray, T. J., Gadag, V., and O'Connor, P. (1999). Does a shift in the T-cell receptor repertoire precede the onset of MS? *Neurology*, 53(3):485–90.

Hale, J. S. and Ahmed, R. (2015). Memory T Follicular Helper CD4 T Cells. *Frontiers in Immunology*, 6:16.

Hammers, C. M., Bieber, K., Kalies, K., Banczyk, D., Ellebrecht, C. T., Ibrahim, S. M., Zillikens, D., Ludwig, R. J., and Westermann, J. (2011). Complement-fixing anti-type VII collagen antibodies are induced in Th1-polarized lymph nodes of epidermolysis bullosa acquisita-susceptible mice. *Journal of Immunology*, 187(10):5043–5050.

Han, J., Swan, D. C., Smith, S. J., Lum, S. H., Sefers, S. E., Unger, E. R., and Tang, Y. W. (2006). Simultaneous amplification and identification of 25 human papillomavirus types with Templex technology. *Journal of Clinical Microbiology*, 44(11):4157–4162.

Harden, J. L., Hamm, D., Gulati, N., Lowes, M. A., and Krueger, J. G. (2015). Deep Sequencing of the T-cell Receptor Repertoire Demonstrates Polyclonal T-cell Infiltrates in Psoriasis. *F1000Research*, 4:460.

Heather, J. M., Ismail, M., Oakes, T., and Chain, B. (2017). High-throughput sequencing of the T-cell receptor repertoire: pitfalls and opportunities. *Briefings in Bioinformatics*, 19(4):bbw138.

Hellemans, J., Mortier, G., De Paepe, A., Speleman, F., and Vandesompele, J. (2007). qBase relative quantification framework and software for management and automated analysis of real-time quantitative PCR data. *Genome Biology*, 8(2):R19.

Hindley, J. P., Ferreira, C., Jones, E., Lauder, S. N., Ladell, K., Wynn, K. K., Betts, G. J., Singh, Y., Price, D. A., Godkin, A. J., Dyson, J., and Gallimore, A. (2011). Analysis of the T-cell receptor repertoires of tumor-infiltrating conventional and regulatory T cells reveals no evidence for conversion in carcinogen-induced tumors. *Cancer Research*, 71(3):736–46.

Homey, B., Steinhoff, M., Ruzicka, T., and Leung, D. Y. (2006). Cytokines and chemokines orchestrate atopic skin inflammation. *Journal of Allergy and Clinical Immunology*, 118(1):178–189.

Horn, H. S. (1966). Measurement of "Overlap" in Comparative Ecological Studies. *American Naturalist*, 100(914):419–424.

Huang, J., Zarnitsyna, V. I., Liu, B., Edwards, L. J., Jiang, N., Evavold, B. D., and Zhu, C. (2010). The kinetics of two-dimensional TCR and pMHC interactions determine T-cell responsiveness. *Nature*, 464(7290):932–936.

Huang, J., Zeng, X., Sigal, N., Lund, P. J., Su, L. F., Huang, H., Chien, Y.-h., and Davis, M. M. (2016). Detection, phenotyping, and quantification of antigen-specific T cells using a peptide-MHC dodecamer. *Proceedings of the National Academy of Sciences*, 113(13):E1890–E1897.

Hunter, R., Strickland, F., and Kézdy, F. (1981). The adjuvant activity of nonionic block polymer surfactants. I. The role of hydrophile-lipophile balance. *Journal of Immunology*, 127(3):1244–50.

Hussein, M. R., Mahammad, F., Ali, N., and Hussein, M. R. (2007). Immunohistological analysis of immune cells in blistering skin lesions. *Journal of Clinical Pathology*, 60:62–71.

Hutloff, A., Dittrich, A. M., Beier, K. C., Eljaschewitsch, B., Kraft, R., Anagnostopoulos, I., and Kroczek, R. A. (1999). ICOS is an inducible T-cell co-stimulator structurally and functionally related to CD28. *Nature*, 397(6716):263–266.

Issekutz, T. B., Stoltz, J. M., and van der Meide, P. (1988). The recruitment of lymphocytes into the skin by T cell lymphokines: the role of gamma-interferon. *Clinical and experimental immunology*, 73(1):70–5.

Iwata, H., Bieber, K., Tiburzy, B., Chrobok, N., Kalies, K., Shimizu, A., Leineweber, S., Ishiko, A., Vorobyev, A., Zillikens, D., Köhl, J., Westermann, J., Seeger, K., Manz, R., and Ludwig, R. J. (2013). B cells, dendritic cells, and macrophages are required to induce an autoreactive CD4 helper T cell response in experimental epidermolysis bullosa acquisita. *Journal of Immunology*, 191(6):2978–2988.

Jaccard, P. (1908). Nouvelles recherches sur la distribution florale. *Bulletin de la Societe Vaudoise des Sciences Naturelles*, 44:223–270.

Jackson, A. M. and Krangel, M. S. (2005). Allele-specific regulation of TCR beta variable gene segment chromatin structure. *Journal of Immunology*, 175(8):5186–91.

Jankovic, D., Kugler, D. G., and Sher, A. (2010). IL-10 production by CD4+ effector T cells: a mechanism for self-regulation. *Mucosal Immunology*, 3(3):239–46.

Jenkins, M. K., Taylor, P. S., Norton, S. D., and Urdahl, K. B. (1991). CD28 delivers a costimulatory signal involved in antigen-specific IL-2 production by human T cells. *Journal of Immunology*, 147(8):2461–6.

Johnston, R. J., Poholek, A. C., DiToro, D., Yusuf, I., Eto, D., Barnett, B., Dent, A. L., Craft, J., and Crotty, S. (2009). Bcl6 and Blimp-1 Are Reciprocal and Antagonistic Regulators of T Follicular Helper Cell Differentiation. *Science*, 325(5943):1006–1010.

Jörg, S., Grohme, D. A., Erzler, M., Binsfeld, M., Haghikia, A., Müller, D. N., Linker, R. A., and Kleinewietfeld, M. (2016). Environmental factors in autoimmune diseases and their role in multiple sclerosis. *Cellular and Molecular Life Sciences*, 73(24):4611–4622.

June, C. H., Bluestone, J. A., Nadler, L. M., and Thompson, C. B. (1994). The B7 and CD28 receptor families. *Immunology Today*, 15(7):321–331.

Kalies, K., Blessenohl, M., Nietsch, J., and Westermann, J. (2006). T Cell Zones of Lymphoid Organs Constitutively Express Th1 Cytokine mRNA: Specific Changes during the Early Phase of an Immune Response. *Journal of Immunology*, 176(2).

Kalies, K., König, P., Zhang, Y. M., Deierling, M., Barthelmann, J., Stamm, C., and Westermann, J. (2008). Nonoverlapping expression of IL10, IL12p40, and IFNgamma mRNA in the marginal zone and T cell zone of the spleen after antigenic stimulation. *Journal of Immunology*, 180(8):5457–5465.

Kaplan, M. H., Sun, Y.-L., Hoey, T., and Grusby, M. J. (1996). Impaired IL-12 responses and enhanced development of Th2 cells in Stat4-deficient mice. *Nature*, 382(6587):174–177.

Kasperkiewicz, M., Müller, R., Manz, R., Magens, M., Hammers, C. M., Somlai, C., Westermann, J., Schmidt, E., Zillikens, D., Ludwig, R. J., and Orosz, A. (2011). Heat-shock protein 90 inhibition in autoimmunity to type VII collagen: evidence that nonmalignant plasma cells are not therapeutic targets. *Blood*, 117(23):6135–6142.

Kasperkiewicz, M., Nimmerjahn, F., Wende, S., Hirose, M., Iwata, H., Jonkman, M. F., Samavedam, U., Gupta, Y., Möller, S., Rentz, E., Hellberg, L., Kalies, K., Yu, X., Schmidt, E., Hasler, R., Laskay, T., Westermann, J., Köhl, J., Zillikens, D., and Ludwig, R. J. (2012). Genetic identification and functional validation of FcgammaRIV as key molecule in autoantibody-induced tissue injury. *Journal of Pathology*, 228(1):8–19.

Kasperkiewicz, M., Sadik, C. D., Bieber, K., Ibrahim, S. M., Manz, R. A., Schmidt, E., Zillikens, D., and Ludwig, R. J. (2016). Epidermolysis Bullosa Acquisita: From Pathophysiology to Novel Therapeutic Options. *Journal of Investigative Dermatology*, 136(1):24–33.

Kaune, K. M., Kasperkiewicz, M., Tams, D., Bergmann, M., and Zutt, M. (2015). Anti-p200/anti-laminin gamma1 pemphigoid and BP180 NC16A/4575- positive mucous membrane pemphigoid : late diagnosis in a patient with disease-related loss of vision and multiple previous surgical interventions. *Hautarzt*, 66(1):60–64.

Kawabe, T., Naka, T., Yoshida, K., Tanaka, T., Fujiwara, H., Suematsu, S., Yoshida, N., Kishimoto, T., and Kikutani, H. (1994). The immune responses in CD40-deficient mice: impaired immunoglobulin class switching and germinal center formation. *Immunity*, 1(3):167–78.

Kirsch, I. R., Watanabe, R., O'Malley, J. T., Williamson, D. W., Scott, L.-L., Elco, C. P., Teague, J. E., Gehad, A., Lowry, E. L., LeBoeuf, N. R., Krueger, J. G., Robins, H. S., Kupper, T. S., and Clark, R. A. (2015). TCR sequencing facilitates diagnosis and identifies mature T cells as the cell of origin in CTCL. *Science Translational Medicine*, 7(308):308ra158–308ra158.

Kita, S., Tsuda, T., Sugisaki, K., Miyazaki, E., and Matsumoto, T. (1995). Characterization of distribution of T lymphocyte subsets and activated T lymphocytes infiltrating into sarcoid lesions. *Internal Medicine*, 34(9):847–855.

Kita, Y., Kuroda, K., Mimori, T., Hashimoto, T., Yamamoto, K., Saito, Y., Iwamoto, I., and Sumida, T. (1998). T Cell Receptor Clonotypes in Skin Lesions from Patients with Systemic Lupus Erythematosus. *Journal of Investigative Dermatology*, 110(1):41–46.

Klein, L., Kyewski, B., Allen, P. M., and Hogquist, K. A. (2014). Positive and negative selection of the T cell repertoire: what thymocytes see (and don't see). *Nature Reviews Immunology*, 14(6):377–391.

Köhler, A. (1893). Ein neues Beleuchtungsverfahren für mikrophotographische Zwecke. *Zeitschrift für wissenschaftliche Mikroskopie und für Mikroskopische Technik*, 10(4):433–440.

Komori, T., Okada, A., Stewart, V., and Alt, F. W. (1993). Lack of N regions in antigen receptor variable region genes of TdT-deficient lymphocytes. *Science*, 261(5125):1171–5.

Krangel, M. S. (2009). Mechanics of T cell receptor gene rearrangement. *Current Opinion in Immunology*, 21(2):133–139.

Krangel, M. S., Carabana, J., Abbarategui, I., Schlimgen, R., and Hawwari, A. (2004). Enforcing order within a complex locus: current perspectives on the control of V(D)J recombination at the murine T-cell receptor alpha/delta locus. *Immunological Reviews*, 200(1):224–232.

Laemmli, U. K. (1970). Cleavage of structural proteins during the assembly of the head of bacteriophage T4. *Nature*, 227(5259):680–5.

Lapiere, J. C., Woodley, D. T., Parente, M. G., Iwasaki, T., Wynn, K. C., Christiano, A. M., and Uitto, J. (1993). Epitope mapping of type VII collagen. Identification of discrete peptide sequences recognized by sera from patients with acquired epidermolysis bullosa. *Journal of Clinical Investigation*, 92(4):1831–9.

Laydon, D. J., Bangham, C. R. M., and Asquith, B. (2015). Estimating T-cell repertoire diversity: limitations of classical estimators and a new approach. *Philosophical Transactions of the Royal Society B: Biological Sciences*, 370(1675).

Lee, S., Silva, D., Martin, J., Pratama, A., Hu, X., Chang, P.-P., Walters, G., and Vinuesa, C. (2012). Interferon-$\gamma$ Excess Leads to Pathogenic Accumulation of Follicular Helper T Cells and Germinal Centers. *Immunity*, 37(5):880–892.

Lefranc, M. P., Giudicelli, V., Duroux, P., Jabado-Michaloud, J., Folch, G., Aouinti, S., Carillon, E., Duvergey, H., Houles, A., Paysan-Lafosse, T., Hadi-Saljoqi, S., Sasorith, S., Lefranc, G., and Kossida, S. (2015). IMGT R, the international ImMunoGeneTics information system R 25 years on. *Nucleic Acids Research*, 43(D1):D413–D422.

Lefranc, M.-P., Giudicelli, V., Kaas, Q., Duprat, E., Jabado-Michaloud, J., Scaviner, D., Ginestoux, C., Clément, O., Chaume, D., and Lefranc, G. (2004). IMGT, the international ImMunoGeneTics information system(R). *Nucleic Acids Research*, 33:D593–D597.

Leyendeckers, H., Schmitz, J., Tasanen, K., Bruckner-Tuderman, L., Zillikens, D., Sitaru, C., and Hunzelmann, N. (2003). Memory B Cells Specific for the NC16A Domain of the 180 kDa Bullous Pemphigoid Autoantigen Can Be Detected in Peripheral Blood of Bullous Pemphigoid Pa-

tients and Induced In Vitro to Synthesize Autoantibodies. *Journal of Investigative Dermatology*, 120(3):372–378.

Ling, D. and Salvaterra, P. M. (2011). Robust RT-qPCR data normalization: validation and selection of internal reference genes during post-experimental data analysis. *PloS one*, 6(3):e17762.

Liu, D., Xu, H., Shih, C., Wan, Z., Ma, X., Ma, W., Luo, D., and Qi, H. (2015). T–B-cell entanglement and ICOSL-driven feed-forward regulation of germinal centre reaction. *Nature*, 517(7533):214–218.

Liu, X., Yan, X., Zhong, B., Nurieva, R. I., Wang, A., Wang, X., Martin-Orozco, N., Wang, Y., Chang, S. H., Esplugues, E., Flavell, R. A., Tian, Q., and Dong, C. (2012). Bcl6 expression specifies the T follicular helper cell program in vivo. *Journal of Experimental Medicine*, 209(10):1841–1852.

Livak, K. J. and Schmittgen, T. D. (2001). Analysis of Relative Gene Expression Data Using Real-Time Quantitative PCR and the 2ΔΔCT Method. *Methods*, 25(4):402–408.

Ludwig, R. J., Recke, A., Bieber, K., Müller, S., Marques, A. d. C., Banczyk, D., Hirose, M., Kasperkiewicz, M., Ishii, N., Schmidt, E., Westermann, J., Zillikens, D., and Ibrahim, S. M. (2011). Generation of Antibodies of Distinct Subclasses and Specificity Is Linked to H2s in an Active Mouse Model of Epidermolysis Bullosa Acquisita. *Journal of Investigative Dermatology*, 131(1):167–176.

Lythe, G., Callard, R. E., Hoare, R. L., and Molina-Paris, C. (2016). How many TCR clonotypes does a body maintain? *Journal of Theoretical Biology*, 389:214–224.

Ma, C. S. and Phan, T. G. (2017). Here, there and everywhere: T follicular helper cells on the move. *Immunology*, 152(3):382–387.

Maass, S. C. (2015). *Das passive Antikörpertransfermodell der Epidermolysis Bullosa Acquisita: Die Produktion endogener Antikörper gegen injizierte Fremdproteine und die Anwesenheit aktivierter T-Zellen in der Haut führen zu verstärkter Blasenbildung.* PhD thesis, University of Lübeck.

Madi, A., Shifrut, E., Reich-Zeliger, S., Gal, H., Best, K., Ndifon, W., Chain, B., Cohen, I. R., and Friedman, N. (2014). T-cell receptor repertoires share a restricted set of public and abundant CDR3 sequences that are associated with self-related immunity. *Genome Research*, 24(10):1603–1612.

Mahnke, Y. D. and Roederer, M. (2007). Optimizing a multicolor immunophenotyping assay. *Clinics in Laboratory Medicine*, 27(3):469–85, v.

Marrack, P., Scott-Browne, J. P., Dai, S., Gapin, L., and Kappler, J. W. (2008). Evolutionarily Conserved Amino Acids That Control TCR-MHC Interaction. *Annual Review of Immunology*, 26(1):171–203.

Matzaraki, V., Kumar, V., Wijmenga, C., and Zhernakova, A. (2017). The MHC locus and genetic susceptibility to autoimmune and infectious diseases. *Genome Biology*, 18(1):76.

McLachlan, J. B. and Jenkins, M. K. (2007). Migration and accumulation of effector CD4+ T cells in nonlymphoid tissues. *Proceedings of the American Thoracic Society*, 4(5):439–42.

Menezes, J. S., van den Elzen, P., Thornes, J., Huffman, D., Droin, N. M., Maverakis, E., and Sercarz, E. E. (2007). A public T cell clonotype within a heterogeneous autoreactive repertoire is dominant in driving EAE. *Journal of Clinical Investigation*, 117(8):2176–2185.

Mihai, S., Chiriac, M. T., Takahashi, K., Thurman, J. M., Holers, V. M., Zillikens, D., Botto, M., and Sitaru, C. (2007). The alternative pathway of complement activation is critical for blister induction in experimental epidermolysis bullosa acquisita. *Journal of Immunology*, 178(10):6514–21.

Mihai, S. and Sitaru, C. (2007). Immunopathology and molecular diagnosis of autoimmune bullous diseases. *Journal of Cellular and Molecular Medicine*, 11(3):462–81.

Miqueu, P., Degauque, N., Guillet, M., Giral, M., Ruiz, C., Pallier, A., Braudeau, C., Roussey-Kesler, G., Ashton-Chess, J., Doré, J.-C., Thervet, E., Legendre, C., Hernandez-Fuentes, M. P., Warrens, A. N., Goldman, M., Volk, H.-D., Janssen, U., Wood, K. J., Lechler, R. I., Bertrand, D., Sébille, V., Soulillou, J.-P., and Brouard, S. (2010). Analysis of the peripheral T-cell repertoire in kidney transplant patients. *European Journal of Immunology*, 40:3280–3290.

Miqueu, P., Guillet, M., Degauque, N., Doré, J.-C., Soulillou, J.-P., and Brouard, S. (2007). Statistical analysis of CDR3 length distributions for the assessment of T and B cell repertoire biases. *Molecular Immunology*, 44(6):1057–1064.

Morgan, D. A., Ruscetti, F. W., and Gallo, R. (1976). Selective in vitro growth of T lymphocytes from normal human bone marrows. *Science*, 193(4257):1007–8.

Morisita, M. (1962). I $\sigma$-Index, a measure of dispersion of individuals. *Researches on Population Ecology*, 4(1):1–7.

Moser, B. (2015). CXCR5, the Defining Marker for Follicular B Helper T (TFH) Cells. *Frontiers in Immunology*, 6:296.

Murphy, K. and Weaver, C. (2016). *Janeway's Immunobiology*. Garland Science, 9th edition.

Murphy, K. M. and Reiner, S. L. (2002). The lineage decisions of helper T cells. *Nature Reviews Immunology*, 2(12):933–944.

Nakayamada, S., Kanno, Y., Takahashi, H., Jankovic, D., Lu, K., Johnson, T., Sun, H.-w., Vahedi, G., Hakim, O., Handon, R., Schwartzberg, P., Hager, G., and O'Shea, J. (2011). Early Th1 Cell Differentiation Is Marked by a Tfh Cell-like Transition. *Immunity*, 35(6):919–931.

Nathan, C. F., Murray, H. W., Wiebe, M. E., and Rubin, B. Y. (1983). Identification of interferon-gamma as the lymphokine that activates human macrophage oxidative metabolism and antimicrobial activity. *Journal of Experimental Medicine*, 158(3):670–89.

Nazarov, V. I., Pogorelyy, M. V., Komech, E. A., Zvyagin, I. V., Bolotin, D. A., Shugay, M., Chudakov, D. M., Lebedev, Y. B., and Mamedov, I. Z. (2015). tcR: an R package for T cell receptor repertoire advanced data analysis. *BMC Bioinformatics*, 16(1):175.

Nepom, G. T. (2012). MHC class II tetramers. *Journal of Immunology*, 188(6):2477–82.

Ng, T. H. S., Britton, G. J., Hill, E. V., Verhagen, J., Burton, B. R., and Wraith, D. C. (2013). Regulation of adaptive immunity; the role of interleukin-10. *Frontiers in Immunology*, 4:129.

Niemi, H. J., Laakso, S., Salminen, J. T., Arstila, T. P., and Tuulasvaara, A. (2015). A normal T cell receptor beta CDR3 length distribution in patients with APECED. *Cellular Immunology*, 295(2):99–104.

Niu, J., Jia, Q., Ni, Q., Yang, Y., Chen, G., Yang, X., Zhai, Z., Yu, H., Guan, P., Lin, R., Song, Z., Li, Q.-J., Hao, F., Zhong, H., and Wan, Y. (2015). Association of CD8+ T lymphocyte repertoire spreading with the severity of DRESS syndrome. *Scientific Reports*, 5(1):9913.

Nurieva, R. I., Chung, Y., Hwang, D., Yang, X. O., Kang, H. S., Ma, L., Wang, Y.-h., Watowich, S. S., Jetten, A. M., Tian, Q., and Dong, C. (2008). Generation of T Follicular Helper Cells Is Mediated by Interleukin-21 but Independent of T Helper 1, 2, or 17 Cell Lineages. *Immunity*, 29(1):138–149.

Nurieva, R. I., Chung, Y., Martinez, G. J., Yang, X. O., Tanaka, S., Matskevitch, T. D., Wang, Y.-H., and Dong, C. (2009). Bcl6 Mediates the Development of T Follicular Helper Cells. *Science*, 325(5943):1001–1005.

Oakes, T., Heather, J. M., Best, K., Byng-Maddick, R., Husovsky, C., Ismail, M., Joshi, K., Maxwell, G., Noursadeghi, M., Riddell, N., Ruehl, T., Turner, C. T., Uddin, I., and Chain, B. (2017a). Quantitative Characterization of the T Cell Receptor Repertoire of Naïve and Memory Subsets Using an Integrated Experimental and Computational Pipeline Which Is Robust, Economical, and Versatile. *Frontiers in Immunology*, 8:1267.

Oakes, T., Popple, A. L., Williams, J., Best, K., Heather, J. M., Ismail, M., Maxwell, G., Gellatly, N., Dearman, R. J., Kimber, I., and Chain, B. (2017b). The T Cell Response to the Contact Sensitizer Paraphenylenediamine Is Characterized by a Polyclonal Diverse Repertoire of Antigen-Specific Receptors. *Frontiers in Immunology*, 8:162.

Oestreich, K. J. and Weinmann, A. S. (2012). Master regulators or lineage-specifying? Changing views on CD4+ T cell transcription factors. *Nature Reviews Immunology*, 12(11):799–804.

O'Garra, A. and Murphy, K. (1996). Role of cytokines in development of Th1 and Th2 cells. *Chemical Immunology*, 63:1–13.

Okajima, M., Wada, T., Nishida, M., Yokoyama, T., Nakayama, Y., Hashida, Y., Shibata, F., Tone, Y., Ishizaki, A., Shimizu, M., Saito, T., Ohta, K., Toma, T., and Yachie, A. (2009). Analysis of T cell receptor Vbeta diversity in peripheral CD4 and CD8 T lymphocytes in patients with autoimmune thyroid diseases. *Clinical and Experimental Immunology*, 155(2):166–72.

Ouyang, W., Ranganath, S. H., Weindel, K., Bhattacharya, D., Murphy, T. L., Sha, W. C., and Murphy, K. M. (1998). Inhibition of Th1 development mediated by GATA-3 through an IL-4-independent mechanism. *Immunity*, 9(5):745–55.

Pannetier, C., Cochet, M., Darche, S., Casrouge, A., Zöller, M., and Kourilsky, P. (1993). The sizes of the CDR3 hypervariable regions of the murine T-cell receptor beta chains vary as a function of the recombined germ-line segments. *Proceedings of the National Academy of Sciences of the United States of America*, 90(9):4319–23.

Pilli, D., Zou, A., Tea, F., Dale, R. C., and Brilot, F. (2017). Expanding Role of T Cells in Human Autoimmune Diseases of the Central Nervous System. *Frontiers in Immunology*, 8:652.

Pogorelyy, M. V., Fedorova, A. D., McLaren, J. E., Ladell, K., Bagaev, D. V., Eliseev, A. V., Mikelov, A. I., Koneva, A. E., Zvyagin, I. V., Price, D. A., Chudakov, D. M., and Shugay, M. (2018). Exploring the pre-immune landscape of antigen-specific T cells. *Genome Medicine*, 10(1):68.

Pollard, T. D. T. D., Earnshaw, W. C., Lippincott-Schwartz, J., and Johnson, G. T. (2017). Extracellular Matrix Molecules. In *Cell Biology (Third Edition)*, pages 505–524. Elsevier, 3rd edition.

Qi, H. (2016). T follicular helper cells in space-time. *Nature Reviews Immunology*, 16(10):612–625.

R Core Team (2015). *R: A Language and Environment for Statistical Computing*. R Foundation for Statistical Computing, Vienna, Austria.

Rao, K. V. N., He, Y.-X., and Kalyanasundaram, R. (2003). Expression of a 28-kilodalton glutathione S-transferase antigen of Schistosoma mansoni on the surface of filamentous phages and evaluation of its vaccine potential. *Clinical and Diagnostic Laboratory Immunology*, 10(4):536–41.

Reinhardt, R. L., Bullard, D. C., Weaver, C. T., and Jenkins, M. K. (2003). Preferential Accumulation of Antigen-specific Effector CD4 T Cells at an Antigen Injection Site Involves CD62E-dependent Migration but Not Local Proliferation. *Journal of Experimental Medicine*, 197(6):751–762.

Ridgway, W. M. and Fathman, C. G. (1998). The association of MHC with autoimmune diseases: understanding the pathogenesis of autoimmune diabetes. *Clinical immunology and immunopathology*, 86(1):3–10.

Rosati, E., Dowds, C. M., Liaskou, E., Henriksen, E. K. K., Karlsen, T. H., and Franke, A. (2017). Overview of methodologies for T-cell receptor repertoire analysis. *BMC Biotechnology*, 17(1):61.

Rudensky, A. Y., Preston-Hurlburt, P., Hong, S.-C., Barlow, A., and Janeway, C. A. (1991). Sequence analysis of peptides bound to MHC class II molecules. *Nature*, 353(6345):622–627.

Sadofsky, M. J. (2001). The RAG proteins in V(D)J recombination: more than just a nuclease. *Nucleic Acids Research*, 29(7):1399–409.

Schatz, D. G. and Spanopoulou, E. (2005). Biochemistry of V(D)J recombination. *Current Topics in Microbiology and Immunology*, 290:49–85.

Schindelin, J., Arganda-Carreras, I., Frise, E., Kaynig, V., Longair, M., Pietzsch, T., Preibisch, S., Rueden, C., Saalfeld, S., Schmid, B., Tinevez, J. Y., White, D. J., Hartenstein, V., Eliceiri, K., Tomancak, P., and Cardona, A. (2012). Fiji: an open-source platform for biological-image analysis. *Nature Methods*, 9(7):676–682.

Selvaraj, R. K. and Geiger, T. L. (2007). A kinetic and dynamic analysis of Foxp3 induced in T cells by TGF-beta. *Journal of Immunology*, 178(12):7667–77.

Sharpe, A. H. and Abbas, A. K. (2006). T-Cell Costimulation — Biology, Therapeutic Potential, and Challenges. *New England Journal of Medicine*, 355(10):973–975.

Shimanovich, I., Mihai, S., Oostingh, G. J., Ilenchuk, T. T., Bröcker, E.-B., Opdenakker, G., Zillikens, D., and Sitaru, C. (2004). Granulocyte-derived elastase and gelatinase B are required for dermal-epidermal separation induced by autoantibodies from patients with epidermolysis bullosa acquisita and bullous pemphigoid. *Journal of Pathology*, 204(5):519–27.

Shulman, Z., Gitlin, A. D., Targ, S., Jankovic, M., Pasqual, G., Nussenzweig, M. C., and Victora, G. D. (2013). T follicular helper cell dynamics in germinal centers. *Science*, 341(6146):673–677.

Sitaru, C., Chiriac, M. T., Mihai, S., Büning, J., Gebert, A., Ishiko, A., and Zillikens, D. (2006). Induction of complement-fixing autoantibodies against type VII collagen results in subepidermal blistering in mice. *Journal of Immunology*, 177(5):3461–3468.

Sitaru, C., Mihai, S., Otto, C., Chiriac, M. T., Hausser, I., Dotterweich, B., Saito, H., Rose, C., Ishiko, A., and Zillikens, D. (2005). Induction of dermal-epidermal separation in mice by passive transfer of antibodies specific to type VII collagen. *Journal of Clinical Investigation*, 115(4):870–878.

Six, A., Mariotti-Ferrandiz, M. E., Chaara, W., Magadan, S., Pham, H.-P., Lefranc, M.-P., Mora, T., Thomas-Vaslin, V., Walczak, A. M., and Boudinot, P. (2013). The Past, Present, and Future of Immune Repertoire Biology – The Rise of Next-Generation Repertoire Analysis. *Frontiers in Immunology*, 4:413.

Starr, T. K., Jameson, S. C., and Hogquist, K. A. (2003). Positive and negative selection of T cells. *Annual Review of Immunology*, 21(1):139–176.

Stavnezer, J., Guikema, J. E. J., and Schrader, C. E. (2008). Mechanism and regulation of class switch recombination. *Annual review of Immunology*, 26:261–92.

Szabo, S. J., Kim, S. T., Costa, G. L., Zhang, X., Fathman, C., and Glimcher, L. H. (2000). A Novel Transcription Factor, T-bet, Directs Th1 Lineage Commitment. *Cell*, 100(6):655–669.

Tal, M., Silberstein, A., and Nusser, E. (1985). Why does Coomassie Brilliant Blue R interact differently with different proteins? A partial answer. *Journal of Biological Chemistry*, 260(18):9976–80.

Taylor, D. K., Mittereder, N., Kuta, E., Delaney, T., Burwell, T., Dacosta, K., Zhao, W., Cheng, L. I., Brown, C., Boutrin, A., Guo, X., White, W. I., Zhu, J., Dong, H., Bowen, M. A., Lin, J., Gao, C., Yu, L., Ramaswamy, M., Gaudreau, M.-C., Woods, R., Herbst, R., and Carlesso, G. (2018). T follicular helper–like cells contribute to skin fibrosis. *Science Translational Medicine*, 10(431):eaaf5307.

Textor, J., Fähnrich, A., Meinhardt, M., Tune, C., Klein, S., Pagel, R., König, P., Kalies, K., and Westermann, J. (2018). Deep Sequencing Reveals Transient Segregation of T Cell Repertoires in Splenic T Cell Zones during an Immune Response. *Journal of Immunology*, 201(2):350–358.

Tiburzy, B., Szyska, M., Iwata, H., Chrobok, N., Kulkarni, U., Hirose, M., Ludwig, R. J., Kalies, K., Westermann, J., Wong, D., and Manz, R. A. (2013). Persistent autoantibody-production by intermediates between short-and long-lived plasma cells in inflamed lymph nodes of experimental epidermolysis bullosa acquisita. *PLoS One*, 8(12):e83631.

Tripathi, S. K. and Lahesmaa, R. (2014). Transcriptional and epigenetic regulation of T-helper lineage specification. *Immunological Reviews*, 261(1):62–83.

Tubo, N. J. and Jenkins, M. K. (2014). TCR signal quantity and quality in CD4+ T cell differentiation. *Trends in Immunology*, 35(12):591–596.

Tubo, N. J., Pagan, A. J., Taylor, J. J., Nelson, R. W., Linehan, J. L., Ertelt, J. M., Huseby, E. S., Way, S. S., and Jenkins, M. K. (2013). Single naive CD4+ T cells from a diverse repertoire produce different effector cell types during infection. *Cell*, 153(4):785–796.

Tukey, J. W. J. W. (1977). *Exploratory data analysis*. Addison-Wesley Publishing Company.

Ueno, H. (2016). Human Circulating T Follicular Helper Cell Subsets in Health and Disease. *Journal of Clinical Immunology*, 36(S1):34–39.

van den Beemd, R., Boor, P. P., van Lochem, E. G., Hop, W. C., Langerak, A. W., Wolvers-Tettero, I. L., Hooijkaas, H., and van Dongen, J. J. (2000). Flow cytometric analysis of the V? repertoire in healthy controls. *Cytometry*, 40(4):336–345.

van Panhuys, N. (2016). TCR Signal Strength Alters T-DC Activation and Interaction Times and Directs the Outcome of Differentiation. *Frontiers in Immunology*, 7:6.

VanderBorght, A., Geusens, P., Vandevyver, C., Raus, J., and Stinissen, P. (2000). Skewed T-cell receptor variable gene usage in the synovium of early and chronic rheumatoid arthritis patients and persistence of clonally expanded T cells in a chronic patient. *Rheumatology*, 39(11):1189–201.

Vandesompele, J., De Preter, K., Pattyn, F., Poppe, B., Van Roy, N., De Paepe, A., and Speleman, F. (2002). Accurate normalization of real-time quantitative RT-PCR data by geometric averaging of multiple internal control genes. *Genome biology*, 3(7):34.

Vojdani, A., Pollard, K. M., and Campbell, A. W. (2014). Environmental triggers and autoimmunity. *Autoimmune Diseases*, 2014:798029.

Wang, C., Sanders, C. M., Yang, Q., Schroeder Jr., H. W., Wang, E., Babrzadeh, F., Gharizadeh, B., Myers, R. M., Hudson Jr., J. R., Davis, R. W., and Han, J. (2010). High throughput sequencing reveals a complex pattern of dynamic interrelationships among human T cell subsets. *Proceedings of the National Academy of Sciences*, 107(4):1518–1523.

Wang, Y., Wang, L., Shi, Y., Wang, F., Yang, H., Han, S., and Bai, Y. (2017). Altered circulating T follicular helper cell subsets in patients with psoriasis vulgaris. *Immunology Letters*, 181:101–108.

Woodley, D. T., Briggaman, R. A., O'Keefe, E. J., Inman, A. O., Queen, L. L., and Gammon, W. R. (1984). Identification of the Skin Basement-Membrane Autoantigen in Epidermolysis Bullosa Acquisita. *New England Journal of Medicine*, 310(16):1007–1013.

Woodsworth, D. J., Castellarin, M., and Holt, R. A. (2013). Sequence analysis of T-cell repertoires in health and disease. *Genome Medicine*, 5(10):98.

Wraith, D. C., Smilek, D. E., and Webb, S. (1992). MHC-binding peptides for immunotherapy of experimental autoimmune disease. *Journal of Autoimmunity*, 5 Suppl A:103–13.

Xu, H., Li, X., Liu, D., Li, J., Zhang, X., Chen, X., Hou, S., Peng, L., Xu, C., Liu, W., Zhang, L., and Qi, H. (2013). Follicular T-helper cell recruitment governed by bystander B cells and ICOS-driven motility. *Nature*, 496(7446):523–527.

Yassai, M. B., Naumov, Y. N., Naumova, E. N., and Gorski, J. (2009). A clonotype nomenclature for T cell receptors. *Immunogenetics*, 61(7):493–502.

Yoshizawa, K., Ota, M., Katsuyama, Y., Ichijo, T., Inada, H., Umemura, T., Tanaka, E., and Kiyosawa, K. (1999). T cell repertoire in the liver of patients with autoimmune hepatitis. *Human Immunology*, 60(9):806–15.

Yu, D., Rao, S., Tsai, L. M., Lee, S. K., He, Y., Sutcliffe, E. L., Srivastava, M., Linterman, M., Zheng, L., Simpson, N., Ellyard, J. I., Parish, I. A., Ma, C. S., Li, Q.-J., Parish, C. R., Mackay, C. R., and Vinuesa, C. G. (2009). The Transcriptional Repressor Bcl-6 Directs T Follicular Helper Cell Lineage Commitment. *Immunity*, 31(3):457–468.

Yuan, R. R., Wong, P., McDevitt, M. R., Doubrovina, E., Leiner, I., Bornmann, W., O'reilly, R., Pamer, E. G., and Scheinberg, D. A. (2004). Targeted deletion of T-cell clones using alpha-emitting suicide MHC tetramers. *Blood*, 104(8):2397–2402.

Zarnitsyna, V. I., Evavold, B. D., Schoettle, L. N., Blattman, J. N., and Antia, R. (2013). Estimating the diversity, completeness, and cross-reactivity of the T cell repertoire. *Frontiers in Immunology*, 4:485.

Zhang, J., Kobert, K., Flouri, T., and Stamatakis, A. (2014). PEAR: A fast and accurate Illumina Paired-End reAd mergeR. *Bioinformatics*, 30(5):614–620.

Zhang, Z., Procissi, D., Li, W., Kim, D.-H., Li, K., Han, G., Huan, Y., and Larson, A. C. (2013). High resolution MRI for non-invasive mouse lymph node mapping. *Journal of Immunological Methods*, 400-401:23–29.

Zhu, J. (2015). T helper 2 (Th2) cell differentiation, type 2 innate lymphoid cell (ILC2) development and regulation of interleukin-4 (IL-4) and IL-13 production. *Cytokine*, 75(1):14–24.

Zhu, J., Yamane, H., Cote-Sierra, J., Guo, L., and Paul, W. E. (2006). GATA-3 promotes Th2 responses through three different mechanisms: induction of Th2 cytokine production, selective growth of Th2 cells and inhibition of Th1 cell-specific factors. *Cell Research*, 16(1):3–10.

Ziegler, S. F. (2006). FOXP3: Of Mice and Men. *Annual Review of Immunology*, 24(1):209–226.

Zvyagin, I. V., Pogorelyy, M. V., Ivanova, M. E., Komech, E. A., Shugay, M., Bolotin, D. A., Shelenkov, A. A., Kurnosov, A. A., Staroverov, D. B., Chudakov, D. M., Lebedev, Y. B., and Mamedov, I. Z. (2014). Distinctive properties of identical twins' TCR repertoires revealed by high-throughput sequencing. *Proceedings of the National Academy of Sciences*, 111(16):5980–5985.

# List of Figures

# List of Tables

## List of Abbreviations

| | |
|---|---|
| AA | Amino acid |
| APAAP | Alkaline Phosphatase - Anti-Alkaline Phosphatase |
| APC | Antigen presenting cells |
| APC (fluorochrome) | Allophycocyanin |
| BCZ | B-lymphocyte zone |
| bp | Base pair |
| BSA | Bovine serum albumin |
| BV421/510 | Brilliant Violet 421/510 |
| CD | Cluster of differentiation |
| cDNA | Complementary DNA |
| CDR | Complementarity-determining region |
| (m)Col7 | (murine) Collagen type VII |
| comp. | compartment |
| $C_T$ | Cycle of threshold |
| Cy5.5/7 | Cyanine 5.5/7 |
| d | Day |
| DAB | 3,3'-Diaminobenzidine |
| DAPI | 4',6-Diamidin-2-phenylindol |
| DIF | Direct immunofluorescence |
| (g)DNA | (Genomic) Deoxyribonucleic acid |
| DNase | Deoxyribonuclease |
| dNTP | Deoxynucleotide triphosphate |
| EDTA | Ethylendiamintetraacetat |
| FACS | Fluorescence-activated cell sorting |
| FMO | Fluorescence minus one |
| FSC | Forward scatter |
| g | Gravitational constant |
| GAPDH | Glycerinaldehyd-3-phosphat-Dehydrogenase |
| GC | Germinal center |
| GST | Glutathione-S-transferase |
| h | Hour |

| | |
|---|---|
| ICOS(L) | Inducible T-cell costimulator (lignad) |
| IF | Immunofluorescence |
| IFN | Interferon |
| Ig | Immune globulin |
| IL | Interleukin |
| i.p. | Intraperitoneal |
| kDa | Kilo-Dalton |
| Ki-67 | Kiel-67 |
| LN | Lymph node |
| mCOL7c-GST | Murine collagen type VII fragment linked to GST |
| MHC | Major Histocompatibility Complex |
| min | Minute |
| ml | Milliliter |
| $\mu$l | Microliter |
| MLN51 | Metastatic lympnnode 51 |
| mRNA | Messenger ribonucleic acid |
| n | Sample size |
| N | Number of individuals |
| NC1 | Non-collagenous domain 1 |
| NCBI | National Center for Biotechnology Information |
| $N_F$ | qRT-PCR normalization factor |
| NGS | Next-Generation Sequencing |
| nm | Nanometer |
| o/n | Overnight |
| PCR | Polymerase chain reaction |
| PE | Phycoerythrin |
| PerCP | Peridinin chlorophyll protein complex |
| PFA | Paraformaldehyde |
| PI | Propidium Iodide |
| qRT-PCR | Quantitative real-time polymerase chain reaction |
| RAG | Recombination-activating gene |
| RNA | Ribonucleic acid |
| ROS | Reactive oxygen species |

| | |
|---|---|
| RT | Room temperature |
| s.c. | Subcutan |
| SD | Standard deviation |
| sec | Second |
| SPF | Specific-pathogen-free |
| TCR | T-lymphocyte receptor |
| TCZ | T-lymphocyte zone |
| $T_{fh}$ | Follicular helper T-lymphocyte |
| TGF | Transforming growth factor |
| $T_H$ | T-lymphocyte helper cells |
| TRBJ | T-lymphocyte receptor J-segment |
| TRBV | T-lymphocyte receptor V-segment |
| $T_{skin}$ | Skin immigrating T-lymphocytes |
| UV | Ultraviolet light |
| V | Volt |
| vWFA2 | von-Willebrand-factor A like domain 2 |

## Acknowledgement

Initially I like to thank and express my sincere gratitude to my supervisor PD. Dr.in rer. nat. Kathrin Kalies for her guidance and continual support. The close collaboration and fruitful discussions helped me throughout the time of research and writing this thesis.

Furthermore I like to thank Prof. Dr. med. Jürgen Westermann not only for the financial support, much more for his continuous reviews and critical questions. This encouraged me to see my project in the bigger picture and appropriately interpret experimental results.

I like to address a very special thank to my GRK mentors Prof. Dr. rer. nat. Rudolf Manz and Dr.in rer. nat. Katja Bieber. Due to your constant and critical feedback during the GRK jour fixes and retreats, I was always motivated to think and question my project. Your view beyond the horizon was always helpful!

Also a deep thank you to the Postdocs and PhD-students of the Anatomy for all the help, support and expertise throughout my entire time. Particularly, Dr.in rer. nat. Anke Fähnrich, Dr. rer. nat. Sebastian Maass, Dr.in rer. nat. Natalia Kunz, Dr. rer. nat. Sebastian Klein, Dr.in rer. physiol. Cornelia Tune, Dr.in rer. nat. Andrea Schampel, Rebecca Reumann, Julia Belde and Lisa-Kristin Schierloh. With you, not only the lab-work was great, especially non-work-activities were a great pleasure.

My sincere thanks goes to all colleagues of the Anatomy. I would like to emphasize Lidija Gutjahr, Petra Lau, Daniela Rieck and René Pagel who supported this study in a number of ways. Your general knowledge and technical expertise made experiments a success and supported me throughout the whole time. A very special thanks for your flexibility and handling the many tings that "should have been done by yesterday".

Many thanks to Susanne Allan from the Institute for Biology. Your help in molecular and protein biology was outstanding and saved me a lot of time and hassle.

Further I like to thank Prof. Dr. med. Ralf Ludwig and the entire LIED team for providing recombinant proteins and their general expertise in the EBA setting.

Special thanks to my parents, who essentially supported my career from the beginning. The unconditional support backed me not only on this way.

My deepest and warmest thank is addressed to Sophie. Your help, support and affection was and is my main motivator. Your devotion for our daughter covered my back and has made all this possible. Just - Thank you!

## Curriculum Vitae